Digging for Answers:

The Effects of Mining Pollution Externalities on Local Agricultural Output in Africa

Mira Korb

Click here for latest version.

Abstract

Mining may affect local agriculture through demand shocks that lower the returns to inputs in the non-agricultural sector or pollution shocks that lower the returns to inputs within agriculture. This paper explores the extent to which pollution externalities from industrial mining affect local agricultural output in Sub-Saharan Africa. I combine mine geolocations, topographical data and satellite-based measures of pollution, yields and weather, to identify areas around mines that are disproportionately exposed to pollution but not the effects of local demand booms. Leveraging the staggered openings of mines across Sub-Saharan Africa, I find that air and water pollution externalities account for 44% of the overall reduction in yields caused by industrial mining. Additionally, I use both standard heterogeneity analysis, as well as machine learning methods, to document that negative pollution externalities on local yields are 2-3 times larger for mines in countries with poor governance and regulatory environments.

1 Introduction

A majority of the countries in Sub-Saharan Africa depend heavily on natural resources for government revenues, export earnings and development potential. Of the 48 countries in Sub-Saharan Africa, 26 are considered "resource-rich" by the International Monetary Fund, meaning at least 20% of exports or fiscal revenue come from natural resources [Cust and Zeufack, 2023]. This dependence on natural resource extraction in Africa is only expected to rise in the future. From smartphones to electric vehicles, the global transition to clean energy has lead to a boom in demand for critical minerals and metals. According to the International Energy Agency, the demand for cobalt and nickel will double, while the demand for lithium will rise by almost ten-fold in the next two decades [Chen et al., 2024].

As Sub-Saharan Africa is home to 30% of the world's critical minerals, policymakers argue that the region should take advantage of rising mineral demand to drive structural transformation [Chen et al., 2024]. In fact, it seems that many African governments are already acting upon this rhetoric by providing tax breaks or other incentives to attract investment from mining companies [Coulibaly and Camara, 2022]. However, an important first order question to ask is how rising mineral extraction may affect local livelihoods in Africa, the majority of which depend heavily on agriculture [Goedde et al., 2019].

The standard model of structural transformation proposes that higher returns to inputs in non-agricultural sectors will increase the opportunity cost of keeping productive inputs in agriculture, encouraging a reallocation of these inputs out of agriculture towards other more productive sectors. However, structural change is not the only mechanism through which industrial activities, like mining, may lead to an observed decline in agriculture. Cross-sector externalities, such as air or water pollution, may lower the returns to agriculture rather than raise the returns of outside options. In this paper, I investigate the extent to which industrial mining affects local agriculture in Sub-Saharan Africa through pollution externalities versus raising the returns to inputs outside of agriculture.

I combine a large geo-spatial dataset of mines across Sub-Saharan Africa from S&P Global Market Intelligence, with topographical data, as well as satellite-based measures of pollution, yields and weather. To isolate the effect of mining pollution from the effects of local demand booms, I leverage the fact that while labor or land price shocks from mining will disproportionately affect areas near mines relative to areas further away, they should not disproportionately affect areas near these mines that are more likely to be exposed to pollution externalities, for instance by being located downwind or downstream from a mine.

To estimate the effect of mining on remotely-sensed pollution, as well as the resulting pollution externalities on remotely-sensed yields, I use the staggered openings of mines across Africa from 2000 to 2022 in two spatial difference-in-difference (DID) designs: (1) an upstream vs. downstream DID for water pollution and (2) a DID with continuous downwind exposure for air pollution. I define a mine opening as the start of commercial-level production. Identification is based on within-mine variation in pollution exposure driven by topography or weather, which are plausibly exogenous to local market conditions. I proxy for local crop yields using the normalized difference vegetation index (NDVI), calculated only over cropland pixels.

For water pollution, I define upstream and downstream cropland around mines located along rivers, measuring river water quality with a novel, remotely sensed indicator, the normalized difference turbidity index (NDTI). The downstream cropland reflects treated areas that might be affected by river water quality through seepage of the contaminated water into surrounding soil or the use of polluted river water for irrigation, while the upstream cropland is used as a control.

Similarly, I use highly localized, daily wind direction data to identify cropland that is more or less exposed to air pollution from mines, which I proxy for with satellite-based measures of aerosol optical density (AOD). I define a continuous measure of downwind exposure for each of the four sides of a circular buffer around the mine's location that indicate the cardinal directions that the wind can blow from the mine. As the wind blows across the mine, "treated" sides that are downwind more frequently will experience higher exposure to pollutants such as particulate matter or sulfur dioxide from activities like drilling, blasting or smelting, while sides that are downwind less frequently act as controls.

2

I find that evidence that mining reduces local yields, with these effects driven by water pollution. Mine openings increase remotely-sensed water pollution, which coincides with a statistically significant 3-4% decline in yields for downstream cropland. However, while mine openings lead to statistically significant increases in remotely-sensed air pollution of about 2-3%, there are no accompanying reductions in yields for areas with higher downwind exposure. This finding is consistent across accounting for both contemporaneous and cumulative effects of air pollution from mines on local cropland.

Next, I benchmark the effects of mining pollution externalities on yields against an estimate of the "overall" effect of industrial mining on local agricultural output, which accounts for the effects of both pollution and raising the returns to inputs outside of agriculture. I use the staggered openings of over 300 large-scale mines in a DID that compares NDVI in areas near mines to areas slightly further away, before and after a mine opening. I find that on average, mine openings lead to a statistically significant 1-2% fall in NDVI for areas within 20 kilometers of the mine. Back-of-the-envelope calculations that take the ratio of pollution effects to the "overall" effect, accounting for the area near mines exposed to pollution, suggest that pollution externalities explain about 44% of the overall effect of mining on local agriculture.

Importantly, the estimated average treatment effects mask substantial heterogeneity, which I first illustrate descriptively by estimating mine-specific treatment effects. Then, I use two approaches to investigate drivers of heterogeneous treatment effects: (1) the "standard" approach from the economics literature involving a triple interaction with the dimension of interest and (2) a novel machine-learning (ML) method that predicts mine-specific treatment effects given a large number of mine characteristics and calculates a measure of "importance" for each of these predictors in explaining treatment effect variation. Across both approaches, I find that the quality of local governance influences the extent to which mines affect local agriculture via pollution. Mines in countries with poor governance lower local yields by two to three times more than those in areas that perform better on governance indicators. This exercise also demonstrates the value of the ML approach for settings where the researcher wishes to be cautious about "data-mining" for heterogeneous treatment effects.

My paper contributes to three growing literatures. First, it adds to the literature studying the local impacts of natural resource extraction by examining the understudied question of how the pollution from extractive industries affects local agricultural output. The discussion of whether natural resources are a blessing or a curse has focused heavily on the effects of natural resource extraction on local economic outcomes, such as re-allocation of labor [Kotsadam and Tolonen, 2016], wealth [von der Goltz and Barnwal, 2019] and income [Aragón and Rud, 2013], as well issues of corruption and governance (Caselli and Michaels [2013]; Asher and Novosad [2023]), conflict [Berman et al., 2017] and crime [Axbard et al., 2021]. In a developing country context, our understanding of the effects of natural resource extraction on outcomes

through the channel of pollution externalities is primarily limited to human health outcomes (von der Goltz and Barnwal [2019], Benshaul-Tolonen [2020]) and human capital development (Bonilla Mejía [2020]; Rau et al. [2015]). With the exception of [Aragón and Rud, 2016], to the best of my knowledge there is no other work quantifying the effects of natural resource extraction on agricultural outcomes in developing countries. My contribution is to document the magnitude of the polluting effects of mines and their resulting externalities on yields, as well as examine heterogeneity in these effects. This is valuable for informing policy on natural resource management in developing countries: in the absence of effective environmental governance local communities may be forced to make a trade off between local economic gains from extractive industries and long run environmental degradation. It is additionally policy-relevant to understand what factors may mitigate or aggravate the extent to which mining pollution affects local agricultural output.

Second, my paper contributes to the literature on "local" structural transformation and agriculture, which suggests that industrialization drives structural change primarily through sectoral reallocation within small areas rather than across large distances [Ekert et al., 2023]. By isolating the effect of pollution externalities from the effects of raising the returns to inputs in the non-agricultural sector, I am able to speak to the extent to which local reductions in yields are driven by pollution rather than structural transformation. Huang et al. [2023] and Kotsadam and Tolonen [2016] both find evidence that mining leads to structural shifts out of agriculture into more productive sectors, like low-skilled services. My finding that pollution externalities alone account for almost half of the effect of mine openings on local yields suggests that we must be wary of interpreting observed declines in agriculture as evidence purely of structural transformation, especially in the long run. While long-lasting effects of pollution externalities may persist even after a mine closes, local economic opportunities may not [Black et al., 2005].

Finally, my paper contributes to an emerging literature that uses remotely-sensed outcomes to address data gaps in developing countries. While existing literature has used NDVI to proxy for crop yields (Sukhtankar [2016]; Emerick [2018]) and AOD to proxy for air pollution (Gendron-Carrier et al. [2022]; Xie and Yuan [2023]; Zou [2021]), to the best of my knowledge I am the first to apply a satellite-based measure of water quality, the normalized difference turbidity index, in a causal inference framework. This innovation is valuable as it can allow researchers to answer questions in developing country settings where ground-measured indicators of water quality are spatially and temporally sparse, or otherwise completely unavailable.

2 Background

Mining pollution can affect crop yields through shocks to land and labor inputs. Shocks to land may arise through channels such as worsening soil quality, direct toxicity of certain pollutants to plant health and interference with plant photosynthetic processes. Labor shocks primarily arise through pollution affecting human health and resulting labor productivity, which has been documented extensively in the air pollution context (Graff Zivin and Neidell [2012]; He et al. [2019]) but sparsely in the water pollution context [Russ et al., 2022]. The following section provides background information on how mining pollution can affect yields through the plant health and soil quality channels, which is are less clear than the labor productivity channel.

2.1 Mining, Air Pollution and Crop Yields: Several small-scale environmental impact assessments and qualitative research suggest that mining can generate air pollution (Mwaanga et al. [2019]; Ghose and Majee [2002]). These studies typically focus on a handful of sites within a single country and time period, using ground-based measures of air pollution. A separate literature examines the extent to which air pollution can affect crop yields (Lobell et al. [2022]; Burney and Ramanathan [2014]; [Schiferl et al., 2018]).

The technologies employed by large-scale mining operations can contribute to air pollution through a variety of ways. First, metal smelting and refining produces gaseous emissions, such as carbon dioxide, sulfur dioxide, and nitrogen oxide, as well as particulate matter [Dudka and Adriano, 1997]. Sulfur dioxide emissions are especially common, as most economically important mineral ores occur as metallic sulfides, which are released into the atmosphere during blasting and smelting operations that expose rocks to the air and other chemicals. Furthermore, smelting and refining operations are major contributors to emissions of heavy metals, such as arsenic, cadmium, copper, lead and zinc. Since most mining operations in developing countries tend to process the raw ores on site before export, the pollution effects of these smelting and refining activities are concentrated in areas local to the mine. Second, activities such as blasting, crushing, stockpiling, loading and transportation of mine rocks also release large amounts of dust [Petavratzi et al., 2005]. This dust contributes to fine particulate matter and heavy metal levels in the atmosphere. In fact, levels of air pollution generated by mining operations can be on par with those produced by power plants or other large-scale industrial activities [Dudka and Adriano, 1997]. Finally, there are two main types of mining: underground mining and surface (also known as open pit) mining. While both types can contribute to air pollution, open pit mining is considered more damaging [Sahu et al., 2015].

Mining-induced air pollution can directly interfere with plant health and photosynthetic processes or indirectly affect crops by worsening soil quality. To begin, activities such as drilling, blasting or smelting

can release pollutants into the atmosphere that affect plant photosynthesis or other plant growth processes. Whether air pollution has a positive or negative effect on plant health depends on the type and intensity of pollution. Some pollutants, like ozone, consistently reduce yields by limiting photosynthesis [Feng and Kobayashi, 2009]. Other pollutants, like particulate matter (PM), have mixed effects due to competing absorption and scattering effects, which can depend on the intensity of pollution. While absorption by PM reduces total solar radiation reaching the surface and thus diminishes a plant's photosynthetic capabilities, scattering by PM increases the fraction of diffuse light available, which can be more effectively used by the plant [Schiferl et al., 2018]. This suggests that the effect of mining-induced air pollution on local crop health could be highly heterogeneous across mines, agro-ecological zones and climates.

Secondly, air pollution can lead to long-run deterioration of soil quality through atmospheric deposition of pollutants on the soil over time. As dust, heavy metals and other pollutants are released into the atmosphere from mining activities, they are carried by the wind and deposited on the ground. While some literature suggests that atmospheric deposition could erode soil quality over time [Liu et al., 2023], other literature finds that atmospheric deposition from polluting industries can actually serve as key nutrient inputs for modern high yield crops [Sanders and Barreca, 2022].

Lastly, I seek to disentangle contemporaneous and cumulative effects of air pollution on yields. Contemporaneous effects refer to when air pollution affects concurrent yields, that is, air pollution occurring within a given season affects yields in that same season. In contrast, cumulative effects refer to when yields are affected by prolonged exposure to air pollution. While yield effects due to deterioration of soil quality will likely occur due to cumulative exposure, yield effects due to plant health or photosynthetic interference could also occur solely from contemporaneous pollution.

2.2 Mining, Water Pollution and Crop Yields:

Mines can pollute surface water and groundwater sources through acid mine drainage (AMD), when water high in sulfates and heavy metals from mining activities is released into the soil or neighboring water bodies [Dudka and Adriano, 1997]. Water contaminated with AMD can then affect crops either by overflow or seepage from contaminated rivers onto neighboring land, movement of pollutants through groundwater or irrigation. The extent to which polluted water affects crops through each of these channels depends on multiple factors, including how widespread the use of river water for irrigation is and local hydrological characteristics that influence the dispersion of pollutants from surface water into groundwater, as well as how pollutants move through groundwater [Lapworth et al., 2017]. In some cases, AMD can reduce yields substantially. Pot experiments reveal that fields contaminated with AMD have 62% lower grain yields than non-contaminated fields [Choudhury et al., 2017].

Like air pollution, water pollution from mines can have both contemporaneous and cumulative effects on

yields. However, unlike air pollution, there is much less temporal variation in which areas are exposed to AMD. While wind direction can vary substantially within a year, blowing air pollutants in different directions around a mine, the direction of water flow is generally consistent over time.

3 Theoretical Framework

To provide a framework for interpreting the extent to which mining affects local agricultural output through pollution externalities versus market-based channels, I assume that farmer i in mining area m produces a single agricultural good with price $p = 1$ in season t, according to the following production function:

$$Y_{imt} = A_{imt} F(L_{imt}, M_{imt}, \epsilon_{imt}) \tag{1}$$

where Y is actual output, A is total factor productivity, M is land, L is labor, ϵ represents unobservable farmer and season-specific shocks to output, and F is a concave production technology. Additionally, households are endowed with labor and land, E_{im}^L and E_{im}^M respectively, which they can use as inputs to farm production or sell in local input markets at prices w, the wage rate, and r, the cost of land.

The farmer then maximizes profits within "perfect" input markets by choosing land and labor inputs accordingly:

$$\max_{L,M} \quad A_{imt} F(L_{imt}, M_{imt}, \epsilon_{imt}) - wL_{imt} - M_{imt} \tag{2}$$

As in Aragón and Rud [2016], I assume that A is a function of three factors: farmer-specific heterogeneity (η_i), time-invariant economic and environmental conditions specific to a given mining area (ρ_m), and time-varying factors correlated with the presence of local mining activity (S_{mt}). I further break down S_{mt} into environmental, E_{mt}, and non-environmental factors, N_{mt}, correlated with the presence of mining activity. Importantly, E_{mt} is directional: environmental impacts generated by local mining activity will disproportionately affect areas near mines that are more likely to be exposed to pollution, due to local geography and weather. For example, water pollution will disproportionately affect areas downstream from a mine, where pollutants from the mine will flow. In contrast, N_{mt} is generally non-directional, in that most non-environmental factors correlated with mining activity will tend to affect all neighboring areas around a mine.

Assuming that farmers are unconstrained, that is they operate in perfectly competitive input markets, the optimal choice of inputs depends only on input prices and total factor productivity. Mining can affect agricultural output through both shocks to inputs and total factor productivity. Firstly, mining can increase demand for inputs, which increases input prices w and r. Unconstrained farmers can benefit from these

shocks by selling their labor and land endowments, which would in turn reduce the amount of land and labor used in agriculture, as these inputs are allocated towards other sectors that support mining activity. Demand for labor may be driven by the introduction of low-skilled mining jobs or the development of small businesses to support large-scale mining activity (referred to as backwards linkages by Aragón and Rud [2013]). Similarly, demand for land may increase as mining companies buy or appropriate land from existing land owners.

Importantly, shocks to input demand are non-directional, that is, all areas near a mine will likely be affected by these wage or land price increases, not only the areas that are more likely to experience pollution. Indeed, existing work has shown that mining increases wealth [von der Goltz and Barnwal, 2019] and employment in the non-agricultural sector [Kotsadam and Tolonen, 2016] in areas near mines, relative to areas further away.

Secondly, mining can affect how productively inputs are used, through shocks to S_{mt}. To begin, mining can generate air and water pollution, which affects the quality of land and labor inputs (as described in Section 2). This enters the model through a negative total factor productivity shock via E_{mt}, which will disproportionately affect areas near a mine that are exposed to pollution, rather than all surrounding areas. Aside from pollution, mining can affect total factor productivity through non-environmental factors such as changing composition of agricultural workers or non-pollution externalities, which are shocks to N_{mt}. While my paper focuses on estimating the effects of shocks to inputs or shocks to total factor productivity through pollution externalities, I discuss the extent to which my research design captures these non-environmental shocks to total factor productivity in Section 11.

My paper seeks to isolate the impact of mining-induced pollution (shocks to E_{mt}) on agricultural output, from the effect of mining on agricultural output through market-based channels. To do this, I leverage the fact that pollution shocks are directional while shocks through market-based channels, such as input price shocks or shocks to non-environmental time-varying factors correlated with mining activity, are non-directional. The literature examining the effects of mining on various economic outcomes predominantly uses a DID design that compares areas near mines to areas slightly further away (Aragón and Rud [2013], Aragón and Rud [2016], Kotsadam and Tolonen [2016], Benshaul-Tolonen [2020], Dietler et al. [2021], von der Goltz and Barnwal [2019]). Importantly, the near versus far DID mixes together the effects of the pollution externalities and market-based channels, both of which would more heavily affect areas closer to mines. This suggests that using a near vs. far DID is insufficient to isolate the pollution externalities of mining on agriculture.

Aragón and Rud [2016] serves as a helpful benchmark for the effects of mining activity on agricultural productivity. The authors estimate an agricultural production function using three rounds of repeated cross-

section household data and a near versus far DID design in the context of 12 gold mines in Ghana. They use cumulative gold production as their proxy for pollution exposure, comparing the effect of increased gold production on household agricultural output in mining areas to that of non-mining areas further away. A household falls in a mining-area if it is located within 20 kilometers of a mine. All other households are considered to be living in non-mining areas. The authors find that a 100-tonne increase in cumulative gold production reduces real agricultural output by about 17% in mining areas, relative to non-mining areas. Of the 12 mines in their sample, 9 were already operating during the first wave of the survey. As a result, their empirical strategy estimates primarily an intensive margin effect of increased mining production on agricultural output.

By controlling for household labor and land use as covariates in their model, Aragón and Rud [2016] are able to remove the influence of market-based input demand shocks when trying to isolate the effect of mining-pollution on agricultural productivity. However, remaining market-based channels that operate by shocking total factor productivity and are correlated with proximity to a mine, such as local demand shocks that change the composition of workers in agriculture, remain a potential endogeneity issue when trying to isolate the pollution effect. This highlights the importance of more carefully defined treatment and control areas.

Furthermore, while the focus on a single commodity and single country over a short time period allows Aragón and Rud [2016] to leverage context-specific information to close down several market-based channels, it limits the ability to study heterogeneous effects of mines on agricultural output. It is policy-relevant to understand whether their finding that mining leads to meaningful reductions in agricultural output is consistent across other countries, commodities, regulatory environments, technologies and time.

4 Data

To investigate the effect of industrial mining on agricultural output in mining communities, I construct a panel of mining areas from 2000-2022. I link mine opening dates and spatial buffers around mine geo-locations, provided by S&P Global Market Intelligence, to remotely sensed measures of pollution, crop yields and weather variables. The unit of observation in my analysis is a mine-side-month, where a "side" refers to part of a buffer around a mine. In this section, I briefly explain the construction of the main variables used in my analysis, with an in-depth discussion detailed in Appendix 12.2.

4.1 Mines S&P Global Market Intelligence provides the geo-locations of the centroids of mining operations for large-scale mines across the world. Appendix Figure 10 shows the geo-locations of the S&P

mines used in my analysis. These centroids are used to construct three different types of spatial buffers, which define treatment and control areas for my analysis. First, to estimate an "overall" effect of mining activity on yields, I define circular buffers around each mine to distinguish between areas near mines and areas slightly further away. Intuitively, areas near mines are more likely to experience both the effects of local labor market shocks and pollution exposure from mining activity, relative to areas further away. I refer to the buffer of radius 20-kilometers around a mine as the "near" group, which I assume is the "treated" area that would be impacted by both market-based and pollution channels. I discuss the specific reasons for choosing the 20-km cutoff in more detail in Section 7.

Second, I buffer river segments near mines to estimate effects of mining-induced water pollution on yields. I use the HydroRIVERS dataset to identify rivers located in Africa. Each mine within 1 km of a river in this network is "snapped" to the closest river segment, then the upstream and downstream river segments from the mine river segment are identified. The upstream and downstream segments are buffered by 1-kilometer on either side of the line to identify land area around the rivers that would be affected by water pollution through seepage, irrigation or labor productivity channels. The choice of a 1-km buffer is based on contaminant transport modelling from mining areas, which shows that sulfates were detected in groundwater up to 2.5 km away from the polluting source, with up to 1.5 km of horizontal dispersion [Myers, 2016]. The "side" of a mine in the water pollution analysis refers to the upstream or downstream buffer.

Lastly, to estimate effects of mining-induced air pollution on yields I use slices of circular buffers around each mine that indicate wind direction from the mine. I start by defining a buffer of radius 60-kilometers around each mine. This radius is chosen based on a spatial decay model shown in Appendix Figure 11, which demonstrates that on average, air pollution increases (as proxied by AOD) from mining are concentrated within 60-km of the mine centroid and statistically indistinguishable from zero beyond this cut-off. Next, for each mine the 60-km buffer is divided into 4 90-degree slices representing the cardinal directions that the wind can blow from the mine centroid. Hence, a "side" of a mine in the air pollution analysis refers to one of these 4 slices of the 60-km buffer around the mine. Note that the circle of radius 5-km around the mine is removed from the 60-km circle, leaving behind a "donut," to limit the influence highly local air pollution effects that would affect all sides of the mine regardless of wind direction.

Figure 1 illustrates the three different types of treatment and control areas constructed for the three types of analysis. The left panel illustrates the near versus far buffers used to estimate an "overall" effect of mining on local yields, where areas within the 20-km buffer are considered "treated." The top right panel shows the upstream and downstream buffers used to estimate the water pollution effect, while the bottom right panel displays the wind direction buffers used to estimate the air pollution effect.

Additionally, the S&P data provides information on the year that commercial production at the mine
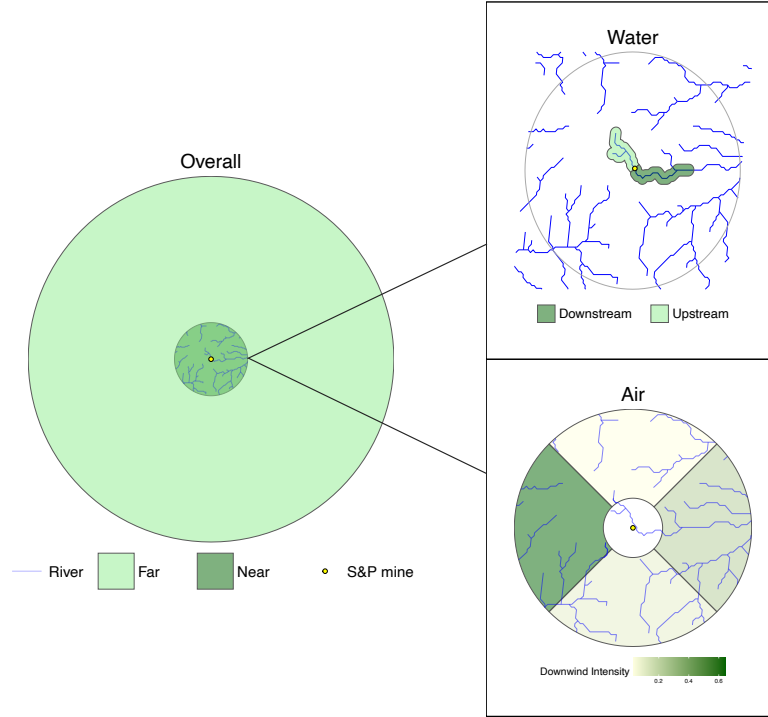
Figure 1: Treatment and Control Buffers

The figure plots the three different types of treatment and control areas used in the analysis. In each sub-figure, the yellow circle indicates the centroid of the mining area. The left panel illustrates the near versus var buffers used to estimate the "overall" effect of mining on local yields. The dark green inner circle has a radius of 20-km and is used to define the "near" group, which is affected by both market-channels and pollution externalities (treated), while the light green outer circle acts as a control. The two sub-figures in the right panel zoom into the near group, showing the treatment and control areas for the water and air pollution analyses. The top right panel shows the downstream (treated) and upstream (control) buffers for the river segments around the S&P mine, while the bottom right panel shows the intensity of downwind exposure (treatment) experienced by each of the four cardinal directions around the mine, defined by 90-degree slices of a circle.

first began, the specific minerals extracted and the extraction method. In line with S&P, I define the start of mining activity, also referred to as the opening of a mine, as the year that "the mine/plant has been commissioned or has produced its first metal, concentrates, or bulk commodity at a commercial rate." Other papers have defined mining activity based on years where a mine had non-zero output (von der Goltz and Barnwal [2019], Benshaul-Tolonen [2020]). Although the S&P data provides yearly production data for some mines, this information is missing or incomplete for many mines in Africa, meaning activity would need to be imputed. As the S&P data on the start year of commercial production is more complete, I opt to define mining activity based on this year instead.

Given that the S&P mining data covers mostly large-scale mines operated by multinationals or national governments, this might suggest that my analysis is not able to speak to the effects of artisanal and small-scale mines (ASM) or those that are illegally operated. As much of ASM and illegal mining operates on the fringes of large-scale mining operations, the mine buffers should encompass areas that are affected by ASM and illegal mining. However, if small-scale mining activities were already contributing to pollution prior to large-scale operations, treatment effects may be underestimated. Since ASM and illegal mining generally uses low capital intensive and high labor intensive technologies, rather than large blasting, drilling and smelting machinery, I do not expect an attenuation of treatment effects in the air pollution analysis. However, underestimation of treatment effects is a potential concern with the water pollution analysis, as ASM or illegal mining often releases heavy metals into the soil and water bodies through the improper and unregulated use of chemicals during the extraction process. For example, artisanal gold mining is associated with mercury pollution as the mercury used in the traditional amalgamation process to separate gold from the ore can leach into the surrounding soil and water [Soe et al., 2022].

4.2 Wind: Wind data for the air pollution analysis is retrieved from the Modern-Era Retrospective analysis for Research and Applications, Version 2 (MERRA2). MERRA2 is a re-analysis product, meaning it combines satellite imagery with algorithms and atmospheric models to create the final data product. I use the daily aggregates of hourly time-averaged U and V wind vector components for heights of 2 meters and 50 meters, at a 0.5 degree $\times$ 0.625 degree resolution.

To measure downwind exposure for each side of a mine, I first determine the direction (in degrees from due North) that the wind is blowing from the mine centroid, on each day from 2000-2022.[1] I then classify this direction into one of the four 90-degree sides defined by the cardinal directions (North, East, South, West). Finally, for each mine-month, I count the number of days that the wind blows from the mine into each of the four sides, as well as determine the average monthly wind speed experienced by each side. Downwind

---

[1] $Direction = 90 - atan2(v, u) \times 180/\pi$

exposure experienced by a given side is defined as the share of days in a month that the side is downwind from the mine.

4.3   Satellite-based air pollution:

Daily measures of aerosol optical density (AOD) are obtained from the Moderate Resolution Imaging Spectroradiometers (MODIS) satellites at a 3-kilometer spatial resolution. In brief, AOD is calculated by comparing the light intensity in a particular band against a reference value and attributing the difference to particulates in the air column. The higher the level of AOD, the higher the level of air pollution as more light is being reflected back due to particulates in the atmosphere. Several studies have shown that AOD is highly predictive of ground-based measures of PM10 and PM2.5. In their preferred specification, Gendron-Carrier et al. [2022] find that one unit of remotely sensed AOD is associated with about 114 $\mu g/m^3$ of PM10 measured by a ground-based instrument.

I rely on global daily rasters of MODIS AOD generated by Gendron-Carrier et al. [2022]. The authors provide daily tifs from July 4, 2002 until August 31, 2018, for the Aqua satellite and February 24, 2000 until July 31, 2020 for the Terra satellite. Given MODIS data availability, the panel used in the air pollution analysis covers 2003 - 2017. From the daily AOD rasters, I construct mean AOD for each mine-side-month by averaging all pixel-days with non-missing AOD readings that fall within each side of a mine in a given month. I calculate this average monthly AOD only using data from the Aqua satellite, as the Terra satellite suffers from more missing values due to satellite detection errors during my time period of interest. More details on AOD data construction are covered in Appendix 12.2.

4.4   Satellite-based water pollution

While satellite-based measures of air pollution have been used extensively to answer causal inference questions related to air pollution ([Gendron-Carrier et al., 2022], Gutiérrez and Teshima [2018]; Chen et al. [2022]), to the best of my knowledge, no paper is yet to conduct causal inference using similar satellite-based measures of water pollution in developing countries.

Satellite-based proxies for pollution have an key advantage in that they allow researchers to answer questions in contexts where ground-based pollution data is unavailable or limited. Importantly, spatial and temporal gaps in ground-based water pollution data can be even larger than those for air pollution in developing countries Virro et al. [2021]. While low cost air quality sensors have been deployed in many African countries, the development and implementation of low cost water quality sensors is in its infancy. These limitations in ground-based water quality monitoring highlight the value of remotely-sensed measures of water pollution, which offer an affordable way to track quality of African water bodies over time.

While the remote sensing literature has developed several promising satellite-based indicators of water quality, these measures are yet to make their way into the social sciences literature. To the best of my

knowledge, I am the first to apply a satellite-based measure of water quality from the remote sensing literature, the normalized difference turbidity index (NDTI), in the context of causal inference. NDTI uses the spectral reflectance of water pixels to estimate turbidity, which is a measure of water clarity. Similar to AOD, turbidity measures the amount of light scattered by particles in the water column. The higher the level of particles in the water, the more light that will be scattered. High turbidity makes water appear cloudy, muddy or discolored. Turbidity is often used to proxy for total suspended solids (TSS), which are a common indicator of water quality. TSS are particles found in the water column that are larger than 2 microns. Increases in TSS can be driven by natural phenomena, such as stirred bottom sediments from heavy precipitation or algal blooms, as well as industrial runoff or wastewater discharge. When TSS levels cannot be measured, changes in turbidity can be used to reflect changes in TSS concentration in water (CITE).

To measure turbidity, NDTI leverages how electromagnetic reflectance is higher in green spectrum than the red spectrum for clear water (Lacaux et al. [2007]; Gardelle et al. [2010]). Increased reflectance of the red spectrum relative to green corresponds to an increase in turbidity [Islam and Sado, 2006]. NDTI is calculated with the red and green spectral bands according to the following formula:

$$NDTI = \frac{\text{Red} - \text{Green}}{\text{Red} + \text{Green}}$$

Generally, NDTI ranges from -0.2 to greater than +0.25, where lower (negative) values indicate clear water and higher (positive) values indicate turbid water [Sharma et al., 2015].

To obtain a remotely-sensed measure of river water pollution, I first identify the precise shape of the upstream and downstream river segments near mines using a water mask based on the normalized difference water index (NDWI). This index is commonly used to detect water bodies in satellite images and is calculated from the green and near-infrared (NIR) bands.[2] I generate the NDWI water mask from a mosaic of cloud-free Sentinel-2 pixels from 2020-2023 at a 15-m resolution, to limit the influence of atmospheric interference on water detection. The NDWI water mask is fixed over time, meaning any estimated effect of mining activity on turbidity does not reflect changes in the extent of water bodies over time.

Next, I calculate monthly NDTI for each identified river pixel from 2000-2022, masking out low quality or cloudy pixels, using Landsat 7 data at a 30-m resolution. Finally, I average monthly NDTI across water pixels within the upstream or downstream river segments, for each mine, to create mine-month-side level measures of river NDTI.

With NDTI, I am able to overcome the poor spatial and temporal resolution of ground-based water

---

[2]
$$NDWI = \frac{\text{Green} - \text{NIR}}{\text{Green} + \text{NIR}}$$

pollution monitoring in Sub-Saharan Africa. Global freshwater quality databases, such as the Global River Quality Archive (GRWQ), which harmonizes five water quality datasets to provide the most comprehensive river water quality data from ground-based sampling sites, have extremely sparse coverage of Sub-Saharan Africa. This makes it challenging to use these datasets to investigate the effects of highly localized polluting activities on water quality over time. In Appendix Table 6, I show that NDTI is highly predictive of ground-measured TSS from the GRWQ database. In my preferred specification, a one unit increase in NDTI is associated with a 887 mg/l increase in ground-measured TSS.

Importantly, while NDTI is successful at detecting changes in the overall levels of particles in water, it cannot distinguish between types of particles. While some particles may be pollutants from mine waste effluent, such as heavy metals or acidic sulfides, others may be sediment from rock or soil disturbed during the extraction process. While heavy metals and sulfides have been shown to substantially reduce crop yields [Choudhury et al., 2017], the effect of excessive sediment in water on local yields is less clear, though some literature suggests potential negative effects. For instance, Gurmu et al. [2022] find that excess sediment in the water can disrupt formal irrigation systems. However, many smallholder farmers either do not use irrigation or use an informal system (e.g. fetching water from river themselves), suggesting that this channel is unlikely to impact local yields around a river. Alternatively, in extreme cases excess sediment in water may lead to harmful algal blooms, which can interfere with the development of plant structures during irrigation or seepage into neighboring lands [Newton and Melaram, 2023]. Since NDTI cannot distinguish between polluting particles and sediment, it is important to interpret observed changes in NDTI due to mining as changes in both harmful pollutants and potentially non-harmful sediment.

4.5 Satellite-based yields: Ideally, I would use data on farm-level yields at a high spatial and temporal resolution around mines. While some high quality plot-level agricultural survey data is available, such as the World Bank Living Standards Measurement Survey - Integrated Surveys on Agriculture (LSMS-ISA), these sources are not suited to my research design for several reasons. To start off, these surveys are limited to a handful countries and do not cover many households near mines, let alone within the precisely defined pollution buffers. Furthermore, surveys are collected infrequently, making it difficult to tie observed effects on yields to the start of mining activity or examine cumulative effects of pollution over time.

To overcome survey data limitations, I proxy for crop yields using the normalized difference vegetation index (NDVI). NDVI is strongly correlated with crop productivity and final yields, especially during the growing season [Panek and Gozdowski, 2021]. I construct a measure of pixel-level daily mean NDVI from 2000 - 2022 using the MODIS MCD43A4 Version 6.1, combined Terra and Aqua product at a 500-m resolution. NDVI is calculated from the MODIS data using readings of light reflected in the near-infrared and red

spectrum.[3]

When aggregating NDVI from the pixel-day to the mine-side-month level, I first mask out pixels that are not classified as cropland according to the Global Food Security Support Analysis Data (GFSAD). This helps ensure that changes in NDVI reflect changes in crop yields rather than changes in forest cover, for instance due to deforestation that might occur during construction of the mine site. The coarse 1-km resolution of the cropland extent data may constrain the ability to detect cropland of very small farms. Consequently, estimates obtained by causal inference may be more informative of the effects of mining on local yields for larger farms captured in the crop mask, rather than smaller farms that are left out. However, given that larger farms are likely more able to adapt to labor market or pollution shocks than smaller farms (CITE), so may mitigate the impact of mining on local yields, one can interpret estimated treatment effects in my setting as a lower bound for the effect of mine openings on local yields for smallholder farmers.

In addition to measurement error introduced by the cropland mask, NDVI may suffer also suffer from errors due to factors like cloud cover, surface reflectance, canopy thickness, the level of atmospheric aerosols and satellite sensor errors. I discuss how measurement error in NDVI might affect estimates from causal inference in Appendix 12.13. However, despite these potential sources of measurement error, Table 5 shows that NDVI is still highly predictive of plot-level yields in Sub-Saharan Africa, though the magnitude of the correlation may be attenuated. I construct my final measures of cropland NDVI for the treatment and control areas by averaging NDVI across all cropland pixel-days within each mine-side-month, within the relevant buffers.

An emerging literature uses machine learning algorithms to predict crop yields based on vegetation indices, like NDVI, and other covariates (Burke and Lobell [2017], Jin et al. [2017]). Unfortunately, most of the mining areas in my analysis are not located near sites where ground truth measures of yields, like cropcuts, are available. Furthermore, high quality ground truth data are not available prior to 2015. Given that machine learning models predict more poorly on observations that are spatially distant from training data samples Proctor et al. [2023] or outside of the time period covered by the training data [Barriga-Cabanillas et al., 2024], I am concerned that using predicted yields as my main outcome of interest would introduce additional measurement error into the estimation of the effect of mining on yields. As a result, I opt to use NDVI as my main measure of agricultural output rather than predicted yields. This allows me to remove prediction error as a source of measurement error, and instead focus solely on understanding how measurement error in the NDVI data itself could be affecting estimated coefficients. Additional discussion of measurement error in NDVI are covered in Appendix 12.13.

---

[3]NDVI $= \frac{NIR-RED}{NIR+RED}$

4.6 Weather Controls: Local weather conditions influence actual yields, as well as the ability for satellites to accurately detect these yields (Gendron-Carrier et al. [2022]; Heino et al. [2023]). I calculate mine-side-month averages of cloud cover percentage, temperature, precipitation, evapotranspiration, vapor pressure and wet day frequency using the Climatic Research Unit gridded dataset, available at a 0.5 degree resolution from Harris et al. [2014]. These monthly averages of key weather variables are the main control variables in my regressions.

4.7 Agricultural Seasons: For each mine, I aggregate daily measures of AOD and NDVI to the monthly level. Aggregating to a less granular temporal resolution allows me to smooth over missing days of data that occur due to cloud cover or other satellite errors. Each mine-month is then linked to one of the following agricultural seasons: planting, early growing, late growing, harvest and non-farm, to investigate whether observed yield effects differ across seasons. I use the Sacks et al. [2010] global raster dataset on planting and harvesting dates for maize to define area-specific agricultural seasons. This data is available at a 5 arc-minute (approximately 10 km × 10 km) spatial resolution. I focus on maize as it is one of the primary crops grown in Africa and has the most complete crop calendar data. Other important crops like cassava or wheat have missing data across most of Africa and Sacks et al. [2010] caution against using interpolated products. Using seasons defined by maize only could potentially introduce measurement error into regressions where season indicators are used as covariates or to stratify the sample. I discuss this issue in more detail in Appendix 12.13.

5 Mining-induced Water Pollution

To estimate the effect of mining-induced water pollution on yields, I use a difference-in-difference (DID) that compares NDVI between the upstream and downstream sides of a mine, before and after a mine opening:

$$NDVI_{smt} = \alpha_{sm} + \lambda_{mt} + \delta Downstream_{sm} + \eta Post_{mt} + \beta_W Downstream_{sm} \times Post_{mt} + \mathbf{X'_{smt}\Gamma} + \epsilon_{smt} \quad (3)$$

where $NDVI_{smt}$ is mean NDVI on side s of mine m in month t. $Downstream_{sm}$ is a dummy variable equal to 1 if side s is downstream from mine m and equal to 0 if it is upstream. $Post_{mt}$ is a dummy variable equal to 1 after mine m opened, 0 otherwise.

I include mine-side fixed effects (α) to control for time invariant unobservables correlated with agricultural output on each side of a mine, such as soil quality, as well as mine-date fixed effects (λ) to control for

mine-specific trends in NDVI over time. Given the mine-side and mine-date fixed effects, β_W is identified by within-month differences in the change in NDVI among areas upstream and downstream from mine openings. Essentially, β_W is a weighted average of mine-specific DIDs generated from almost 40 mine openings used in this analysis. To address the influence of weather shocks to yields that vary across sides and time, I control for linear and quadratic terms of mean cloud cover, vapor pressure, temperature, precipitation, evapotranspiration and wet days.

Estimating the causal effect of mining-induced water pollution on yields requires that the timing and placement of a mine opening is plausibly exogenous to local changes in NDVI. While the placement of mineral deposits is random, the discovery of these deposits may depend on a variety of non-random factors, including local governance quality, business environments, infrastructure access and input prices [Benshaul-Tolonen, 2020]. This issue should not pose a threat to identification in the upstream versus downstream DID, as both sides of the river will be similarly affected by these factors within the narrowly defined buffers.

I estimate Equation 3 over a partially balanced panel of 38 mines within 1 km of a river, where non-missing NDVI is observed on both the upstream and downstream sides of the mine, for at least 6 months of every year, for at least 2 years pre- and 2 years post-mine opening. Additionally, I estimate an event study version that replaces the single *Post* dummy with a series of event time dummies indicating the number of years since a mine opened. As NDVI during the growing season is more strongly correlated with actual crop yields than NDVI during the non-growing season, I also estimate the DID and event study models separately over months in the growing season and non-growing seasons. Standard errors are clustered at the mine-level.

To establish the first-stage effect of mining activity on water pollution, I estimate Equation 3 with normalized difference turbidity index (NDTI) as the outcome of interest. Monthly NDTI measures are missing more frequently, since NDTI is calculated over narrowly defined river pixels and so are more affected by cloud cover or other atmospheric interference. As a result, I estimate the event study and DID regressions for turbidity over a subset of the mines used in the NDVI analysis.

Figure 2 shows that on average after a mine opens, downstream river turbidity increases significantly. Larger increases in turbidity during the growing seasons could be explained by increased precipitation causing more runoff from mining areas into rivers. Figure 3 reveals a complementary pattern of reductions in NDVI for downstream cropland after a mine opening, with stronger negative effects during the growing seasons.
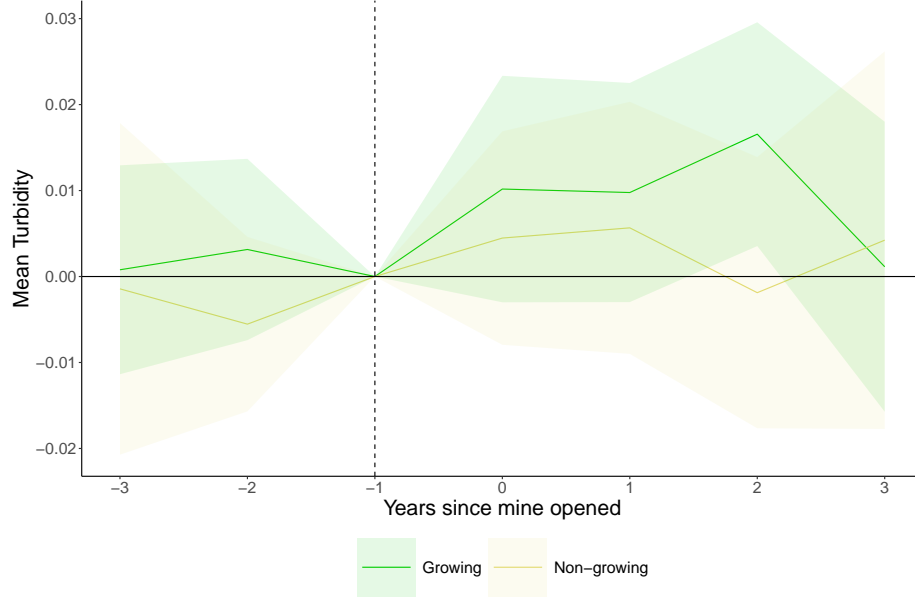
Figure 2: Average effect of mining-induced water pollution on NDTI - event study

The figure plots coefficient estimates from two separate event study regressions of mean normalized difference turbidity index on a dummy for whether a side is downstream from a mine interacted with a series of event time dummies for years since a mine first opened. The unit of analysis is a mine-side-month, though event time coefficients are binned into yearly increments. The event study regressions are estimated separately over growing season months (early growing and late growing) and non-growing season months (planting, harvest and non-farm). The dotted lines show point-wise 95 percent confidence intervals for the coefficients of the event-time path of mean NDTI. Coefficients can be interpreted as estimated effects relative to the period one year before the mine opened. Both regressions includes linear and quadratic controls for mean temperature, precipitation, vapor pressure, wet days, evapotranspiration and cloud cover, as well as mine-side and mine-year-month fixed effects. The sample includes the 30 mines for which non-missing NDTI is observed on the upstream and downstream sides for at least 2 months in each year, for at least 2 years pre- and 2 years post-mine opening. Event times less than -2 or greater than 2 are binned into two end points.
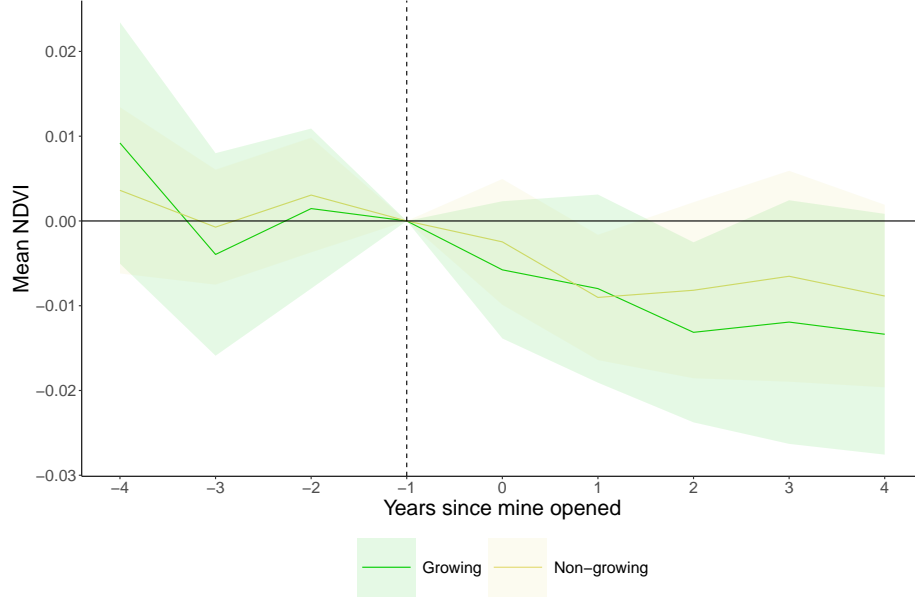
Figure 3: Average effect of mining-induced water pollution on NDVI - event study

The figure plots coefficient estimates from two separate event study regressions of mean NDVI on a dummy for whether a side is downstream from a mine interacted with a series of event time dummies for years since a mine first opened. The unit of analysis is a mine-side-month, though event time coefficients are binned into yearly increments. The event study regressions are estimated separately over growing season months (early growing and late growing) and non-growing season months (planting, harvest and non-farm). The dotted lines show pointwise 95 percent confidence intervals for the coefficients of the event-time path of mean NDVI. Coefficients can be interpreted as estimated effects relative to the period one year before the mine opened. Both regressions includes linear and quadratic controls for mean temperature, precipitation, vapor pressure, wet days, evapotranspiration and cloud cover, as well as mine-side and mine-year-month fixed effects. The sample includes the 38 mines for which non-missing NDVI is observed on the upstream and downstream sides for at least 6 months in each year, for at least 3 years pre- and 3 years post-mine opening. Event times less than -3 or greater than 3 are binned into two end points.

To better quantify the impact of industrial mining, I use the DID regression model outlined in Equation 3. As NDTI is imperfectly correlated with polluting particles in water that may affect yields, I opt to estimate the first-stage and reduced form results separately, rather than as a two-stage least squares model with the downwind and post interaction instrumenting for NDTI. Table 1 presents the main results for remotely sensed turbidity and yields, estimated on all months pooled together, as well as separately by growing and non-growing seasons.

Panel A consistently shows that mining increases remotely sensed water turbidity, though these estimates are statistically insignificant, likely due to lack of power. The increase in turbidity is on the magnitude of 12-50% relative to NDTI in the pre-period. Rather than give substantial weight to the magnitude of these effects, I cautiously interpret the reduced form results as evidence of an extensive margin effect of mining on water pollution. Furthermore, the observed increase in NDTI is capturing both increased sediment and increased pollution, meaning that only a fraction of the large effect size is likely attributable to increased water pollution. Using Column 2 of Appendix Table 6 to convert NDTI to total suspended solids suggests that on average, mine openings increase total suspended solids in downstream water by 4.33 - 4.83 mg/l.

Similarly, the reduced form results in Panel B show consistent and statistically significant reductions in remotely sensed yields in downstream areas relative to upstream areas, after a mine opens. These estimates correspond to a 3-4% drop in NDVI, with larger effects observed during months in the growing season. The observed reductions of NDVI in downstream cropland suggest that at least part of the observed increase in remotely-sensed turbidity can be attributed to increased pollution, given that increases in sediment in water are unlikely to affect local yields.

To understand the extent to which water pollution may be affecting local crop yields through irrigation, I estimate Equation 3 using only NDVI over irrigated cropland as the outcome of interest. The GFSAD cropland extent data identifies rainfed versus irrigated cropland pixels, allowing me to to identify cropland near rivers that may be negatively affected by the use of polluted water during irrigation. Appendix Table 7 shows that estimated reductions in NDVI due to mining are about 25% larger for irrigated downstream cropland compared to non-irrigated areas, suggesting that irrigation with polluted water is indeed an important channel through which mining-induced water pollution may affect local yields.

However, irrigation use in smallholder African farming is low: Sheahan and Barrett [2017] find that less than 5% of households in the LSMS use some form of irrigation. This suggests that irrigation alone cannot be the main driver of observed reductions in downstream yields. Existing work from the hydrological sciences suggests that it is reasonable to posit that pollutants from surface water can move through groundwater and affect cropland within 1-km of the polluted river. Myers [2016] finds that sulfates from mining operations can be detected up to 2.5 kilometers away from a polluting source, while Xiang et al. [2019] demonstrate that

Table 1: Relationship Between Industrial Mine Openings, Remotely-Sensed Water Turbidity and Crop Yields

	(1)	(2)	(3)
	All seasons	Growing	Non-growing
Panel A: First Stage for Turbidity			
Downstream × Post	0.00488	0.00426	0.00544
	(0.00649)	(0.00761)	(0.00636)
Mines	30	30	30
Observations	11,330	5,304	6,026
Mean NDTI (t-1)	.01	-.01	.04
Panel B: Reduced Form for Yields			
Downstream × Post	−0.01404**	−0.01770**	−0.01093**
	(0.00587)	(0.00714)	(0.00531)
Mines	38	38	38
Observations	20,518	9,888	10,630
Mean NDVI (t-1)	.47	.54	.39
Mine-side FE	Yes	Yes	Yes
Mine-year-month FE	Yes	Yes	Yes
Weather	Yes	Yes	Yes

Notes: Each column reports the results of a linear regression. The unit of analysis is a mine-side-month. In Panel A, the dependent variable is the mean normalized difference turbidity index (NDTI) of the river water on the upstream or downstream side of a mine, in a given month. I derive remotely sensed turbidity from Landsat 7. In Panel B, the dependent variable is the mean normalized difference vegetation index (NDVI) of the land within the 1km buffer along the river on either the upstream or downstream side of a mine, in a given month. I derive remotely sensed yields from the MODIS Combined Terra and Aqua product (MCD43A4.061). *Downstream* is equal to 1 if the side is downstream from the mine and 0 if it is upstream from the mine. *Post* is equal to 1 after the mine opened, 0 otherwise. All models include linear and quadratic controls for mean temperature, precipitation, vapor pressure, wet days, evapotranspiration and cloud cover, as well as mine-side and mine-year-month fixed effects. For turbidity, the sample includes the 30 mines for which non-missing NDTI is observed on the upstream and downstream sides for at least 2 months in each year, for at least 2 years pre and 2 years post-mine opening. For yields, the sample includes the 38 mines for which non-missing NDVI is observed on the upstream and downstream sides for at least 6 months in each year, for at least 2 years pre- and 2 years post-mine opening. Column 1 reports results estimated by pooling months over all 5 seasons: planting, early growing, late growing, harvest and non-farm. Column 2 reports results estimated only over months in the early growing and late growing seasons and Column 3 reports results estimated only over months in non-growing seasons: planting, harvest and non-farm. Standard errors in parentheses are clustered by mine.

pollutants can disperse from a point source to areas 100m to 15km away. Unfortunately, a careful analysis of the extent to which movements of pollutants through groundwater may deteriorate soil quality requires detailed information on soil type, hydraulic gradients and pollution concentrations, so is beyond the scope of this paper.

6 Mining-induced Air Pollution

To identify areas near mines that are disproportionately exposed to air pollution, I rely on the assumption that wind blows pollutants from the mine towards the downwind side of the mine. I apply high-frequency data on wind direction and the staggered openings of over 100 large-scale mines in two methods that estimate the effect of mining-induced air pollution on local yields: (1) a DID and event study that primarily capture the effects of contemporaneous exposure to air pollution and (2) a distributed lag model that allows for cumulative effects of prolonged exposure to air pollution.

6.1 Contemporaneous effect: The model capturing contemporaneous effects of mining-induced air pollution on local yields is specified as follows:

$$NDVI_{smt} = \alpha_{sm} + \lambda_{mt} + \delta Wind_{smt} + \eta Post_{mt} + \beta_A Wind_{smt} \times Post_{mt} + \mathbf{X'_{smt}\Gamma} + \epsilon_{smt} \qquad (4)$$

where $NDVI_{smt}$ is mean NDVI on side s of the 60-km buffer around mine m on date t. $Wind_{smt}$ is the share of days in month t that side s is downwind from mine m, while $Post_{mt}$ is a dummy variable equal to 1 after mine m opened. As in the water pollution specification, I include weather controls, as well as mine-side and mine-year-month fixed effects. Standard errors are clustered at the mine-level. Additionally, I estimate an event study version of Equation 4, which replaces the single $Post_{mt}$ dummy with a series of dummy variables for years since the opening of mine m.

As wind direction is exogenous to local conditions, factors that may be correlated with the timing and placement of mine openings, as well as yields, are likely constant across all four directional sides of the buffer around a mine. Essentially, β_A is estimated by comparing sides of a mine that receive more wind to sides of a mine that receive less wind, before and after a mine opening, across over 100 mines. In other words, β_A is identified from within-month variation in exposure to wind from the mine, across four directional sides.

To establish that mining activity does indeed increase air pollution, I use an almost identical model to the one outlined in Equation 4, with mean AOD as the outcome of interest. Unlike the NDVI data, the AOD data is available only for 2003-2017 and has more missing values due to errors in AOD detection from cloud

cover. To ensure a consistent sample of mines between the NDVI and AOD regressions, I use a partially balanced panel of 102 mines, where each mine must be observed on all sides for at least 4 months of every year, for at least 5 years pre- and 5 years post-mine opening. To address measurement error in AOD, I additionally control for the number of non-missing pixel days used to construct mean monthly AOD.

6.2 Cumulative effect:

Importantly, the DID and event study designs outlined above are limited in that they primarily estimate the effect of contemporaneous air pollution exposure on yields. This is because the mine-side and mine-date fixed effects ensure a comparison of sides of the same mine, within the same time period, which does not account for pollution exposure in prior time periods. Due to seasonality in winds, the side of a mine that is most frequently downwind varies within the year. This means that the downwind exposure of a given side in one month may not necessarily be similar to that side's exposure in prior months.

To overcome this limitation, I use a distributed lag model that allows me to estimate the effect of cumulative air pollution exposure from mines on yields:

$$NDVI_{smt} = \alpha_{sm} + \lambda_{mt} + \sum_{p=0}^{P} \beta_p Wind_{sm,t-p} + \sum_{p=0}^{P} \delta_p Wind_{sm,t-p} \times Post_{m,t-p} + \mathbf{X'_{smt}}\mathbf{\Gamma} + \epsilon_{imt} \quad (5)$$

$NDVI_{smt}$ is mean NDVI on side s of mine m at time t, while $Wind_{sm,t-p}$ is downwind exposure on side s of mine m, p months before t. Downwind exposure is defined as the number of days a side is downwind from the mine, normalized so that one unit corresponds to 30 days of downwind exposure. $Post_{m,t-p}$ is an indicator for when production first began at mine m, lagged by p months. By interacting lagged wind exposure with a lagged indicator for mining activity, I ensure that only wind exposure in the months after a mine opening is included in the cumulative effect estimated for the post period. I include a vector of contemporaneous mine-side-month controls for weather and wind speed, as well as mine-side fixed effects and mine-date fixed effects. Standard errors are clustered at the mine-level.

Before a mine opening, the cumulative effect of exposure to air pollution during the current month and the P months prior is $\sum_{p=0}^{P} \beta_p$. The cumulative effect of pollution exposure after a mine opening is $\sum_{p=0}^{P} \beta_p + \delta_p$. Thus, we can interpret $\sum_{p=0}^{P} \delta_p$ as the difference in the cumulative effect of exposure to air pollution during the current and P prior months, between the pre- and post-mine opening periods. Standard errors, p-values and confidence intervals for each lag structure are obtained by testing whether $\sum_{p=0}^{P} \delta_p = 0$, for each P. In my main specification, I include lagged months up to 2 years prior (24 months) so estimate 25 total coefficients (1 contemporaneous and 24 lagged).

To estimate the distributed lag model, I define a different sample of mines from the set used in the AOD and contemporaneous yield effect estimation shown in Table 2. First, I expand the set of mines to include those where AOD data may be missing or incomplete for certain months, as estimating the coefficients on the main effects and interaction terms for each of the lagged variables in Equation 5 is computationally demanding. Second, I restrict to only the set of mines where NDVI is observed on all four sides, for all 12 months of every year, for at least 5 years pre- and 5 years post-mine opening. This ensures that NDVI for each mine-side-month is observed for all lags included in the main specification, so that the composition of mines does not vary with the lag structure.

6.3   Results: The AOD event study in Figure 4 reveals that on average, sides of a mine that are downwind more frequently experience higher levels of AOD after a mine opening. This increase in AOD begins about 3 years before the mine officially starts commercial production and remains relatively constant over time. Prior to this 3-year period before a mine opens, we see evidence of parallel trends between areas with high downwind exposure and areas with low downwind exposure.

Why would air pollution occur before a mine officially starts producing? To answer this question, it is helpful to reconceptualize mining activity as a gradual ramp up over time rather than a binary "on/off." Detailed work histories of the mines in the S&P database provide evidence in support of this gradual increase in activity. S&P roughly classifies mining activity into the following phases: discovery, exploration/feasibility study, construction/pre-production, production and closure. The discovery phase describes the time at which mineral potential was first determined in a mining area. Exploration and feasibility studies encompass activities such as drilling and testing, which are used to estimate the quality and quantity of reserves. Construction and pre-production include activities related to the building of infrastructure needed for large-scale mineral extraction (e.g. roads, electricity grid, buildings). Production refers to industrial-level extraction and processing of raw materials. Closure refers to the permanent shut-down of a mine and the associated reclamation activities that are supposed to return the land to its previous state.

Literature estimating emissions rates from different activities at a mine site suggests that air pollutants are most likely to be released during the exploration, construction/pre-production and production phases [Patra et al., 2016]. In particular, the use of heavy machinery or vehicles during exploration, as well as the clearing of overburden or construction may contribute to local air pollution levels before the official start of production. As a result, it is not unreasonable to observe increased air pollution in downwind areas prior to the official start of mine production.

To better understand the polluting effects of the different phases of a mine's life cycle, I use satellite data to estimate a structural break in the mean of remotely sensed nighttime light intensity for each mine that
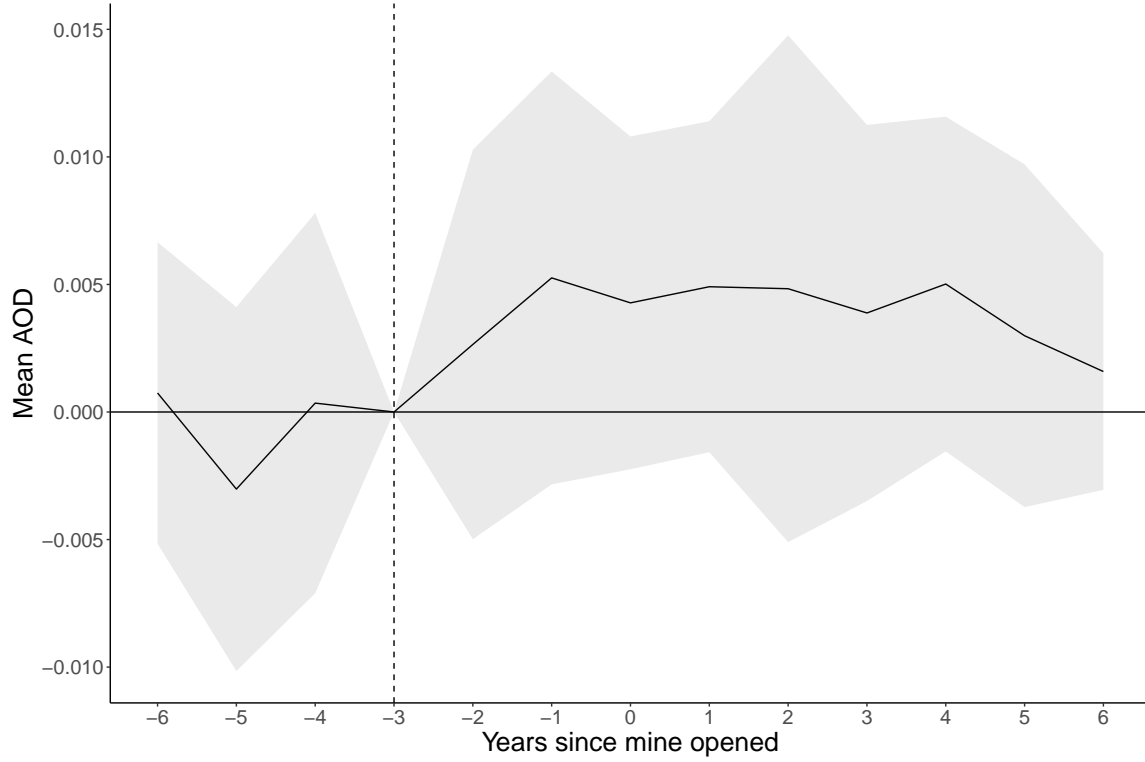
Figure 4: Average effect of mine openings on air pollution - event study

The figure plots coefficient estimates from a regression of mean AOD on the share of days in a month that a side is downwind from a mine, interacted with a series of event time dummies for years since a mine first opened. The unit of analysis is a mine-side-month, though event time coefficients are binned into yearly increments. The dotted lines show pointwise 95 percent confidence intervals for the coefficients of the event-time path of mean AOD. Coefficients can be interpreted as estimated effects relative to the period three years before the mine opened. The regression includes linear and quadratic controls for mean temperature, precipitation, vapor pressure, wet days, evapotranspiration and cloud cover, as well as mine-side fixed effects, mine-year-month fixed effects, mean wind speed and a linear control for the number of non-missing pixel days used to form mean AOD. The sample includes only the 102 mines for which non-missing AOD is observed on all 4 sides of the mine, for at least 4 months in each year, for at least 5 years pre- and 5 years post-mine opening. Event times less than -5 or greater than 5 are binned into two end points.

opened between 2003 and 2012 using the methods of Andrews [1993] and Andrews and Ploberger [1994].[4] I hypothesize that the construction of infrastructure in mining areas would lead to a dramatic increase in nightlights and so interpret the structural break in nightlights as aligning with the construction/pre-production phase. Additional details on the structural breaks estimation procedure are covered in the Appendix 12.12.

For the average mine, I find that a structural break in nightlights occurs about 3 years prior to the S&P start date of commercial production. This is similar to Benshaul-Tolonen [2020], who also uses nightlights to demonstrate an "investment phase" of mining activity occurring 2 years before the start of production. In addition, this finding supports Figure 4, which shows that increases in air pollution begin about 3 years before mines start commercial production. I cautiously interpret this result as evidence that air pollutants generated during the construction and pre-production phase of a mine are major drivers of local air pollution from mines, which aligns with emission rate studies from mine sites [Patra et al., 2016].

After establishing that mining starts to increase air pollution in downwind areas about 3 years before a mine officially begins producing, I turn to estimating the effect of contemporaneous air pollution on remotely sensed yields in mining areas. The event study in Figure 5 reveals no economically or statistically significant effects of contemporaneous exposure to air pollution on NDVI in either the growing or non-growing seasons, at any point in a mine's life cycle. Importantly, these event study estimates are likely only capturing how concurrent exposure to air pollution a certain number of years after a mine opened affects yields, rather than the effect of prolonged exposure to air pollution from a mine. This is because the direction that the wind blows from a mine varies substantially across months within the same year, for most mines in the sample.

The event study findings for both AOD and NDVI are supported by the DID estimates shown in Table 2. Given that mines start to release air pollution about 3 years before official production begins, I define $(Post_{mt} - 3)$ to be equal to 1 after the "investment" phase of a mine begins, which is 3 years prior to the official S&P start year. Panel A of Table 2 shows that relative to sides a mine that are downwind less frequently, sides of a mine that are downwind more frequently experience about a statistically significant increase in AOD after the "investment" phase of a mine begins. The magnitude of this effect is equivalent to roughly a 2% increase and is larger when focusing only on "strongly treated cases:" mine-months where the side that is downwind from the mine most frequently out of all four sides experiences at least 20 days of wind exposure from the mine in a month. In contrast, Panel B shows no economically or statistically significant effect of contemporaneous air pollution on NDVI.

Next, I use the distributed lag model in Equation 5 to examine how cumulative exposure to air pollution

---

[4]In 2013 there was a switch from the DMSP OLS to the VIIRS instrument as the source of nightlights. Since this switch introduced an artificial break in nightlights in 2013, I only estimate structural breaks for mines that opened prior to 2013.
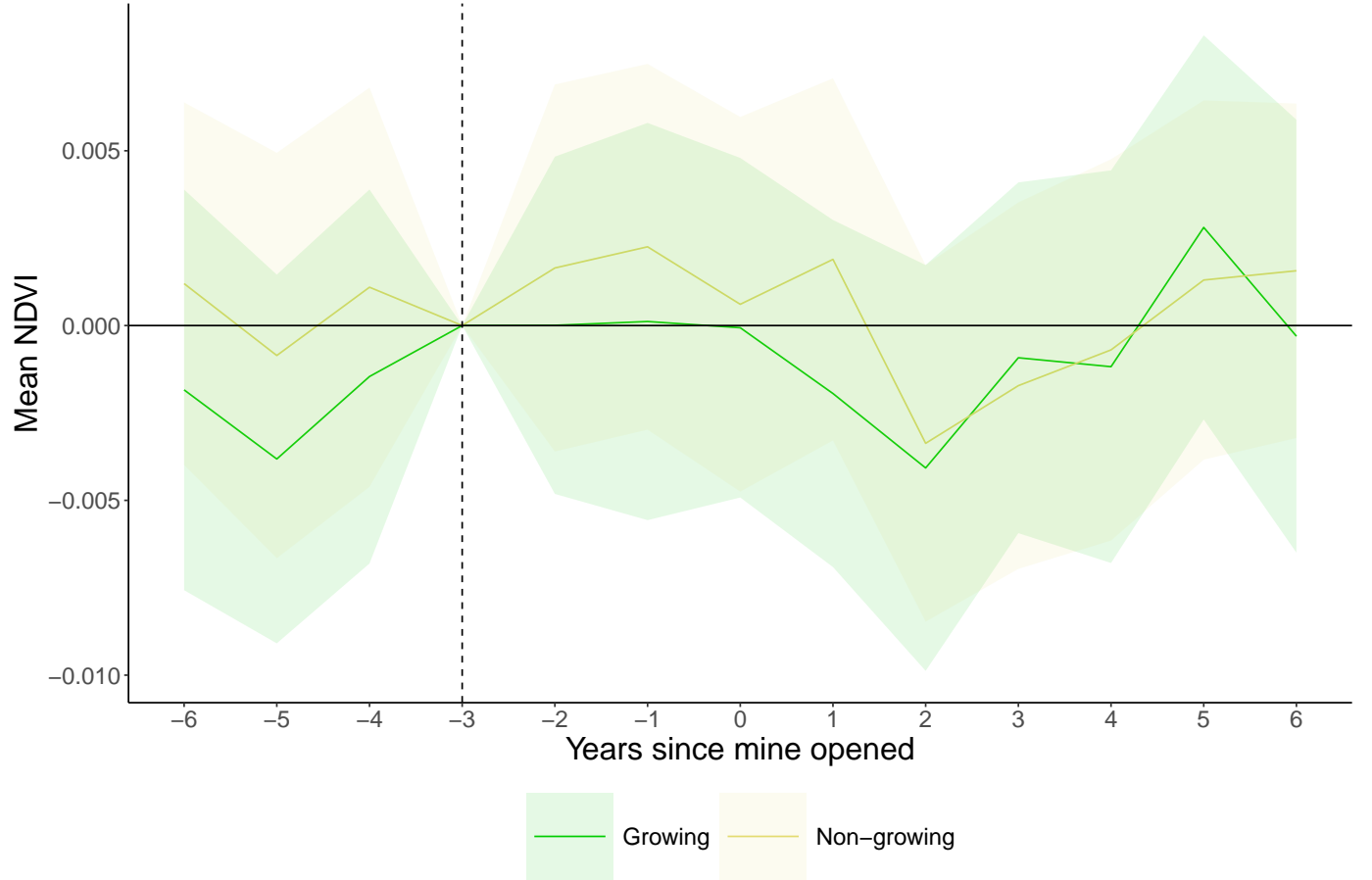
Figure 5: Average effect of contemporaneous mining-induced air pollution on NDVI

The figure plots coefficient estimates from two separate event-study regressions of mean NDVI on the concurrent share of days in a month that a side is downwind from a mine, interacted with a series of event time dummies for years since a mine first opened. The unit of analysis is a mine-side-month, though event time coefficients are binned into yearly increments. The regressions are estimated separately over growing season months (early and late growing) and non-growing season months (planting, harvest and non-farm). The dotted lines show pointwise 95 percent confidence intervals for the coefficients of the event-time path of mean NDVI. Coefficients can be interpreted as estimated effects relative to the period three years before the mine opened. The regression includes linear and quadratic controls for mean temperature, precipitation, vapor pressure, wet days, evapotranspiration and cloud cover, as well as mine-side, mine-year-month fixed effects and mean wind speed. The sample includes only the 102 mines for which non-missing NDVI and AOD is observed on all 4 sides of the mine, for at least 4 months each year, for at least 5 years pre- and 5 years post-mine opening. Event times less than -5 or greater than 5 are binned into two end points.

Table 2: Relationship Between Industrial Mine Openings, Remotely-Sensed Air Pollution and Crop Yields

	(1)	(2)	(3)
	All	20+ days downwind	25+ days downwind
Panel A: First Stage for AOD			
Wind × (Post - 3)	0.00403***	0.00443***	0.00601***
	(0.00147)	(0.00158)	(0.00212)
Mines	102	102	71
Observations	72,596	31,384	16,852
Mean AOD (t-3)	.22	.22	.22
Panel B: Reduced Form for Yields			
Wind × (Post - 3)	0.00028	0.00061	0.00009
	(0.00146)	(0.00140)	(0.00158)
Mines	102	102	71
Observations	72,596	31,384	16,852
Mean NDVI (t-3)	.49	.49	.49
Mine-side FE	Yes	Yes	Yes
Mine-year-month FE	Yes	Yes	Yes
Weather	Yes	Yes	Yes

Notes: Each column reports the results of a linear regression. The unit of analysis is a mine-side-month. In Panel A, the dependent variable is mean aerosol optical depth (AOD) for one of the four sides (N,S, E, W) of a mine within a 60km buffer, in a given month. I derive AOD from the MODIS Aqua Level 2 Daily product (MYD04_3K). In Panel B, the dependent variable is mean normalized difference vegetation index (NDVI) for one of the four sides of a mine within a 60km buffer, in a given month. I derive remotely sensed yields from the MODIS Combined Terra and Aqua product (MCD43A4.061). *Wind* is defined as the share of days in a month that a side is downwind from the mine. *Post - 3* is equal to 1 after the investment phase of a mine, which occurs 3 years before the mine opened, 0 otherwise. All models include linear and quadratic controls for mean temperature, precipitation, vapor pressure, wet days, evapotranspiration and cloud cover, as well as mine-side fixed effects, mine-year-month fixed effects and mean wind speed. The sample includes the 102 mines for which non-missing AOD and NDVI are observed on all four sides of the mine for at least 4 months in each year, for at least 5 years pre and 5 years post-mine opening. Column 1 reports results from a model estimated over all mine months while Column 2 (3) subsets to only mine-months where the side that is downwind most frequently receives at least 20 (25) days of wind from the mine. Standard errors in parentheses are clustered by mine.

over an extended period of time affects crop yields. Instead of being determined solely by contemporaneous wind, air pollution exposure is now a vector of monthly downwind exposure from the current month all the way back to 24 months prior. Pooling all seasons together, Figure 6 reports point estimates and 95 percent confidence intervals for the cumulative effect of lagged and concurrent pollution exposure, proxied by days of wind downwind from a mine. Along the horizontal axis, I increase the maximum response delay from $P = 1$ to $P = 24$ months, estimating a separate distributed lag model for each lag increment. On the vertical axis, I report the NDVI effect for a $+30$ day increase wind sustained over the $P + 1$ preceding and concurrent months. For example, at $P = 12$ lagged months on the horizontal axis, Figure 6 reports the pre-post difference in cumulative effects, $\sum_{p=0}^{12} \delta_p$, of a sustained 30 day increase in wind from a mine on NDVI over the prior 12 months and the current month. For interpretation, I normalize the coefficients using mean NDVI from 3 years before a mine opens. Appendix Table 16 presents the coefficients, standard errors and p-values for each of the lag increments.

On average, I find no effect of cumulative mining-induced air pollution on NDVI in downwind areas, both when pooling all months (Figure 6) as well as when estimating the model separately by growing and non-growing seasons (Appendix Figure 13). Importantly, these average treatment effects mask substantial heterogeneity. For instance, Appendix Table 14 Column 2 shows that downwind areas near open pit mines experience a small but statistically significant reduction in NDVI due to contemporaneous mining-induced air pollution exposure. This aligns with literature suggesting that open pit mines tend to pollute more than underground mines [Sahu et al., 2015]. Other dimensions of heterogeneity are discussed in more detail in Section 9.
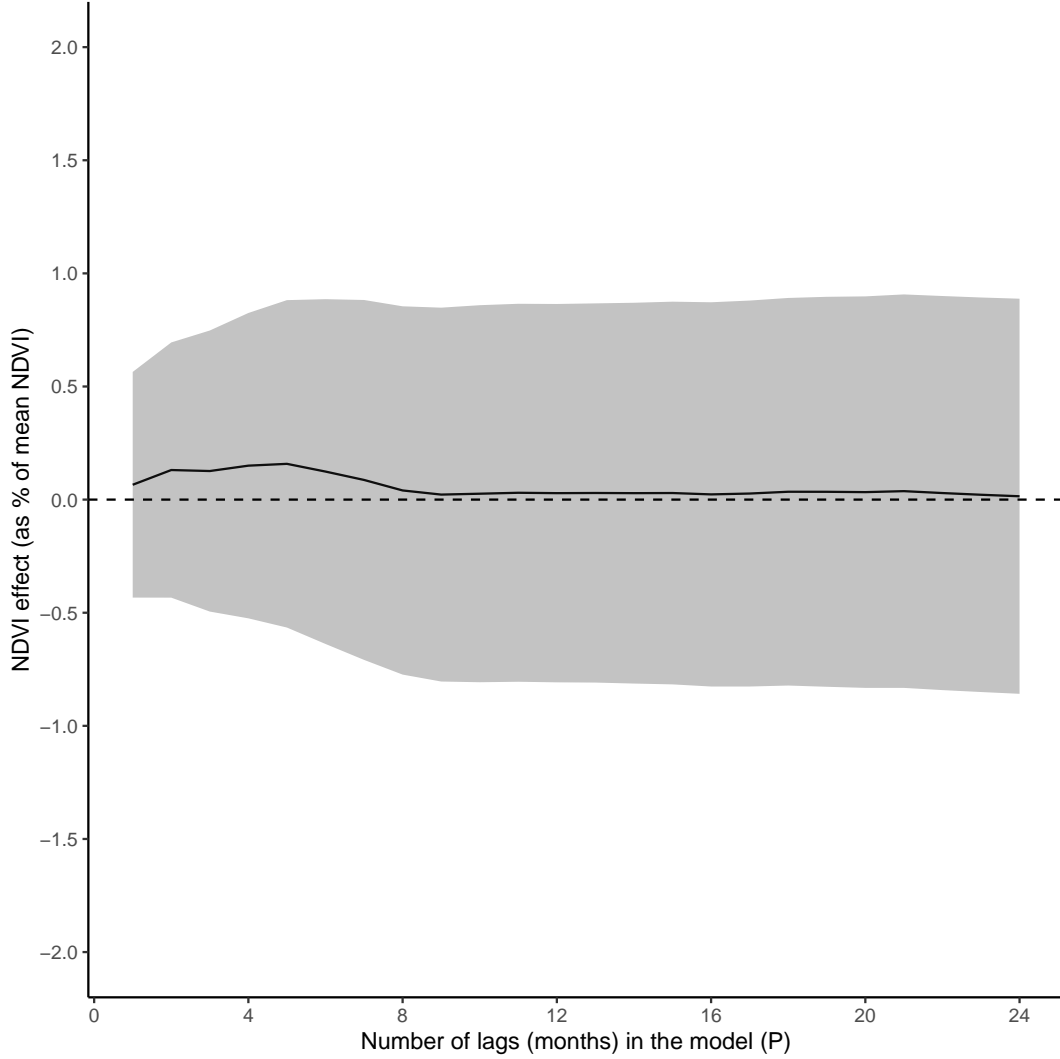
Figure 6: Average effect of cumulative exposure to mining-induced air pollution on mean NDVI - pooling seasons

The figure plots the cumulative impact on mean NDVI of +30 days of downwind exposure to air pollution from a mine in each of the concurrent and previous P months. Each value reports the point estimate and 95 percent CI on $\sum_{p=0}^{P} \delta_p$ from a different distributed lag model, as I increase P along the horizontal axis. $\sum_{p=0}^{P} \delta_p$ can be interpreted as the average difference in cumulative effects of air pollution on NDVI between the pre and post period, where the post period is defined as the time period after a mine opens. The sample includes the set of 219 mines with non-missing NDVI data observed on all 4 sides, for all 12 months in each year, for at least 5 years pre- and 5 years post-mine opening. Each distributed lag model is estimated using mine-side-months observed after the time period 3 years before a mine first opens, to ensure that lagged wind exposure is observed for at least 2 years before the current month. Each distributed lag model is estimated over months in all seasons.

7 Mixing Pollution Externalities and Market-based Channels

To estimate an "overall" effect of industrial mining on agricultural output through both pollution externalities and market-based channels, I use the staggered openings of 308 mines across Sub-Saharan Africa in a DID that compares NDVI between areas near mines to areas further away, before and after a mine opening. Causal identification of this effect relies on the assumption that areas near mines and areas further away are similarly affected by unobservables that may be correlated with mine openings and local yields, but proximal areas are more affected by both market and pollution shocks.

First, to motivate the assumption that market channels will disproportionately affect areas near mines, I use findings from existing literature to define the spatial extent of local markets around mining areas. Empirical evidence on commuting distances in urban and rural Africa suggests that areas of 5, 10 or 15 km are likely integrated markets (Amoh-Gyimah and Aidoo [2013]; Kung et al. [2014], Shafer [2000]). Furthermore, wealth increases and structural transformation effects are concentrated within 20-km of a mine. Kotsadam and Tolonen [2016] find that mining leads to large and statistically significant shifts out of agriculture into services for households up to 25-km away, while von der Goltz and Barnwal [2019] find statistically significant wealth increases for households up to 20-km away, with negligible effects further away. Taken together, this literature suggests that areas within 20-km of a mine likely define integrated markets that will be affected by mining activity.

Second, to demonstrate that pollution effects will be concentrated close to mines, I estimate a spatial lag model with AOD as the outcome of interest. Appendix Figure 11 shows that AOD increases after mine openings are largest within 20-km of a mine, though smaller, statistically significant effects persist up to 60-km away, with no statistically distinguishable effects at greater distances.

After establishing that market effects and pollution externalities are likely concentrated within 20-km of a mine, I define the following specification to estimate the overall effect of mining on yields:

$$NDVI_{gmt} = \alpha_{gm} + \lambda_{mt} + \delta Near_{gm} + \eta Post_{mt} + \beta_O Near_{gm} \times Post_{mt} + \mathbf{X'_{gmt}\Gamma} + \epsilon_{gmt} \qquad (6)$$

where g indexes the distance group (near or far), m indexes the mine and t indexes the date. The near group for each mine is defined as the buffer of radius 20 kilometers around the mine centroid, while the far group is defined as the ring between the buffer of 100 km and the buffer of 150 km away from the mine. This radius is chosen based on a spatial lag model: Appendix Figure 12 shows that the largest reduction in NDVI occurs within 20 kilometers of a mine, with smaller reductions in NDVI occurring between 20-60 kilometers

of a mine and no statistically significant effect at greater distances.[5] As a result, I define $Near_{gm}$ equal to 1 within the 20 kilometer buffer and 0 for the 100-150km ring. $Post_{mt}$ is equal to 1 after mine m opened, 0 otherwise. Standard errors are clustered at the mine level.

I include mine-distance group and mine-date fixed effects, as well as linear and quadratic controls for mean temperature, vapor pressure, wet days, precipitation, evapotranspiration and cloud cover. The main parameter of interest is β_O, which captures the differential impact of an open mine on cropland "near" the mine, relative to cropland further away. Given that the model includes mine-by-distance and mine-by-date fixed effects, β_O is identified by within-month differences in the change in NDVI in cropland "near" and further away from a mine opening.

It is theoretically ambiguous whether β_O should be larger in magnitude than the effect of the pollution channels alone on yields. While market channels can generate negative effects on crop yields, for instance by drawing workers out of agriculture into other sectors, they can also increase local household wealth, which may allow households to invest more in inputs to agriculture or switch to crops that may be less sensitive to pollution, helping them adapt to the effects of mining pollution on yields. If the effect of market channels on local yields are net negative, we would expect that the joint effect of pollution and market based channels estimated through the near-far DID to be larger than the pollution-only effect. The opposite would hold if market effects on yields are net positive or mitigate some of the pollution effect.

Table 3 shows that on average, mine openings lead to a statistically significant decrease in NDVI of about 1.5% in areas near mines relative to areas further away, with slightly larger effects in the growing season. These results provide a helpful baseline against which the estimates generated by isolating the pollution effect can be compared to.

---

[5]In the spatial lag model, the omitted category is the 100-150km ring.

Table 3: Average effect of mine openings on NDVI - mixing pollution and market channels

	(1) Pooled	(2) Growing only	(3) Non-growing only
Near × Post	-0.00638***	-0.00691***	-0.00589***
	(0.000980)	(0.000990)	(0.00108)
Number of mines	307	307	307
Obs.	168626	80582	88044
Mine-distance group FE	Yes	Yes	Yes
Mine-year-month FE	Yes	Yes	Yes
Weather	Yes	Yes	Yes
Mean NDVI (t-1)	.476	.543	.415

Each column reports the results of a linear regression. The unit of analysis is a mine-distance group-month. The dependent variable is mean NDVI within a given distance group, in a given month. *Near* is equal to 1 for area within the 20km buffer around the mine and equal to 0 for the area in the ring between the buffers of 100km and 150km. *Post* is equal to 1 after the mine opened, 0 otherwise. All models include linear and quadratic controls for mean temperature, precipitation, vapor pressure, wet days, evapotranspiration and cloud cover, as well as mine and year-month fixed effects. The sample includes the mines for which non-missing NDVI is observed in both distance groups for at least 4 months in each year, for at least 3 years pre- and 3 years post-mine opening. Column 1 reports results estimated by pooling months over all 5 seasons: planting, early growing, late growing, harvest and non-farm. Column 2 reports results estimated only over months in the early growing and late growing seasons and Column 3 reports results estimated only over months in non-growing seasons: planting, harvest and non-farm. Standard errors in parentheses are clustered by mine.

8   Explaining small average treatment effects

I find that on average mining leads to statistically significant, but economically small, declines in local yields, for both the overall effect and the effect of pollution externalities alone. Most strikingly, my finding that mine openings decrease yields in areas near mines by about 1.5% relative to areas further away stands in stark contrast to the findings of Aragón and Rud [2016], who use survey data for households near 11 gold mines in Ghana in a similar near versus far DID design to show that a 100-tonne increase in gold production in mining regions of Ghana decreases real agricultural output by about 15% and maize yields by about 40%. Relative to the mean increase in gold production for the average mine in Ghana of about 40 tonnes, these findings suggest effect sizes of 6.5% and 17% respectively.

I consider measurement error in NDVI and treatment effect heterogeneity as two possible explanations for the discrepancy between effect sizes I obtain and those estimated by Aragón and Rud [2016]. Like many remotely-sensed variables, NDVI is an imperfect measure of the true plot-level yields and subject to different types of measurement error, some of which may be non-classical. Mean-reverting measurement error, common to remotely sensed variables, would attenuate estimated coefficients when affecting the dependent variable, in some cases quite significantly. Estimates of the magnitude of mean-reverting measurement error by Proctor et al. [2023] suggest that estimated coefficients from regressions using mismeasured remotely sensed variables may biased downward by up to 50%.

While some methods exist to correct for measurement error in remotely-sensed variables, such as the

multiple imputation method proposed by Proctor et al. [2023], these methods generally require ground-truth data within at least 2 km of the area of interest to perform well. Potential sources of plot-level cropcuts data, such as the LSMS-ISA or One Acre Fund, do not satisfy this criteria as they are not available for sites proximal to mining areas used in my analysis. Appendix 12.13 discusses NDVI measurement error, as well as the data limitations that prevent me from addressing these issues, in more detail.

Aside from measurement error, the small average effect of mine openings on yields may be explained by heterogeneity in treatment effects across mines. Unlike Aragón and Rud [2016], who focus on a single country (Ghana) and a single commodity (gold), my sample contains mines that cover over 26 commodities across 29 countries in Africa. Given the mine-side and mine-year-month fixed effects, the DID estimate obtained from Equation 6 is provides an average of the underlying mine-specific estimates that would be derived from over 300 mine openings, some of which may be negative, others positive. Even if a majority of the underlying DID estimates that make up the average effect are negative, positive mine-specific DID estimates might attenuate the average effect across all mines. In the next section, I explore the extent to which the small average treatment effects reported in Tables 1, 2 and 3 may mask treatment effect heterogeneity, as well as what factors might drive larger yield reductions.

9   Heterogeneous Treatment Effects

An advantage of my empirical design is that I am able to observe a treatment and control area for every mine in my analysis, before and after the mine opening date, allowing me to estimate mine-specific DID estimates. Each mine-specific DID is estimated by running a separate regression for each mine, where the outcome is NDVI on a side of the mine in a given month, with controls for weather and robust standard errors.[6]

Figure 7 plots the distribution of mine-specific "overall", water and air pollution effects on yields, revealing substantial heterogeneity across mines for all three types of analysis. The top panel, which shows the distribution of "overall" effects of mining on local yields, highlights that the majority of treatment effects are negative and concentrated between 0 to -5%. Furthermore, it is not unreasonable to observe some cases where mining increases local yields. For instance, if local demand booms from mining increase incomes, some of this may be reinvested in improved inputs or technologies used in agriculture.

Similarly, the bottom left panel reveals that downstream yields decrease after a mine opening in the

---

[6]When estimating the "overall" specification separately for each mine, only the main effects and interaction terms of Near with Post, along with controls for weather, are included as covariates in the regression. I exclude the side and year-month fixed effects as they are correlated with the Near and Post dummies, respectively. The same holds true for the water pollution specification, but with the Downwind dummy. For the air pollution specification, I include side fixed effects since downwind intensity varies across sides and time, as well as the main effects and interactions of downwind exposure and the Post dummy. Year-month fixed effects are excluded as they are collinear with the Post dummy.

majority of cases, with these reductions larger than those observed for the "overall" effect. This might be explained by some kind of pollution-offsetting effect may be occurring through market-based channels, which is captured by the near vs. far DID but not the water pollution DID. Yield increases in cropland downstream from a mine might be explained by a composition of mine wastewater that is low in heavy metals but high in nutrients needed for plant growth, which may improve pre-existing soil nutrient concentration or pH (Wang et al. [2022]; Xu et al. [2022]).

In contrast, the bottom right panel of Figure 7 highlights that contemporaneous mining-induced air pollution increases yields in roughly half of the sample but decreases yields in the other half. This aligns with literature documenting a theoretically ambiguous effect of air pollution on local yields, which can depend on local pollution regimes, such as the extent to which the scattering versus absorbing effect of particulate matter dominates, as well as other atmospheric conditions [Schiferl et al., 2018]. One proposed explanation for these findings is the intensity of pollution: Behrer and Wang [2024] show that high density smoke plumes from wildfires decrease yields while low density plumes increase yields. Indeed, Appendix Figure 17, which plots the normalized AOD DID estimates against the normalized NDVI estimates for each mine, shows that small increases in AOD lead to small increases in yields, while larger increases in AOD lead to yield reductions.

The fact that all three distributions show how mining increases yields in a substantial number of mine-specific DIDs helps explain why observed average treatment effects generated by pooling all mines together are smaller than those documented by Aragón and Rud [2016] for Ghana. By focusing on the set of mines closer to the sample used by Aragón and Rud [2016], I am able to recover treatment effects that are much closer in magnitude to what they find. Mine-specific estimates obtained from individual near versus far DID regressions reveals that treatment effects for 19 Ghanaian mines are all negative and can be as large as 11%.

Importantly, the variation in treatment effects observed in Figure 7 is much larger than what would be observed due to sampling variation alone, as shown in Appendix Figure 14. This illustrates the value of further investigation into what might be driving meaningful heterogeneity in treatment effects.

9.1 Dimensions explored I investigate heterogeneity across four key dimensions: (1) governance/regulatory environments, (2) mine characteristics, (3) local economic factors and (4) local environmental conditions. First, to explore the role that governance plays in the local effects of mines, I use the country-level World Bank World Governance Indicators from 2000, the year prior to the start of my NDVI panel. I focus on five main indicators: control of corruption, government effectiveness, regulatory quality, rule of law, and voice and accountability.[7] Each indicator is based on data from multiple sources, such as survey data, commercial

---

[7]Kaufmann et al. [2010] define each of the indicators as follows: "Control of corruption captures perceptions of the extent to which public power is exercised for private gain, as well as elite or private capture. Government effectiveness captures
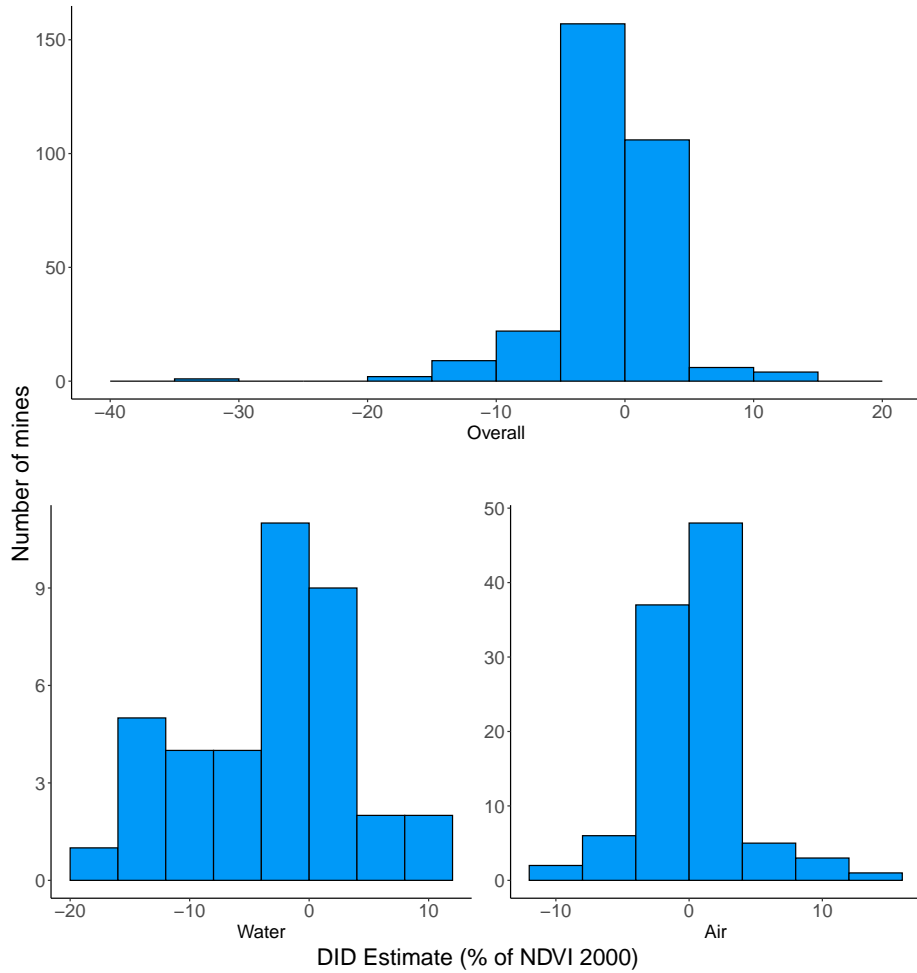
Figure 7: Distribution of Mine-Specific DIDs

The figure plots three histograms showing the distribution of mine-specific DID estimates. Each DID is estimated from a separate regression for each mine. The top panel shows the distribution of mine-specific near vs. far DID estimates obtained by estimating a version of Equation 6 for each mine: I regress NDVI on a side (near or far) on the Near dummy interacted with the Post dummy, along with the main effects and controls for weather. The bottom left panel shows the distribution of mine-specific downstream vs. upstream DID estimates obtained by estimating a version of Equation 3 for each mine: I regress NDVI on a side (downstream or upstreamm) on the Downstream dummy interacted with the Post dummy, along with the main effects and controls for weather. The bottom right panel shows the distribution of mine-specific continuous wind intensity DID estimates obtained by estimating a version of Equation 4 for each mine: I regress NDVI on a side (N, S, E, W) on the share of days a side is downwind from the mine in a given month interacted with the Post dummy, the main effects, side fixed effects and weather controls. Across all regressions, I estimate robust standard errors. Each mine-specific DID estimate is normalized by mean NDVI in 2000 for that mine, then multiplied by 100 to represent the magnitude of the effect relative to the mean of the outcome at the start of the panel in percent terms.

business information providers or non-governmental organizations. The underlying data is aggregated into a score for each of the five indicators, in units of a standard normal distribution from approximately -2.5 to 2.5. Additionally, I examine whether the mine country's membership to the Extractive Industries Transparency Initiative (EITI), designed to promote transparency and accountability in national resource extraction, can explain variation in the local effects of mining.

Second, I examine heterogeneity in effects on NDVI according to the following mine-specific characteristics: extraction method (open pit or non-open pit), commodity type, mine age, distance to the nearest neighboring mine, distance to the nearest town. Finally, I test for heterogeneity by the following economic factors: mineral rents as share of GDP in 2000, GDP in 2000 and population in 2000, as well as the following local environmental conditions: initial air and water pollution exposure (AOD in 2003 and NDTI in 2000), initial crop land productivity (NDVI in 2000) and precipitation in 2000. Additional details on data construction for the variables used in the heterogeneity analysis are covered in 12.2.

9.2 "Standard" heterogeneity analysis To start off, I implement the "standard" practice for heterogeneity analysis used in the economics literature. To estimate heterogeneity in the overall effect of mining on yields I include a triple interaction of the Near dummy, the Post dummy and the dimension of heterogeneity in Equation 6. Similar triple interactions are included in the water and contemporaneous air pollution specifications, with the downstream dummy and the continuous measure of downwind exposure respectively. Lastly, to test for heterogeneous treatment effects of prolonged exposure to air pollution on NDVI, I estimate Equation 5 separately over different sub-groups defined by the dimension of heterogeneity of interest.

Across the overall, water and air pollution analyses, weak governance and regulatory environments are revealed to be important drivers of the negative effect of mining activity on yields. Table 4 reveals that reductions in NDVI are 2-3 times larger in areas near mines located in countries with below median performance on governance indicators. The triple interactions are negative, sizable in magnitude and statistically significant across all governance indicators, with the largest negative effect detected for mines located in countries that are not members of the EITI.

Similar patterns in heterogeneous treatment effects are uncovered from the air and water regressions. Appendix Table 17 shows that the triple interactions with the governance and EITI indicators from the water pollution regressions are overwhelmingly negative, though not statistically significant, likely due to

perceptions of the quality of public services, the quality of policy formulation/implementation and the credibility of government commitment to these policies. Regulatory quality captures perceptions of the government's ability to formulate and implement sound regulations. Rule of law captures perceptions of the extent to which agents have confidence in and follow the rules of society, such as the quality of contract enforcement, property rights, the police and the courts. Voice and accountability captures perceptions of the extent to which a country's citizens can exercise rights to freedom of expression, freedom of association and free media, as well as whether they can participate in free and fair elections."

Table 4: Heterogeneous Treatment Effects - Governance and Regulatory Environments

	Base	Not EITI Member	Control of Corruption	Govt. Effectiveness	Rule of Law	Reg. Quality	Voice and Accountability
Near × Post	-0.00638***	-0.00278***	-0.00405***	-0.00415***	-0.00429***	-0.00426***	-0.00436***
	(0.000980)	(0.000900)	(0.00108)	(0.00110)	(0.00108)	(0.00108)	(0.00111)
Near × Post × Z		-0.00714***	-0.00499**	-0.00472**	-0.00453**	-0.00472**	-0.00414**
		(0.00191)	(0.00198)	(0.00197)	(0.00200)	(0.00202)	(0.00196)
Number of mines	307	307	307	307	307	307	307
Mean NDVI (t-1)	.476	.476	.476	.476	.476	.476	.476

Standard errors in parentheses
* $p < 0.10$, ** $p < 0.05$, *** $p < 0.01$

the small sample size. For air pollution, Appendix Figures 20 - 22, which show the heterogeneous treatment effects from the air pollution distributed lag model, reveal that there is a consistent pattern of decreases in NDVI occurring only for mines with below median governance indicators of government effectiveness, regulatory quality and accountability. Most strikingly, Figure 8, shown below, highlights how statistically significant reductions in NDVI occur for mines located in countries that are not members of the EITI, after about 8 months of exposure to air pollution from mines.

My findings that yield reductions from pollution externalities are larger for mining areas in countries with weak environmental governance aligns with a burgeoning literature that documents the role of public governance on local environmental footprints. Lipscomb and Mobarak [2017] demonstrate the importance of governance in explaining the spatial patterns of water pollution in Brazil, Burgess et al. [2012] find that weak governance worsens deforestation in Indonesia and Cust et al. [2023] show that forest loss near oil wells is lower in countries with stronger public governance. Additionally, my results fit into a larger economics literature that highlights the importance of well-functioning political institutions for economic development [Acemoglu et al., 2005].

In addition to weak governance, I find that exposure to pollution before a mine opens influences the extent to which mining activity impacts local agriculture. Across both the air and water pollution analyses, NDVI reductions are higher for cropland in areas initially exposed to lower pollution levels. Appendix Table 14 Column 2 highlights how NDVI reductions are about twice as large in cropland near rivers that had below median levels of initial turbidity, with the triple interaction being statistically significant. Similarly, Appendix Figure 33 illustrates how statistically significant NDVI reductions occur only for cropland initially exposed to lower levels of AOD. These effects could be explained by plant or farmer adaptation. Crops growing in areas initially exposed to higher pollution levels may have adapted to growing in sub-optimal conditions and so may be less affected by small increases in air and water pollution due to mining (Hutchinson [1984]; Oksanen and Kontunen-Soppela [2021]). Alternatively, farmers used to growing crops in more polluted areas may have already developed strategies to mitigate the effects of pollution on their crops, such as investing in fertilizer to improve soil quality that has been depleted by atmospheric deposition or irrigation with contaminated
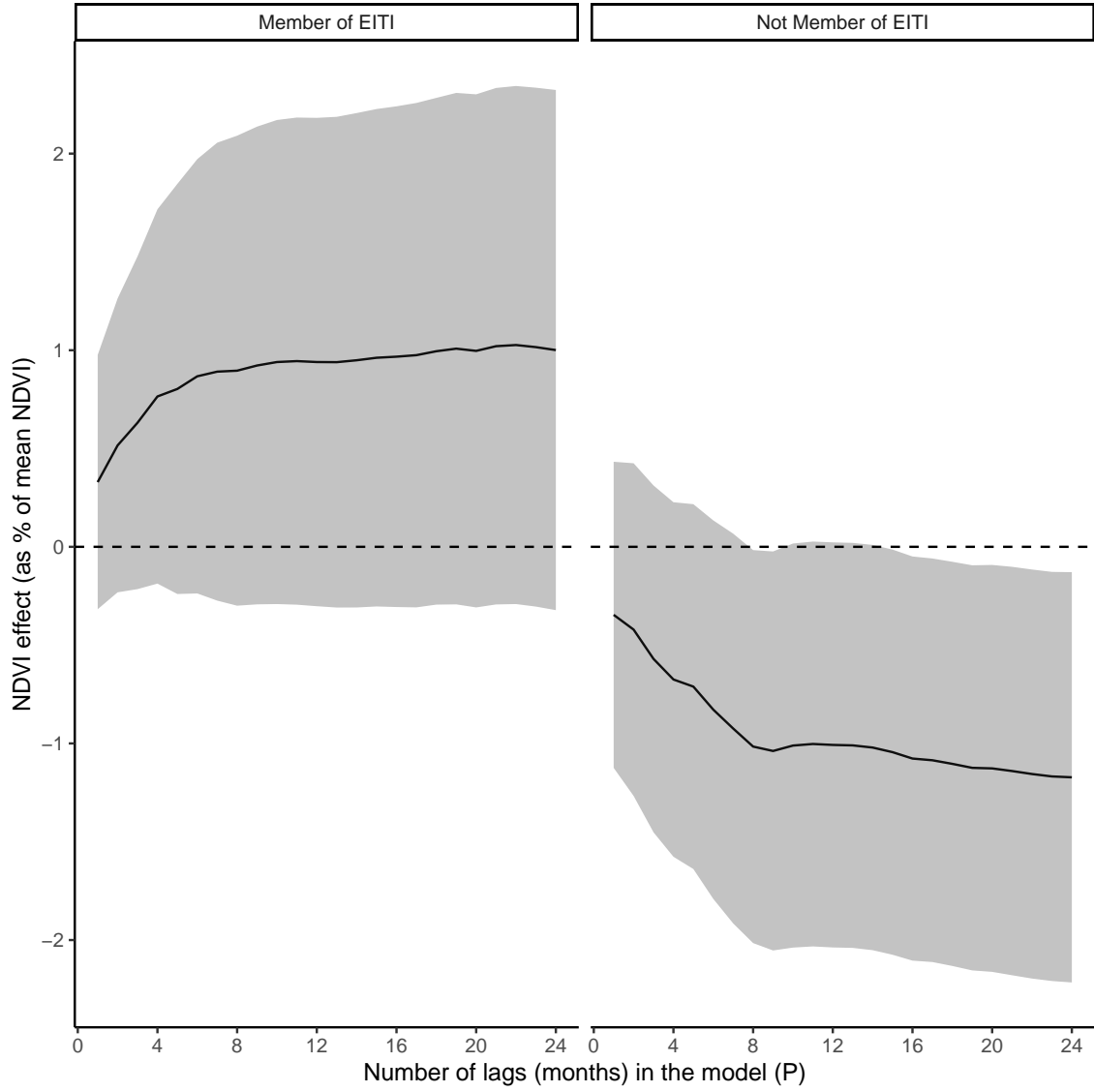
Figure 8: Average cumulative effect of mining air pollution on NDVI - heterogeneity by EITI membership

Each panel in the figure plots the cumulative impact on mean NDVI of +30 days of downwind exposure to air pollution from a mine in each of the concurrent and previous P months. The left panel plots the cumulative impact for mines located in countries that are EITI members, while the right panel plots it for mines in non-member countries. Each value reports the point estimate and 95 percent CI on $\sum_{p=0}^{P} \delta_p$ from a different distributed lag model, as I increase P along the horizontal axis. $\sum_{p=0}^{P} \delta_p$ can be interpreted as the average difference in cumulative effects of mining air pollution on NDVI between the pre and post period, where the post period is defined as the time period after a mine opens. The sample includes only the set of mines with non-missing NDVI data observed on all 4 sides, for all 12 months in each year, for at least 5 years pre- and 5 years post-mine opening. Each distributed lag model is estimated using mine-side-months observed after the time period 3 years before a mine first opens, to ensure that lagged wind exposure and NDVI is observed for at least 4 years before the current month.

water (Magesa et al. [2023], Villamayor-Tomas et al. [2024]).

9.3 Machine-learning heterogeneity analysis In addition to the "standard" heterogeneity analysis, I train a machine learning model to predict mine-specific treatment effects given a large number of mine and country-level characteristics. This data-driven approach allows me to identify dimensions of heterogeneity that drive differences in treatment effects and see whether these findings are complementary to those uncovered in the "standard" heterogeneity analysis. While my approach is similar in spirit to the methods of Wager and Athey [2017], who use causal forests to uncover meaningful dimensions of heterogeneity by estimating conditional average treatment effects, it differs a key way. While I can match the treated area to a control area for every mine, allowing me to estimate unit specific treatment effects, Wager and Athey [2017] do not observe a control unit that can be matched to a treated unit, so use random forests to non-parametrically define groups of treated and control units that are comparable across observables. The exercise I conduct is complementary to their work, as it can be applied to other settings where unit-specific treatment effects can be estimated and treatment effect heterogeneity may be explained by a variety of factors, such that the researcher wishes to demonstrate that statistically significant findings from "standard" heterogeneity analysis are not spurious.

I train a collection of ML models to predict treatment effects, based on 8 algorithms, including linear regression models such as OLS, LASSO, Ridge and elastic net, as well as non-parametric models such as random forest, a classification and regression tree (CART) and a bagged CART. The unit of observation is a mine, where the outcome of interest is the mine-specific DID estimate for the "overall" effect of mining activity on yields. The main predictors include the five governance indicators, a dummy variable for whether the mine is located in an EITI-member country, GDP in 2000 for the mining area, population in 2000 for the mining area, mineral rents as a share of GDP in 2000, dummy variables for mine type, dummy variables for commodity extracted, dummy variables indicating the country that the mine is located in, distance to the nearest mine and distance to the nearest town.[8]

The ML models are trained on the set of 304 mines for which DID estimates are generated and non-missing data for all predictors is available, using 75% of observations for training and the remaining 25% for validation. Model hyperparameters are selected based on a grid search. Out-of-sample accuracy measures values are calculated using 5 fold cross-validation of the training dataset. I therefore obtain 25 hyperparameters combinations for each model (except for OLS), totaling 176 different ML models.

Out of all models trained, the random forest model is identified as the "best" performing model, defined

---

[8]For the country, commodity and mine type variables, which are originally categorical, categories accounting for less than 5% of the observations in the sample are binned together into "other."

by lowest out-of-sample root mean-squared error (RMSE).[9] I re-train this random forest model over the entire dataset of DIDs and obtain a measure of variable importance for each predictor.

To estimate variable importance, I construct a measure of "permutation importance," which leverages the out-of-bag samples for each tree according to the following method. First, the RMSE on the out-of-bag sample is calculated. Then, the values of the predictor of interest in the out-of-bag-sample are randomly shuffled, keeping the values of all other predictors the same. Finally, the decrease in RMSE on the shuffled data is measured. Larger reductions in RMSE after permutation imply that a variable is more "important" in contributing to predictive capacity. I opt for permutation importance over Gini impurity, a common alternative measure of variable importance for random forest models, as impurity-based importance is less reliable in settings where many predictors are dummies.

Figure 9 plots the ten most important variables from the best random forest model, based on permutation importance. One striking result is that all five country-level governance indicators are determined to be highly important. This aligns with the results from the "standard" heterogeneity analysis of Table 4, which finds the triple interactions on these five indicators to be highly statistically significant. Similarly, the indicator for whether the mine is located in an EITI-member country, which was also statistically significant in Table 4, falls in the set of the ten most important predictors. These consistent findings between the standard and ML heterogeneity analysis lend credibility to the interpretation that local governance and regulatory environments are important drivers of the extent to which mining activity negatively impacts local agriculture.

However, I note instances where the findings from the "standard" and ML heterogeneity analyses diverge. While the estimates on the triple interactions with mineral rents as a share of 2000 GDP and distance to the nearest neighboring mine are both large and statistically significant in the standard heterogeneity analysis, both variables are in the set of 10 least important variables determined by the ML model (shown in Appendix Figure 15).

In summary, this exercise highlights the value of conducting ML heterogeneity analysis to cross-check "standard" heterogeneity analysis in settings where unit-specific treatment effects can be estimated. In Appendix Figure 16, I also show that the main conclusions drawn from the ML analysis discussed above are robust to estimating a classification model, where the outcome is a dummy variable equal to one if the mine-specific DID estimate is negative. While the ranking of the most important variables slightly changes, four of the five country-level governance indicators still rank within the top five most important predictors.

---

[9]The best random forest model is grown on 1000 trees, with 1 predictor randomly sampled at each split and a minimum of 15 data points in each node required for additional splitting to occur.
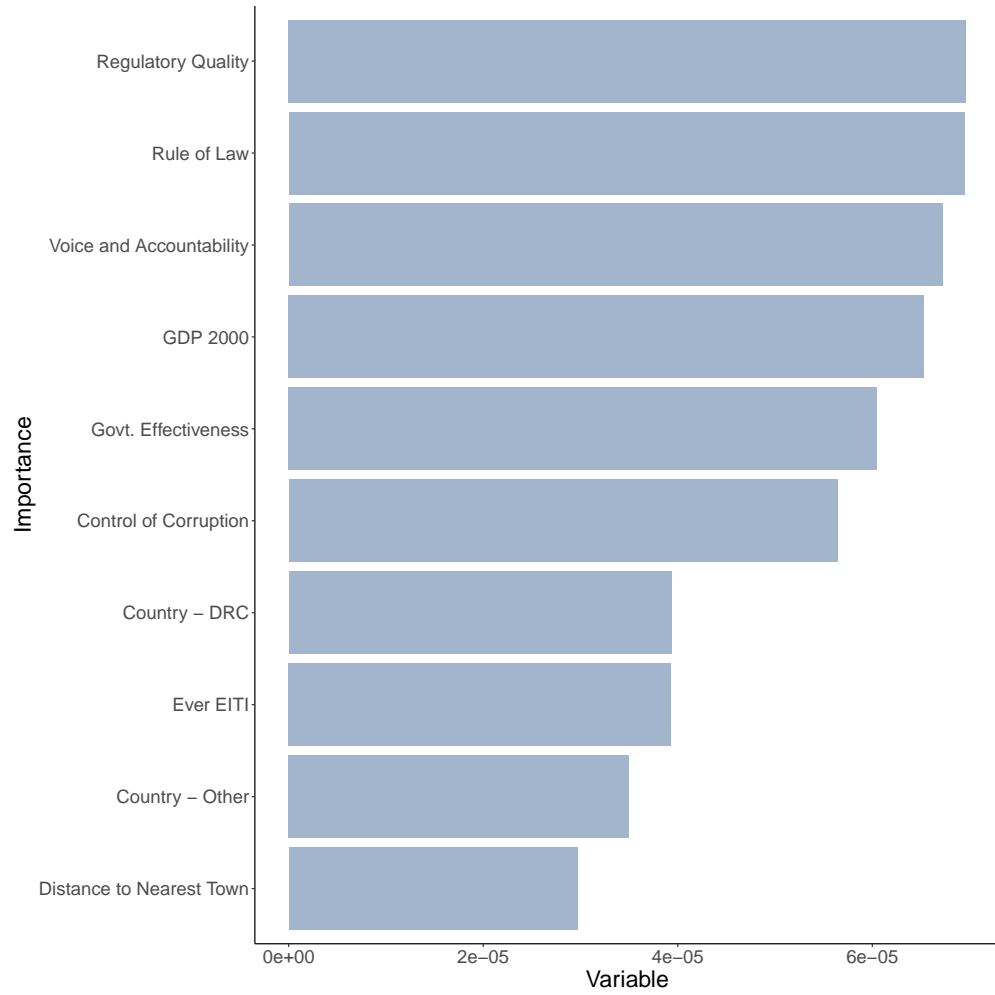
Figure 9: Most Important Variables from Best Random Forest Model

10   Quantifying Results

In this section, I ask two important questions to quantify the effect of mining on yields. First, what share of the average "overall" effect of industrial mining on local agricultural output can be explained by pollution alone? Second, how can we map the estimated effects in NDVI units to effects on actual yields in kilograms per hectare?

10.1   Estimating Share of Effect on Yields Driven By Pollution

I conduct a back-of-the-envelope calculation to estimate the share of the "overall" effect of mining on yields that is driven by pollution externalities by taking the ratio of the pollution-only treatment effects estimated with the air and water pollution DIDs, scaled to account for the area in the near buffer exposed to pollution, to the overall effect estimated with the near vs. far DID.

From the distributed lag results in Table 16, we see that at most NDVI falls by 0.0007 units in downwind areas due to cumulative and contemporaneous mining-induced air pollution. I scale this estimate by 0.25, to reflect the fact that on average, 25% of the 20-km near buffer around mine is downwind most frequently in a given month. This yields a very small scaled treatment effect of 0.000175 for air pollution.

In contrast, we see a much larger effect when looking at exposure to water pollution: Table 1 Column 2 shows that on average, NDVI is 0.0177 lower in downstream areas during the growing seasons. I re-scale this treatment effect by 0.17, which is the 25th percentile of the share of the 20km buffer that is at a lower elevation than the mine, and so could be affected by water flow from the mine, across all mines within 1km of a river. The resulting scaled effect of water pollution on NDVI is 0.003009, which serves as a lower bound for the combined effect of both air and water pollution on local yields.

Taking the ratio of the scaled pollution effect to the overall effect of industrial mining on growing season NDVI of -0.00691, from Column 2 of Table 3 suggests that approximately 44% of the overall effect of mining on NDVI can be explained by air and water pollution externalities. When interpreting this share, it is important to keep in mind several caveats. First, the heterogeneity analysis suggests that this share likely varies substantially across mines. Second, higher returns to inputs outside of agriculture generated by mining could generate a pollution-offsetting effect for areas near mines, which may attenuate the near-far DID estimate and make the share of this effect attributed to pollution appear larger. As wealth increases from local mining activity are non-directional, they should not bias the air and water pollution DID estimates. However, wealth increases will disproportionately affect areas near mines and could offset some of the negative effects of pollution also experienced by these areas. For example, increased wealth could be invested into inputs, such as fertilizer, or more productive technologies that may counteract the effects of mining-induced

pollution on crop health. Alternatively, increased wealth could be used to treat health issues arising from exposure to polluted air or water.

Is it realistic for increased wealth from mining activity to offset the effects of increased pollution? Existing work has documented large and statistically significant wealth increases from mining, with household wealth in the medium run rising by about 0.3 standard deviations for those in the vicinity of a mine [von der Goltz and Barnwal, 2019]. The authors argue that this effect is comparable to having an electricity connection or living in a dwelling with finished flooring in the case of Peru in the year 2000, and to the effect of owning a motorbike or mobile phone in the case of Burkina Faso, in the year 2010.

A thorough investigation of the magnitude and the mechanisms through which increased wealth may offset pollution from mines would require detailed geo-located survey data that covers household agricultural input use and health behaviors, before and after a mine opening. While some data sources that cover this information do exist, such as the LSMS-ISA, their spatial and temporal coverage does not align with the timing and location of mine openings in my sample. As a result, this analysis is beyond the scope of my paper.

Importantly, while the overall and pollution-specific DID estimates may suffer from attenuation bias due to measurement error in remotely-sensed NDVI, as discussed in Section FIXME, this bias should not effect the estimate of the share of the overall effect attributed to pollution. Assuming that conditional on covariates, NDVI errors are uncorrelated with the timing of a mine opening, as well as proximity to a mine or topographical placement relative to the mine, we can still uncover a consistent estimate of the share of the overall effect attributed to pollution as the remaining mean-reverting measurement error that is common to remotely-sensed variables will cancel out when taking the ratio of the pollution effect to the overall effect. Further details are discussed in Appendix 12.13. This suggests that my finding that pollution explains almost half of the overall reductions of yields caused by mining is still informative, even in the presence of measurement error.

10.2 Translating NDVI Effects to Yield Effects

To map NDVI effects to yield effects, I estimate the correlation between actual maize yields from plots of smallholder farmers across Africa and NDVI local to these plots. Data on maize yields, defined in kilograms of maize produced per hectare, are obtained from Aramburu-Merlos et al. [2024]. This dataset covers over 13,000 smallholder farms across 7 countries: Burundi, Uganda, Nigeria, Tanzania, Kenya, Rwanda and Zambia. It is a repeated-cross section, where measurements are taken over the 2016-2022 time period from different plots located in similar areas. The data from Aramburu-Merlos et al. [2024] was collected by One Acre Fund, an NGO that provides smallholder farmers with access to credit, training, crop insurance and farming supplies. Maize yields for

each farmer at the time of harvest were measured in two randomly spaced boxes of 36 square meters, avoiding field edges. While farm size is not provided in the public data of Aramburu-Merlos et al. [2024], African agriculture is dominated by small farms, typically defined as less than 1 acre [Carletto et al., 2015].

To link plot-level yields to NDVI, I define a grid of 1km x 1km cells over the study areas in Aramburu-Merlos et al. [2024]. Each plot is linked to a grid-cell using plot GPS coordinates. I opt for the 1km x 1km grid cell to limit the influence of inaccuracies in plot coordinates [Jin et al., 2017]. While I do not observe the same plots over time, most grid cells can be observed for at least 2 different years. For each grid cell, I calculate mean NDVI across pixels falling within the cell for each season from 2016-2022. Mean seasonal NDVI at the cell-year level is then linked to the average of observed yields across all plots in the corresponding cell-year.

I run the following regression to estimate the relationship between remotely-sensed yields and actual yields measured from One Acre Fund cropcuts, separately for each season:

$$Yield_{ct} = \alpha_c + \lambda_t + \beta_{NDVI} NDVI_{ct} + \Gamma X_{pct} + \epsilon_{pct} \tag{7}$$

where $Yield_{ct}$ is mean maize yields in kg/ha across all plots p in cell c in year t and $NDVI_{ct}$ is mean NDVI in one of the five seasons. I include grid-cell and year fixed effects, as well as cell-level controls for the average number of maize growing degree days, average precipitation over the maize season and average temperature over the maize season from Aramburu-Merlos et al. [2024], across all plots within a cell-year. I also include cell-level weather variables, such as mean cloud cover and evapotranspiration from Harris et al. [2014]. $NDVI_{ct}$ is scaled so that β_{NDVI} reflects the effect of a 0.01 unit increase in NDVI on maize yields. Inclusion of weather controls and fixed effects help limit omitted variable bias in estimation of β_{NDVI} due to NDVI detection errors. These errors can driven by a variety of factors, most notably cloud cover, but also surface reflectance, canopy thickness, the level of atmospheric aerosols and sensor errors. Detection errors make NDVI observed from satellite data an imperfect measure of NDVI in the presence of no detection errors. While some types of detection errors, such as satellite sensor errors, are likely uncorrelated with plot-level yields, detection errors driven by cloud cover or aerosol loading could be correlated with plot-level yields through the direct effect of atmospheric determinants on crop health.

Table 5 shows that on average, a 0.01 unit increase in NDVI is associated with a statistically significant 52.10 kg/ha increase in maize yields during the early growing season, with smaller increases in other seasons. This is supported by existing literature, which also finds that NDVI is a strong predictor of yields specifically during the early stages of growing [Panek and Gozdowski, 2021]. Linking this result to the overall effect of mining on NDVI of -0.00691 suggests that on average, industrial mining reduces actual yields for a

smallholder farmer by about 36 kilograms per hectare. This corresponds to about a 1.2 % decrease in actual yields relative to the mean of 3000 kg/ha, which is a fifth of the magnitude of the reduction in yields caused by an additional dust storm in Iran [Birjandi-Feriz and Yousefi, 2017] or the reduction in yields caused by the Acid Rain Program in the USA [Sanders and Barreca, 2022]. Importantly, these other estimates were generated using administrative data on yields, so may not not suffer from attenuation bias due to measurement error common to remotely sensed variables. Furthermore, this 1.2% decrease represents an "average" effect: yield reductions in areas with poor governance and regulatory quality can be over 3 times larger, which would be on par with the magnitudes estimated in other contexts.

Table 5: Relationship between Cell-level NDVI and Cell-level Yields, cell-size = 1000m

| | (1) | (2) | (3) | (4) | (5) |
	Planting	Early Growing	Late Growing	Harvest	Nonfarm
Mean NDVI	11.83	52.10**	20.25	24.43	9.937
	(16.42)	(22.04)	(21.11)	(17.69)	(14.62)
Year FE	Yes	Yes	Yes	Yes	Yes
Grid cell FE	Yes	Yes	Yes	Yes	Yes
Include weather controls	Yes	Yes	Yes	Yes	Yes
Mean Yields	3005.643	3005.643	3005.643	3005.643	3005.643
Obs.	1127	1153	1153	1141	1153
R-sq	0.631	0.638	0.632	0.634	0.632

Each column reports the results of an OLS regression. The unit of observation is a cell-year. The dependent variable is mean plot-level yields in kg/ha across all plots falling within a cell, in a given year. *Mean NDVI* is the average NDVI in the cell of size 1000m containing the plot, across days in a particular season during the year that maize on the plot was harvested. The columns indicate the season for which NDVI is calculated during the year the plot was harvested. *Mean NDVI* is scaled so that one unit represents a 0.01 increase in NDVI. Each regression includes linear controls for cell-level averages of growing degree days, temperature and precipitation during the maize season across plots falling within the cell, as well as cell-level controls for mean temperature, precipitation, vapor pressure, cloud cover, evapotranspiration and wet days. Year and cell-level fixed effects are included in the regressions.

Table 5 also shows that the NDVI model at the cell-level explains over 50% of the variation in plot-level yields, which is similar to the R^2 found in other work linking the One Acre Fund data to remotely sensed yields (Burke and Lobell [2017]; Jin et al. [2017]). Conditional on observing a sufficiently high R^2, in Appendix 12.13 I discuss whether the estimated relationship between NDVI and local yields from Equation 7 may be biased in my setting, even after controlling for fixed effects and weather. Furthermore, Appendix Tables 21 - 23 demonstrate robustness to varying the size of the grid cell used in the quantification exercise, consistently showing that NDVI during the growing season is most strongly correlated with observed plot-level yields.

11 Discussion

This paper quantifies the extent to which industrial mining affects local agricultural output through pollution externalities versus local demand shocks that raise the returns to inputs outside of agriculture. To isolate

the effect of pollution, I link mine geo-locations to remotely sensed measures of pollution and crop yields in a spatial difference-in-difference design that leverages variation in pollution exposure around a mine driven by topography or weather, which are plausibly exogenous to local market conditions.

A main contribution of my paper is to document the magnitude of increased air and water pollution from mining activity, then estimate the resulting externalities on local yields. While mining increases water and air pollution in exposed areas, the externalities on yields are economically small, on average. Mining leads to statistically significant reductions in yields of about 3-4% through the water pollution channel, with no effect on local yields occurring via air pollution.

Differential cost of abatement is one potential explanation for the larger effect of water pollution. In contrast to technologies designed to abate air pollution from mines, such as gas scrubbers to remove sulfur dioxide or frequent water spraying to limit dust pollution, abatement technologies for acid mine drainage are relatively new and more expensive, often requiring the construction of a separate wastewater treatment plant (Matebese et al. [2024], Hilson [2000], Ghose and Majee [2001]).

Additionally, water pollution from mining may be more challenging to regulate than air pollution due higher monitoring costs and larger contributions of informal mining operations to pollution. While low cost air quality monitors that collect frequent data are readily available, equivalents for water pollution are not. For instance, testing only ten water samples can cost 200 USD, which is equivalent to the cost of a Purple Air monitor that can collect real-time air pollution data over two years. This lack of cost-effective options creates a dearth of up-to-date measures of water quality in African mining areas, which makes monitoring and enforcement of mining companies difficult. Furthermore, while air pollution is usually generated by the advanced machinery used by large-scale mining companies, water pollution is often linked to artisanal and illegal mines (ASM) operating on the fringes of large-scale operations near streams and rivers (Duncan [2020], Darko et al. [2023]). ASM often uses more harmful extraction methods than those used by large-scale companies, such as highly toxic mercury to separate gold from the ore. However, while large-scale companies face government monitoring and regulation, informal ASM operations are not subject to the same level of scrutiny.

To understand the extent to which pollution drives the observed decline in agriculture caused by mining, I benchmark my estimates of the effects of air and water pollution on yields against an estimate of the "overall" effect of mining on yields that captures both pollution externalities and raising the returns to inputs outside of agriculture. I find that pollution externalities account for almost half of the overall effect on yields, suggesting that declines in local agriculture should not be interpreted as purely driven by positive structural transformation. Importantly, average effects mask substantial heterogeneity across mines, with both "standard" heterogeneity analysis and a machine learning approach revealing that poor governance and

regulatory environments drive larger reductions in local yields.

At first glance, my findings of small negative pollution externalities coupled with evidence on mining's large, positive structural transformation effects (Aragón and Rud [2013], Huang et al. [2023], Kotsadam and Tolonen [2016], Benshaul-Tolonen [2020], von der Goltz and Barnwal [2019]) might suggest that local governments should promote investment in mining activities. However, this policy implication fails to account for persistence of mining pollution externalities and structural transformation in the long run. Given that structural transformation in mining areas seems to be driven by backwards linkages [Aragón and Rud, 2013], that is the development of new industries and services to support the mine, absent sufficiently large agglomeration effects local economic booms from natural resource extraction may fade once a mine has closed [Black et al., 2005]. In contrast, the effects of mining pollution on local agriculture may last for decades [Akcil and Koldas, 2006]. If pollution has driven the agricultural sector to a lower, less productive equilibrium, a shift back into agriculture following the closure of a mine may result in lower standards of living for mining communities than those that had existed before the mine first opened.

Policymakers in Sub-Saharan Africa may be averse to enacting more stringent environmental regulations and penalties on mining companies, out of fear of discouraging investment that may boost local development [Keller and Levinson, 2002]. An attractive alternative policy option may be one that encourages the persistence of structural transformation effects by subsidizing the outputs of non-agricultural sectors stimulated by mining's backward linkages, or one that provides incentives for restoration of agricultural land at the end of a mine's operations. Designing the right type of policy to address the trade-off between local economic development and environmental quality in mining communities may be best informed by a model of the long-run welfare effects of mining on local communities that allows for the simulation of counterfactual policy scenarios. While this type of analysis is beyond the scope of this paper, it is a ripe area for future research.

References

Daron Acemoglu, Simon Johnson, and James Robinson. Institutions as the fundamental cause of long-run growth. *The Handbook of Economic Growth*, 2005. URL https://www.wcfia.harvard.edu/sites/projects.iq.harvard.edu/files/wcfia/files/894_jr_handbook9sj.pdf.

Ata Akcil and Soner Koldas. Acid Mine Drainage (AMD): causes, treatment and case studies. *Journal of Cleaner Production*, 14(12):1139–1145, January 2006. ISSN 0959-6526. doi: 10.1016/j.jclepro.2004.09.006. URL https://www.sciencedirect.com/science/article/pii/S0959652605000600.

Richard Amoh-Gyimah and Eric Nimako Aidoo. Mode of transport to work by government employees in the Kumasi metropolis, Ghana. *Journal of Transport Geography*, 31:35–43, July 2013. ISSN 0966-6923. doi: 10.1016/j.jtrangeo.2013.05.008. URL `https://www.sciencedirect.com/science/article/pii/S0966692313000859`.

Donald W. K. Andrews. Tests for Parameter Instability and Structural Change With Unknown Change Point. *Econometrica*, 61(4):821–856, 1993. ISSN 0012-9682. doi: 10.2307/2951764. URL `https://www.jstor.org/stable/2951764`. Publisher: [Wiley, Econometric Society].

Donald W. K. Andrews and Werner Ploberger. Optimal Tests when a Nuisance Parameter is Present Only Under the Alternative. *Econometrica*, 62(6):1383–1414, 1994. ISSN 0012-9682. doi: 10.2307/2951753. URL `https://www.jstor.org/stable/2951753`. Publisher: [Wiley, Econometric Society].

Fernando M. Aragón and Juan Pablo Rud. Natural Resources and Local Communities: Evidence from a Peruvian Gold Mine. *American Economic Journal: Economic Policy*, 5(2):1–25, May 2013. ISSN 1945-7731. doi: 10.1257/pol.5.2.1. URL `https://www.aeaweb.org/articles?id=10.1257/pol.5.2.1`.

Fernando M. Aragón and Juan Pablo Rud. Polluting Industries and Agricultural Productivity: Evidence from Mining in Ghana. *The Economic Journal*, 126(597):1980–2011, 2016. ISSN 1468-0297. doi: 10.1111/ecoj.12244. URL `https://onlinelibrary.wiley.com/doi/abs/10.1111/ecoj.12244`. _eprint: https://onlinelibrary.wiley.com/doi/pdf/10.1111/ecoj.12244.

Fernando Aramburu-Merlos, Fatima A. M. Tenorio, Nester Mashingaidze, Alex Sananka, Stephen Aston, Jonathan J. Ojeda, and Patricio Grassini. Adopting yield-improving practices to meet maize demand in Sub-Saharan Africa without cropland expansion. *Nature Communications*, 15(1):4492, May 2024. ISSN 2041-1723. doi: 10.1038/s41467-024-48859-0. URL `https://www.nature.com/articles/s41467-024-48859-0`. Publisher: Nature Publishing Group.

Sam Asher and Paul Novosad. Rent-Seeking and Criminal Politicians: Evidence from Mining Booms | The Review of Economics and Statistics | MIT Press. *The Review of Economics and Statistics*, 2023. URL `https://direct.mit.edu/rest/article/105/1/20/102838/Rent-Seeking-and-Criminal-Politicians-Evidence`.

Sebastian Axbard, Anja Benshaul-Tolonen, and Jonas Poulsen. Natural resource wealth and crime: The role of international price shocks and public policy. *Journal of Environmental Economics and Management*, 110:102527, October 2021. ISSN 0095-0696. doi: 10.1016/j.jeem.2021.102527. URL `https://www.sciencedirect.com/science/article/pii/S0095069621000905`.

Oscar Barriga-Cabanillas, Mira Korb, and Travis Lybbert. Time is (not) Money: The decay of machine learning models to predict wealth using cellphone data. *Working Paper*, 2024.

A. Patrick Behrer and Sherrie Wang. Current benefits of wildfire smoke for yields in the US Midwest may dissipate by 2050. *Environmental Research Letters*, 19(8):084010, July 2024. ISSN 1748-9326. doi: 10.1088/1748-9326/ad5458. URL `https://dx.doi.org/10.1088/1748-9326/ad5458`. Publisher: IOP Publishing.

Anja Benshaul-Tolonen. Local Industrial Shocks and Infant Mortality. *The Economic Journal*, n/a(n/a), 2020. ISSN 1468-0297. doi: 10.1111/ecoj.12625. URL `https://onlinelibrary.wiley.com/doi/abs/10.1111/ecoj.12625`. _eprint: https://onlinelibrary.wiley.com/doi/pdf/10.1111/ecoj.12625.

Nicolas Berman, Mathieu Couttenier, Dominic Rohner, and Mathias Thoenig. This Mine is Mine! How Minerals Fuel Conflicts in Africa. *American Economic Review*, 107(6):1564–1610, June 2017. ISSN 0002-8282. doi: 10.1257/aer.20150774. URL `https://pubs.aeaweb.org/doi/10.1257/aer.20150774`.

Maliheh Birjandi-Feriz and Kowsar Yousefi. When the Dust Settles: Productivity and Economic Losses Following Dust Storms, November 2017. URL `https://papers.ssrn.com/abstract=3230265`.

Dan Black, Terra McKinnish, and Seth Sanders. The Economic Impact of the Coal Boom and Bust. *The Economic Journal*, 115(503):449–476, April 2005. ISSN 0013-0133. doi: 10.1111/j.1468-0297.2005.00996.x. URL `https://doi.org/10.1111/j.1468-0297.2005.00996.x`.

Leonardo Bonilla Mejía. Mining and human capital accumulation: Evidence from the Colombian gold rush. *Journal of Development Economics*, 145:102471, June 2020. ISSN 0304-3878. doi: 10.1016/j.jdeveco.2020.102471. URL `https://www.sciencedirect.com/science/article/pii/S0304387820300468`.

Robin Burgess, Matthew Hansen, Benjamin A. Olken, Peter Potapov, and Stefanie Sieber. The Political Economy of Deforestation in the Tropics*. *The Quarterly Journal of Economics*, 127(4):1707–1754, November 2012. ISSN 0033-5533. doi: 10.1093/qje/qjs034. URL `https://doi.org/10.1093/qje/qjs034`.

Marshall Burke and David B. Lobell. Satellite-based assessment of yield variation and its determinants in smallholder African systems. *Proceedings of the National Academy of Sciences*, 114(9):2189–2194, February 2017. doi: 10.1073/pnas.1616919114. URL `https://www.pnas.org/doi/abs/10.1073/pnas.1616919114`. Publisher: Proceedings of the National Academy of Sciences.

Jennifer Burney and V. Ramanathan. Recent climate and air pollution impacts on indian agriculture. *PNAS*, 111, 2014. doi: 10.1073/pnas.1317275111. URL `https://www.pnas.org/doi/10.1073/pnas.1317275111`.

Calogero Carletto, Sydney Gourlay, and Paul Winters. From Guesstimates to GPStimates: Land Area Measurement and Implications for Agricultural Analysis. *Journal of African Economies*, 24(5):593–628, November 2015. ISSN 0963-8024, 1464-3723. doi: 10.1093/jae/ejv011. URL `https://academic.oup.com/jae/article-lookup/doi/10.1093/jae/ejv011`.

Francesco Caselli and Guy Michaels. Do Oil Windfalls Improve Living Standards? Evidence from Brazil. *American Economic Journal: Applied Economics*, 5(1):208–238, January 2013. ISSN 1945-7782. doi: 10.1257/app.5.1.208. URL `https://www.aeaweb.org/articles?id=10.1257/app.5.1.208`.

Shuai Chen, Paulina Oliva, and Peng Zhang. The effect of air pollution on migration: Evidence from China. *Journal of Development Economics*, 156:102833, May 2022. ISSN 0304-3878. doi: 10.1016/j.jdeveco.2022.102833. URL `https://www.sciencedirect.com/science/article/pii/S0304387822000153`.

Wenjie Chen, Paola Ganum, Athene Laws, Hamza Mighri, Balazs Stadler, Nico Valckx, and David Zeledon. Digging for opportunity: Harnessing sub-saharan africa's wealth in critical minerals. *The International Monetary Fund, Regional Economic Outlook: Sub-Saharan Africa*, 2024. URL `https://www.imf.org/en/Publications/REO/SSA/Issues/2024/04/19/regional-economic-outlook-for-sub-saharan-africa-april-2024`.

Burhan U. Choudhury, Akbar Malang, Richard Webster, Kamal P. Mohapatra, Bibhash C. Verma, Manoj Kumar, Anup Das, Mokidul Islam, and Samarendra Hazarika. Acid drainage from coal mining: Effect on paddy soil and productivity of rice. *The Science of the Total Environment*, 583:344–351, April 2017. ISSN 1879-1026. doi: 10.1016/j.scitotenv.2017.01.074.

Seydou Coulibaly and Abdramane Camara. The end of tax incentives in mining? Tax policy and mining foreign direct investment in Africa. *African Development Review*, 34(S1):S177–S194, 2022. ISSN 1467-8268. doi: 10.1111/1467-8268.12651. URL `https://onlinelibrary.wiley.com/doi/abs/10.1111/1467-8268.12651`. _eprint: https://onlinelibrary.wiley.com/doi/pdf/10.1111/1467-8268.12651.

James Cust and Albert Zeufack. Africa's Resource Future. 2023. URL `https://documents.worldbank.org/en/publication/documents-reports/documentdetail/099080123145011993/p16722906c03ca09409ace06cb32991395b`.

James Cust, Torfinn Harding, Hanna Krings, and Alexis Rivera-Ballesteros. Public governance versus corporate governance: Evidence from oil drilling in forests. *Journal of Development Economics*, 163:103070, June 2023. ISSN 0304-3878. doi: 10.1016/j.jdeveco.2023.103070. URL `https://www.sciencedirect.com/science/article/pii/S0304387823000251`.

Humphrey Ferdinand Darko, Anthony Yaw Karikari, Anthony Appiah Duah, Bismark Awinbire Akurugu, Victor Mante, and Frank Oblim Teye. Effect of small-scale illegal mining on surface water and sediment quality in Ghana. *International Journal of River Basin Management*, July 2023. ISSN 1571-5124. URL `https://www.tandfonline.com/doi/abs/10.1080/15715124.2021.2002345`. Publisher: Taylor & Francis.

Dominik Dietler, Andrea Farnham, Georg Loss, Günther Fink, and Mirko S. Winkler. Impact of mining projects on water and sanitation infrastructures and associated child health outcomes: a multi-country analysis of Demographic and Health Surveys (DHS) in sub-Saharan Africa. *Globalization and Health*, 17 (1):70, June 2021. ISSN 1744-8603. doi: 10.1186/s12992-021-00723-2.

Stanislaw Dudka and Domy C. Adriano. Environmental Impacts of Metal Ore Mining and Processing: A Review. *Journal of Environmental Quality*, 26(3):590–602, 1997. ISSN 1537-2537. doi: 10.2134/jeq1997.00472425002600030003x. URL `https://onlinelibrary.wiley.com/doi/abs/10.2134/jeq1997.00472425002600030003x`. _eprint: https://onlinelibrary.wiley.com/doi/pdf/10.2134/jeq1997.00472425002600030003x.

Albert Ebo Duncan. The Dangerous Couple: Illegal Mining and Water Pollution—A Case Study in Fena River in the Ashanti Region of Ghana. *Journal of Chemistry*, 2020(1):2378560, 2020. ISSN 2090-9071. doi: 10.1155/2020/2378560. URL `https://onlinelibrary.wiley.com/doi/abs/10.1155/2020/2378560`. _eprint: https://onlinelibrary.wiley.com/doi/pdf/10.1155/2020/2378560.

Fabian Ekert, John Juneau, and Michael Peters. Sprouting Cities: How Rural America Industrialized. *AEA Papers and Proceedings*, 113:87–92, May 2023. doi: 10.1257/pandp.20231075. URL `https://ideas.repec.org/a/aea/apandp/v113y2023p87-92.html`.

Kyle Emerick. Trading frictions in Indian village economies. *Journal of Development Economics*, 132:32–56, May 2018. ISSN 0304-3878. doi: 10.1016/j.jdeveco.2017.12.010. URL `https://www.sciencedirect.com/science/article/pii/S0304387817301293`.

Zhaozhong Feng and Kazuhiko Kobayashi. Assessing the impacts of current and future concentrations of surface ozone on crop yield with meta-analysis. *Atmospheric Environment*, 43(8):1510–1519, March 2009. ISSN 1352-2310. doi: 10.1016/j.atmosenv.2008.11.033. URL `https://www.sciencedirect.com/science/article/pii/S1352231008010972`.

J. Gardelle, P. Hiernaux, L. Kergoat, and M. Grippa. Less rain, more water in ponds: a remote sensing study of the dynamics of surface waters from 1950 to present in pastoral sahel (gourma region, mali).

Hydrology and Earth System Sciences, 14(2):309–324, 2010. doi: 10.5194/hess-14-309-2010. URL `https://hess.copernicus.org/articles/14/309/2010/`.

Nicolas Gendron-Carrier, Marco Gonzalez-Navarro, Stefano Polloni, and Matthew A. Turner. Subways and Urban Air Pollution. *American Economic Journal: Applied Economics*, 14(1):164–196, January 2022. ISSN 1945-7782. doi: 10.1257/app.20180168. URL `https://www.aeaweb.org/articles?id=10.1257/app.20180168`.

M. K. Ghose and S. R. Majee. Air pollution caused by opencast mining and its abatement measures in India. *Journal of Environmental Management*, 63(2):193–202, October 2001. ISSN 0301-4797. doi: 10.1006/jema.2001.0434. URL `https://www.sciencedirect.com/science/article/pii/S0301479701904347`.

M. K. Ghose and S. R. Majee. Assessment of the Status of Work Zone Air Environment Due to Opencast Coal Mining. *Environmental Monitoring and Assessment*, 77(1):51–60, July 2002. ISSN 1573-2959. doi: 10.1023/A:1015719625745. URL `https://doi.org/10.1023/A:1015719625745`.

Lutz Goedde, Amandla Ooko-Ombaka, and Gillian Pais. Winning in Africa's agricultural market, 2019. URL `https://www.mckinsey.com/industries/agriculture/our-insights/winning-in-africas-agricultural-market`.

Joshua Graff Zivin and Matthew Neidell. The Impact of Pollution on Worker Productivity. *American Economic Review*, 102(7):3652–3673, December 2012. ISSN 0002-8282. doi: 10.1257/aer.102.7.3652. URL `https://www.aeaweb.org/articles?id=10.1257/aer.102.7.3652`.

Zerihun Anbesa Gurmu, Henk Ritzema, Charlotte de Fraiture, and Mekonen Ayana. Sedimentation in small-scale irrigation schemes in Ethiopia: Its sources and management. *International Journal of Sediment Research*, 37(5):576–588, October 2022. ISSN 1001-6279. doi: 10.1016/j.ijsrc.2022.02.006. URL `https://www.sciencedirect.com/science/article/pii/S1001627922000129`.

Emilio Gutiérrez and Kensuke Teshima. Abatement expenditures, technology choice, and environmental performance: Evidence from firm responses to import competition in Mexico. *Journal of Development Economics*, 133:264–274, July 2018. ISSN 0304-3878. doi: 10.1016/j.jdeveco.2017.11.004. URL `https://www.sciencedirect.com/science/article/pii/S0304387817301037`.

I. Harris, P.D Jones, T.J. Osborn, , and D.H. Lister. Updated high-resolution grids of monthly climatic observations—cru ts3.26 dataset. *International Journal of Climatology*, 2014.

Jiaxiu He, Haoming Liu, and Alberto Salvo. Severe Air Pollution and Labor Productivity: Evidence from Industrial Towns in China. *American Economic Review*, 11, 2019. doi: 10.1257/app.20170286. URL `https://www.aeaweb.org/articles?id=10.1257/app.20170286`.

Matias Heino, Pekka Kinnunen, Weston Anderson, Deepak K. Ray, Michael J. Puma, Olli Varis, Stefan Siebert, and Matti Kummu. Increased probability of hot and dry weather extremes during the growing season threatens global crop yields. *Scientific Reports*, 13(1):3583, March 2023. ISSN 2045-2322. doi: 10. 1038/s41598-023-29378-2. URL `https://www.nature.com/articles/s41598-023-29378-2`. Publisher: Nature Publishing Group.

Gavin Hilson. Pollution prevention and cleaner production in the mining industry: an analysis of current issues. *Journal of Cleaner Production*, 8(2):119–126, April 2000. ISSN 0959-6526. doi: 10.1016/S0959-6526(99)00320-0. URL `https://www.sciencedirect.com/science/article/pii/S0959652699003200`.

Qing Huang, Victoria Wenxin Xie, and Wei You. Resource Rents, Urbanization, and Structural Transformation. *SSRN Electronic Journal*, 2023. ISSN 1556-5068. doi: 10.2139/ssrn.4543449. URL `https://www.ssrn.com/abstract=4543449`.

Thomas C. Hutchinson. Adaptation of Plants to Atmospheric Pollutants. In *Ciba Foundation Symposium 102 - Origins and Development of Adaptation*, pages 52–72. John Wiley & Sons, Ltd, 1984. ISBN 978-0-470-72083-7. doi: 10.1002/9780470720837.ch5. URL `https://onlinelibrary.wiley.com/doi/abs/10.1002/9780470720837.ch5`. Section: 5 _eprint: https://onlinelibrary.wiley.com/doi/pdf/10.1002/9780470720837.ch5.

Md. Monirul Islam and Kimiteru Sado. Analyses of aster and spectroradiometer data with in situ measurements for turbidity and transparency study of lake abashiri. *International journal of geoinformatics*, 2, 2006. URL `https://api.semanticscholar.org/CorpusID:126540631`.

Zhenong Jin, George Azzari, Marshall Burke, Stephen Aston, and David B. Lobell. Mapping Smallholder Yield Heterogeneity at Multiple Scales in Eastern Africa. *Remote Sensing*, 9(9):931, September 2017. ISSN 2072-4292. doi: 10.3390/rs9090931. URL `https://www.mdpi.com/2072-4292/9/9/931`. Number: 9 Publisher: Multidisciplinary Digital Publishing Institute.

Daniel Kaufmann, Aart Kraay, and Massimo Mastruzzi. The Worldwide Governance Indicators: Methodology and Analytical Issues, September 2010. URL `https://papers.ssrn.com/abstract=1682130`.

Wolfgang Keller and Arik Levinson. Pollution Abatement Costs and Foreign Direct Investment Inflows to U.S. States. *The Review of Economics and Statistics*, 84(4):691–703, November 2002. ISSN 0034-6535. doi: 10.1162/003465302760556503. URL `https://doi.org/10.1162/003465302760556503`.

Andreas Kotsadam and Anja Tolonen. African Mining, Gender, and Local Employment. *World Development*, 83:325–339, July 2016. ISSN 0305-750X. doi: 10.1016/j.worlddev.2016.01.007. URL `https://www.sciencedirect.com/science/article/pii/S0305750X1600005X`.

Kevin S. Kung, Kael Greco, Stanislav Sobolevsky, and Carlo Ratti. Exploring Universal Patterns in Human Home-Work Commuting from Mobile Phone Data. *PLOS ONE*, 9(6):e96180, June 2014. ISSN 1932-6203. doi: 10.1371/journal.pone.0096180. URL `https://journals.plos.org/plosone/article?id=10.1371/journal.pone.0096180`. Publisher: Public Library of Science.

J. P. Lacaux, Y. M. Tourre, C. Vignolles, J. A. Ndione, and M. Lafaye. Classification of ponds from high-spatial resolution remote sensing: Application to Rift Valley Fever epidemics in Senegal. *Remote Sensing of Environment*, 106(1):66–74, January 2007. ISSN 0034-4257. doi: 10.1016/j.rse.2006.07.012. URL `https://www.sciencedirect.com/science/article/pii/S0034425706002811`.

D. J. Lapworth, D. C. W. Nkhuwa, J. Okotto-Okotto, S. Pedley, M. E. Stuart, M. N. Tijani, and J. Wright. Urban groundwater quality in sub-Saharan Africa: current status and implications for water security and public health. *Hydrogeology Journal*, 25(4):1093–1116, 2017. ISSN 1431-2174. doi: 10.1007/s10040-016-1516-6. URL `https://www.ncbi.nlm.nih.gov/pmc/articles/PMC6991975/`.

R.C. Levy, S. Mattoo, L.A. Munchak, L.A. Remer, A.M. Sayer, F. Patadia, and N.C. Hsu. The collection 6 modis aerosol products over land and ocean. *Atmospheric Measurement Techniques*, 2013.

Molly Lipscomb and Ahmed Mushfiq Mobarak. Decentralization and Pollution Spillovers: Evidence from the Re-drawing of County Borders in Brazil*. *The Review of Economic Studies*, 84(1):464–502, January 2017. ISSN 0034-6527. doi: 10.1093/restud/rdw023. URL `https://doi.org/10.1093/restud/rdw023`.

Peng Liu, Qiumei Wu, Wenyou Hu, Kang Tian, Biao Huang, and Yongcun Zhao. Effects of atmospheric deposition on heavy metals accumulation in agricultural soils: Evidence from field monitoring and Pb isotope analysis. *Environmental Pollution*, 330:121740, August 2023. ISSN 0269-7491. doi: 10.1016/j.envpol.2023.121740. URL `https://www.sciencedirect.com/science/article/pii/S026974912300742X`.

Xiang Liu and Ankur R. Desai. Significant Reductions in Crop Yields From Air Pollution and Heat Stress in the United States. *Earth's Future*, 9(8):e2021EF002000, 2021. ISSN 2328-4277. doi:

10.1029/2021EF002000. URL `https://onlinelibrary.wiley.com/doi/abs/10.1029/2021EF002000`. _eprint: https://onlinelibrary.wiley.com/doi/pdf/10.1029/2021EF002000.

Davis Lobell, Stefania Di Tomasso, and Jennifer Burney. Globally ubiquitous negative effects of nitrogen dioxide on crop growth. *Science Advances*, 2022. doi: 10.1126/sciadv.abm9909. URL `https://www.science.org/doi/10.1126/sciadv.abm9909`.

Bahati A. Magesa, Geetha Mohan, Hirotaka Matsuda, Indrek Melts, Mohamed Kefi, and Kensuke Fukushi. Understanding the farmers' choices and adoption of adaptation strategies, and plans to climate change impact in Africa: A systematic review. *Climate Services*, 30:100362, April 2023. ISSN 2405-8807. doi: 10.1016/j.cliser.2023.100362. URL `https://www.sciencedirect.com/science/article/pii/S2405880723000237`.

Funeka Matebese, Alseno K. Mosai, Hlanganani Tutu, and Zenixole R. Tshentu. Mining wastewater treatment technologies and resource recovery techniques: A review. *Heliyon*, 10(3):e24730, February 2024. ISSN 2405-8440. doi: 10.1016/j.heliyon.2024.e24730. URL `https://www.sciencedirect.com/science/article/pii/S2405844024007618`.

Phenny Mwaanga, Mathews Silondwa, George Kasali, and Paul M. Banda. Preliminary review of mine air pollution in Zambia. *Heliyon*, 5(9):e02485, September 2019. ISSN 2405-8440. doi: 10.1016/j.heliyon.2019.e02485. URL `https://www.sciencedirect.com/science/article/pii/S2405844019361456`.

Tom Myers. Acid mine drainage risks – A modeling approach to siting mine facilities in Northern Minnesota USA. *Journal of Hydrology*, 533:277–290, February 2016. ISSN 00221694. doi: 10.1016/j.jhydrol.2015.12.020. URL `https://linkinghub.elsevier.com/retrieve/pii/S0022169415009683`.

Amanda Rose Newton and Rajesh Melaram. Harmful algal blooms in agricultural irrigation: risks, benefits, and management. *Frontiers in Water*, 5, November 2023. ISSN 2624-9375. doi: 10.3389/frwa.2023.1325300. URL `https://www.frontiersin.org/journals/water/articles/10.3389/frwa.2023.1325300/full`. Publisher: Frontiers.

Elina Oksanen and Sari Kontunen-Soppela. Plants have different strategies to defend against air pollutants. *Current Opinion in Environmental Science & Health*, 19:100222, February 2021. ISSN 2468-5844. doi: 10.1016/j.coesh.2020.10.010. URL `https://www.sciencedirect.com/science/article/pii/S2468584420300738`.

Ewa Panek and Dariusz Gozdowski. Relationship between MODIS Derived NDVI and Yield of Cereals for Selected European Countries. *Agronomy*, 11(2):340, February 2021. ISSN 2073-4395. doi:

10.3390/agronomy11020340. URL `https://www.mdpi.com/2073-4395/11/2/340`. Number: 2 Publisher: Multidisciplinary Digital Publishing Institute.

Aditya Kumar Patra, Sneha Gautam, and Prashant Kumar. Emissions and human health impact of particulate matter from surface mining operation—A review. *Environmental Technology & Innovation*, 5: 233–249, April 2016. ISSN 2352-1864. doi: 10.1016/j.eti.2016.04.002. URL `https://www.sciencedirect.com/science/article/pii/S2352186416300153`.

E. Petavratzi, S. Kingman, and I. Lowndes. Particulates from mining operations: A review of sources, effects and regulations. *Minerals Engineering*, 18(12):1183–1199, October 2005. ISSN 0892-6875. doi: 10.1016/j.mineng.2005.06.017. URL `https://www.sciencedirect.com/science/article/pii/S0892687505002050`.

Jonathan Proctor, Tamma Carleton, and Sandy Sum. Parameter Recovery Using Remotely Sensed Variables. *NBER Working Paper*, 2023. URL `http://www.nber.org/papers/w30861`.

Tomás Rau, Sergio Urzúa, and Loreto Reyes. Early Exposure to Hazardous Waste and Academic Achievement: Evidence from a Case of Environmental Negligence. *Journal of the Association of Environmental and Resource Economists*, 2(4):527–563, December 2015. ISSN 2333-5955. doi: 10.1086/683112. URL `https://www.journals.uchicago.edu/doi/full/10.1086/683112`. Publisher: The University of Chicago Press.

Jason Russ, Esha Zaveri, Sebastien Desbureaux, Richard Damania, and Aude-Sophie Rodella. The impact of water quality on GDP growth: Evidence from around the world. *Water Security*, 17:100130, December 2022. ISSN 2468-3124. doi: 10.1016/j.wasec.2022.100130. URL `https://www.sciencedirect.com/science/article/pii/S2468312422000219`.

William J. Sacks, Delphine Deryng, Jonathan A. Foley, and Navin Ramankutty. Crop planting dates: an analysis of global patterns. *Global Ecology and Biogeography*, 19(5):607–620, 2010. ISSN 1466-8238. doi: 10.1111/j.1466-8238.2010.00551.x. URL `https://onlinelibrary.wiley.com/doi/abs/10.1111/j.1466-8238.2010.00551.x`. _eprint: https://onlinelibrary.wiley.com/doi/pdf/10.1111/j.1466-8238.2010.00551.x.

H. B. Sahu, N. Prakash, and S. Jayanthu. Underground Mining for Meeting Environmental Concerns – A Strategic Approach for Sustainable Mining in Future. *Procedia Earth and Planetary Science*, 11:232–241, January 2015. ISSN 1878-5220. doi: 10.1016/j.proeps.2015.06.030. URL `https://www.sciencedirect.com/science/article/pii/S1878522015000818`.

Nicholas J. Sanders and Alan I. Barreca. Adaptation to Environmental Change: Agriculture and the Unexpected Incidence of the Acid Rain Program. *American Economic Journal: Economic Policy*, 14(1): 373–401, February 2022. ISSN 1945-7731. doi: 10.1257/pol.20190060. URL `https://www.aeaweb.org/articles?id=10.1257/pol.20190060`.

Luke D. Schiferl, Colette L. Heald, and David Kelly. Resource and physiological constraints on global crop production enhancements from atmospheric particulate matter and nitrogen deposition. *Biogeosciences*, 15(14):4301–4315, July 2018. ISSN 1726-4170. doi: 10.5194/bg-15-4301-2018. URL `https://bg.copernicus.org/articles/15/4301/2018/`. Publisher: Copernicus GmbH.

Andreas Shafer. Regularities in Travel Demand: An International Perspective. *Journal of Transportation and Statistics*, 2000. URL `https://rosap.ntl.bts.gov/view/dot/4809`.

Alka Sharma, Sushma Panigrahy, T. S. Singh, J. G. Patel, and Hemant Tanwar. Wetland information system using remote sensing and gis in himach pradesh, india. *Asian Journal of Geoinformatics*, 14, 2015. URL `https://api.semanticscholar.org/CorpusID:128677550`.

Megan Sheahan and Christopher B. Barrett. Ten striking facts about agricultural input use in Sub-Saharan Africa. *Food Policy*, 67:12–25, February 2017. ISSN 0306-9192. doi: 10.1016/j.foodpol.2016.09.010. URL `https://www.sciencedirect.com/science/article/pii/S0306919216303773`.

Pyae Sone Soe, Win Thiri Kyaw, Koji Arizono, Yasuhiro Ishibashi, and Tetsuro Agusa. Mercury Pollution from Artisanal and Small-Scale Gold Mining in Myanmar and Other Southeast Asian Countries. *International Journal of Environmental Research and Public Health*, 19(10):6290, May 2022. ISSN 1660-4601. doi: 10.3390/ijerph19106290.

Sandip Sukhtankar. Does firm ownership structure matter? Evidence from sugar mills in India. *Journal of Development Economics*, 122:46–62, September 2016. ISSN 0304-3878. doi: 10.1016/j.jdeveco.2016.04.002. URL `https://www.sciencedirect.com/science/article/pii/S0304387816300232`.

Sergio Villamayor-Tomas, Alexander Bisaro, Kevin Moull, Amaia Albizua, Isabel Mank, Jochen Hinkel, Gerald Leppert, and Martin Noltze. Developing countries can adapt to climate change effectively using nature-based solutions. *Communications Earth & Environment*, 5(1):1–11, April 2024. ISSN 2662-4435. doi: 10.1038/s43247-024-01356-0. URL `https://www.nature.com/articles/s43247-024-01356-0`. Publisher: Nature Publishing Group.

Holger Virro, Giuseppe Amatulli, Alexander Kmoch, Longzhu Shen, and Evelyn Uuemaa. Grqa: Global river water quality archive. *Earth System Science Data*, 13, 2021. doi: 10.5194/essd-13-5483-2021.

Jan von der Goltz and Prabhat Barnwal. Mines: The local wealth and health effects of mineral mining in developing countries. *Journal of Development Economics*, 139:1–16, June 2019. ISSN 0304-3878. doi: 10.1016/j.jdeveco.2018.05.005. URL `https://www.sciencedirect.com/science/article/pii/S0304387818304875`.

Stefan Wager and Susan Athey. Estimation and Inference of Heterogeneous Treatment Effects using Random Forests, July 2017. URL `http://arxiv.org/abs/1510.04342`. arXiv:1510.04342.

Han-jie Wang, Jingjing Wang, and Xiaohua Yu. Wastewater irrigation and crop yield: A meta-analysis. *Journal of Integrative Agriculture*, 21(4):1215–1224, April 2022. ISSN 2095-3119. doi: 10.1016/S2095-3119(21)63853-4. URL `https://www.sciencedirect.com/science/article/pii/S2095311921638534`.

Rui Xiang, Ya Xu, Yu-Qiang Liu, Guo-Yuan Lei, Jing-Cai Liu, and Qi-Fei Huang. Isolation distance between municipal solid waste landfills and drinking water wells for bacteria attenuation and safe drinking. *Scientific Reports*, 9:17881, November 2019. ISSN 2045-2322. doi: 10.1038/s41598-019-54506-2. URL `https://www.ncbi.nlm.nih.gov/pmc/articles/PMC6884615/`.

Tingting Xie and Ye Yuan. Go with the wind: Spatial impacts of environmental regulations on economic activities in China. *Journal of Development Economics*, 164:103139, September 2023. ISSN 0304-3878. doi: 10.1016/j.jdeveco.2023.103139. URL `https://www.sciencedirect.com/science/article/pii/S0304387823000949`.

Lianman Xu, Linlin Du, Yajing Li, Weizhe Li, and Hasa Wu. Effects of mine water on growth characteristics of ryegrass and soil matrix properties. *Scientific Reports*, 12(1):17758, October 2022. ISSN 2045-2322. doi: 10.1038/s41598-022-22625-y. URL `https://www.nature.com/articles/s41598-022-22625-y`. Publisher: Nature Publishing Group.

Eric Yongchen Zou. Unwatched Pollution: The Effect of Intermittent Monitoring on Air Quality. *American Economic Review*, 111, 2021. doi: 10.1257/aer.20181346. URL `https://www.aeaweb.org/articles?id=10.1257/aer.20181346`.

12 Appendix

12.1 Mine Locations Figure 10 plots the set of 307 mines from the S&P dataset used to estimate the "overall" effect of mining on local yields. Each yellow point indicates the centroid of a mining operation, while the countries shaded in blue are those that contain at least one mine used in the analysis.

Figure 10: Map of mines used in analysis

12.2 Data Construction

12.2.1 Water Pollution First, I define the buffers used for the water pollution analysis. I select only mines that are within 1 kilometer of a river. I use the HydroRIVERS data to identify rivers located in Africa. This dataset is a vectorized line network of rivers that have a catchment area of at least 10 km^2, an average river flow of at least 0.1 m^3/sec, or both. Each observation in this dataset is a river segment, where segment end points are defined by splitting rivers or streams at nodes where they fork. Each mine within 1

km of a river in this network is "snapped" to the closest river segment, then the upstream and downstream river segments from the mine river segment are identified. Mines that are snapped to river segment end points, for which an upstream or downstream segment is missing, are excluded from the analysis. Parts of the upstream or downstream river segments that extend beyond a buffer of radius 10-km from the snapped mine point are removed. The upstream and downstream segments are buffered by 1-kilometer on either side of the line to identify land area around the rivers that would likely be affected by acid mine drainage either through seepage or irrigation. The "side" of a mine in the water pollution analysis refers to the upstream or downstream buffer.

Next, I calculate the satellite-based measure of water pollution, NDTI, over river water pixels. I first identify the precise shape of the upstream and downstream river segments near mines using a water mask based on the normalized difference water index (NDWI). This index is commonly used to detect water bodies in satellite images and is calculated from the green and near-infrared (NIR) bands.[10] I generate the NDWI water mask from a mosaic of cloud-free Sentinel-2 pixels from 2020-2023 at a 15-m resolution for the entire area within the 10-km buffer around the snapped mine point. Pixels identified as water based on a positive NDWI value are marked as river pixels.

Then, I calculate monthly mean NDTI for each river pixel according to the following formula: $NDTI = \frac{\text{Red}-\text{Green}}{\text{Red}+\text{Green}}$. I use Landsat 7 data at a 30-m resolution, as it is the highest resolution data available that covers the time period of 2000-2024.[11] I mask out pixels marked as "low quality" due to cloud cover, shadow or other atmospheric interference. Finally, I average monthly NDTI across water pixels within the upstream or downstream river segments, for each mine, to create mine-month-side level measures of river NDTI.

12.2.2   Air Pollution   The algorithm detecting AOD can perform poorly in certain cases, which generates missing values. Levy et al. [2013] find that the algorithm performs poorly over light surfaces, such as desert or snowy regions. To address this limitation, I exclude mining areas that are adjacent to the desert, such as parts of Burkina Faso and Mali that neighbor the Sahel. In addition, the MODIS instruments can only detect AOD on cloud-free days, so missing data in certain regions or on certain days tend to reflect high levels of cloud cover. This results in seasonality of missingness in the MODIS data; I manage this issue by using mine-year-month fixed effects in my model, which account for mine-specific monthly variations in weather patterns correlated with satellite errors. Furthermore, in regressions with AOD as the outcome variable, I control for the number of non-missing pixels used to construct mean monthly AOD. I opt for a

---

[10]

$$NDWI = \frac{\text{Green}-\text{NIR}}{\text{Green}+\text{NIR}}$$

[11]The Sentinel-2 satellite only launched in 2015

linear control of non-missing pixel count over interpolating missing AOD as interpolation algorithms may introduce measurement error that is difficult to interpret.

12.2.3 Agricultural Seasons For each mining area, I observe 4-5 agricultural seasons. Like Sacks et al. [2010], I define the seasons for planting and harvest using start and end dates, and define the growing season as the days in between the planting end date and the harvest start date. As the biological sciences literature suggests that pollution can affect crops more strongly during the reproductive phase of the plant, which occurs early in the growing season, I divide this growing season in half to make early and late growing seasons Liu and Desai [2021]. Finally, I define the non-farming season as the time between the harvest end date of one year and the planting start date of the next year. In mining areas where the harvesting period of one year overlaps with the planting period of the subsequent year, I define the harvest season as ending at the start of next year's planting season. I assign each mining area the modal season dates across all cells falling within the buffer linked to that mine.

12.3 NDTI vs. ground-based turbidity measurements

To estimate the relationship between NDTI and ground-based turbidity, I use geo-located data on ground-based measures of total suspended solids from the Global River Water Quality (GRWQ) data. I calculate NDTI over water pixels located within a 500-m radius of the GRWQ sampling point, during the month that the sample was collected, again using Landsat 7 data.

Table 6: Relationship between Total Suspended Solids from Ground-based Sampling and Remotely-Sensed Turbidity

	(1)	(2)
Normalized Difference Turbidity Index	940.9***	887.1**
	(341.4)	(364.7)
Number of sampling sites	178	178
Include weather controls	No	Yes
TSS mean	147.012	147.012
NDTI mean	.007	.007

Each column reports the results of a linear regression. The unit of analysis is a sampling site on the date that the water sampling occurred. The dependent variable is the level of total suspended solids identified from ground-based water sampling and testing at the sampling site, on a specific date. The independent variable is the mean normalized difference turbidity index for the river segment falling within a 500 meter buffer around the sampling site, in the month corresponding to the sampling date. All models include linear and quadratic controls for mean temperature, precipitation, vapor pressure, wet days, evapotranspiration and cloud cover. Robust standard errors are reported in parentheses

12.4 AOD Spatial Lag Model

To estimate the spatial lag model for AOD, I define concentric rings around a mine point with the following distances: 0-10km, 10-20km, 20-40km, 40-60km, 60-100km, 100-150km, 150-200km. Each of these rings is divided into four 90-degree slices indicating the cardinal directions. For each mine-month, I calculate the number of days the wind is blowing from the mine into a given side, as well as the average wind speed experienced by that side. I estimate a version of Equation 4, with an additional interaction between the post dummy, wind intensity and a dummy for each distance ring, with the 150-200km ring being the ommitted category. Figure 11 plots the coefficients of these triple interactions, which show the DID estimates for the effect of mining on AOD at increasing distances from the mine centroid.
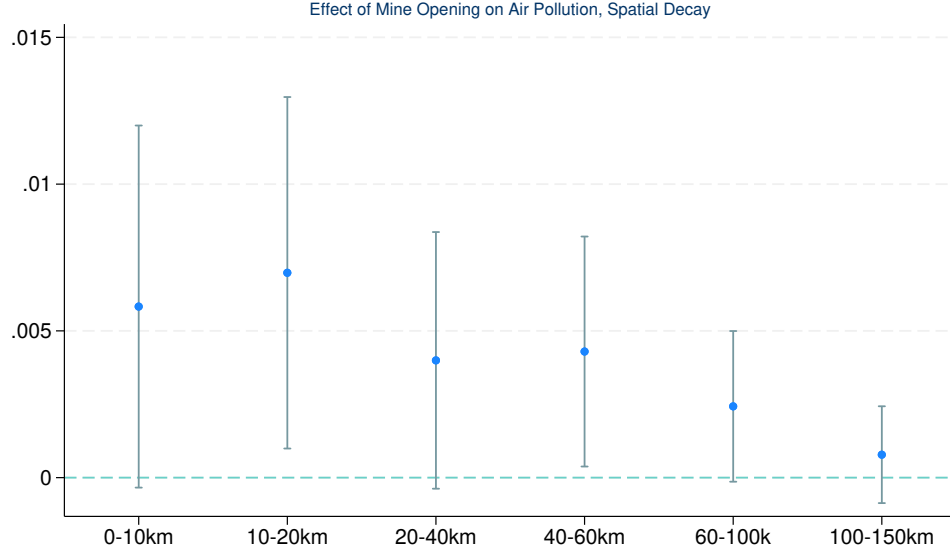
Figure 11: Mean AOD Spatial Decay Model

12.5 NDVI Spatial Lag Model To estimate the spatial lag model for AOD, I define concentric rings around a mine point with the following distances: 0-20km, 20-40km, 40-60km, 60-100km, 100-150km. I estimate a version of Equation 6 that replaces the Near dummy with a series of dummies for each of the distance rings, with the 100-150km ring being the omitted category. Figure 12 plots the coefficients on the interactions between the post dummy and each of the distance ring dummies, showing the DID effect of mining on NDVI at increasing distances from the mine centroid.
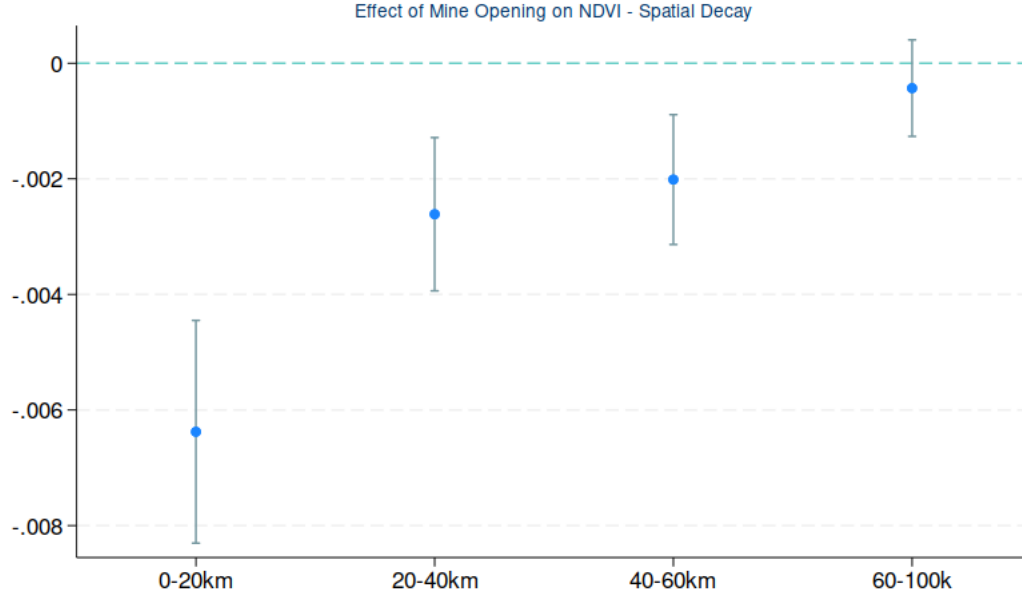
Figure 12: Mean NDVI Spatial Decay Model

12.6   Water Pollution Robustness

12.6.1   Irrigated pixels only   The table below reports the results for estimating equation 3 using mean NDVI calculated over only irrigated cropland pixels within water buffers as the outcome of interest.

Table 7

	Mean NDVI - Irrigated Cropland Only
Downstream × Post	-0.0206
	(0.0233)
Number of mines	4
Mine-side FE	Yes
Mine-year-month FE	Yes
Mean NDVI (t-1)	.46

Standard errors in parentheses

* $p < 0.10$, ** $p < 0.05$, *** $p < 0.01$

12.7 Distributed Lag Results

12.7.1 Average effects: distributed lag as table

Effect of Cumulative Air Pollution Exposure on NDVI

Number of Months Prior	$\sum_p^P \delta_p$	$\frac{\sum_p^P \delta_p}{\text{Mean NDVI}}$	Standard error	p
1	0.0003	0.0656	0.0011	0.7956
2	0.0006	0.1307	0.0012	0.6483
3	0.0005	0.1263	0.0014	0.6890
4	0.0007	0.1501	0.0015	0.6616
5	0.0007	0.1581	0.0016	0.6672
6	0.0005	0.1240	0.0017	0.7488
7	0.0004	0.0869	0.0018	0.8297
8	0.0002	0.0405	0.0018	0.9220
9	0.0001	0.0222	0.0018	0.9579
10	0.0001	0.0260	0.0018	0.9509
11	0.0001	0.0302	0.0018	0.9432
12	0.0001	0.0285	0.0018	0.9464
13	0.0001	0.0293	0.0018	0.9451
14	0.0001	0.0285	0.0019	0.9468
15	0.0001	0.0291	0.0019	0.9460
16	0.0001	0.0231	0.0019	0.9574
17	0.0001	0.0268	0.0019	0.9506
18	0.0002	0.0348	0.0019	0.9363
19	0.0002	0.0345	0.0019	0.9371
20	0.0001	0.0330	0.0019	0.9401
21	0.0002	0.0374	0.0019	0.9326
22	0.0001	0.0290	0.0019	0.9478
23	0.0001	0.0214	0.0019	0.9614
24	0.0001	0.0148	0.0019	0.9734

Figure 13: Average effect of cumulative mining-induced air pollution exposure on NDVI - growing vs. non-growing seasons

12.8 Heterogeneity - Near vs. Far

12.8.1 Mine-specific treatment effects The figure below plots a histogram of the mine-specific DID estimates of the overall effect of mining on local yields against a histogram of simulated DID estimates. To generate the observed mine-specific DID estimates, I regress NDVI on the side of a mine (near/far) on a dummy variable for Near interacted with the dummy variable for Post, the main effects and controls for weather. To generate the observed DID estimates, I make random draws from a normal distribution with a mean equal to the average "overall" treatment effect, -0.00638, shown in Table 3 Column 1, and standard deviation equal to the standard error of the average "overall" treatment effect, 0.000980.
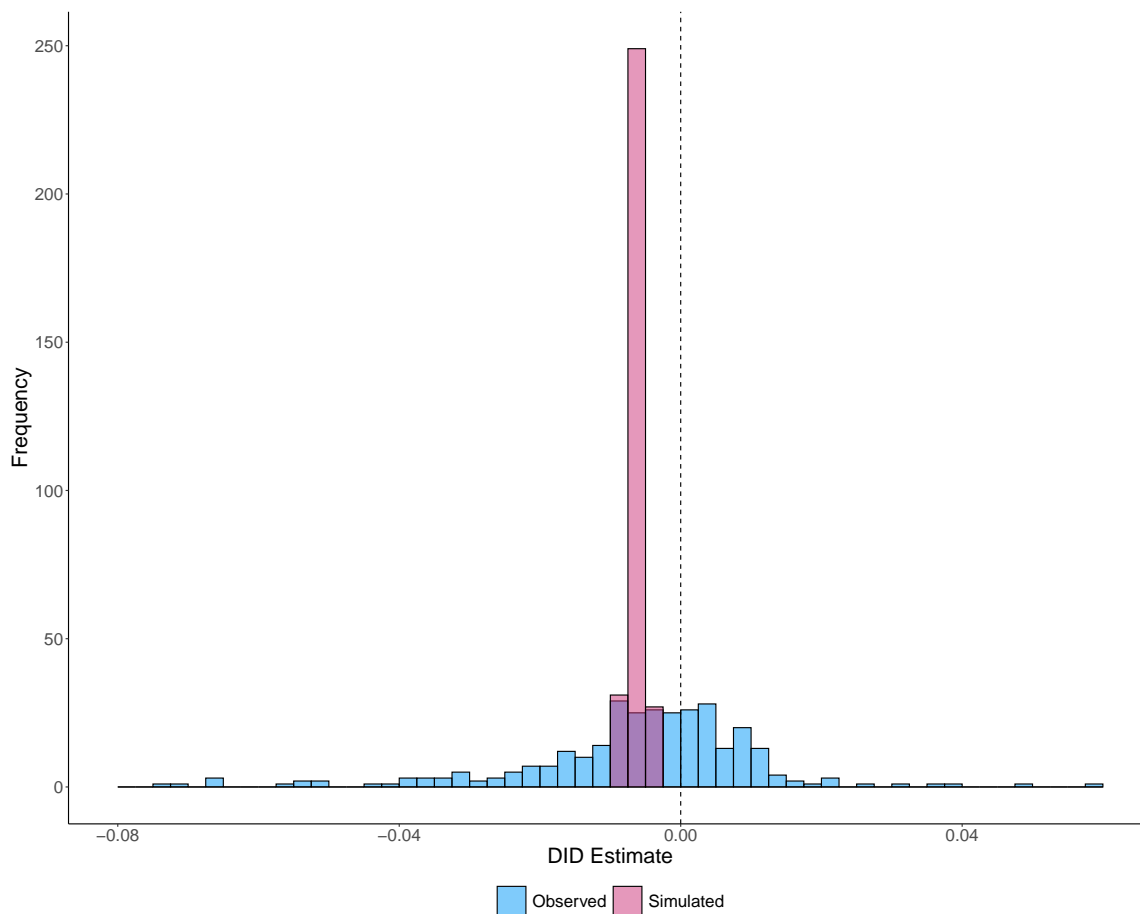
Figure 14: Variation in observed mine-specific DIDs is greater than what we would expect due to sampling variation

12.8.2 Standard heterogeneity analysis

Table 9: Heterogeneous Treatment Effects - Economic Factors

	Base	Above Med. Mineral Rents	Above Med. GDP - 2000	Above Med. Pop - 2000
Near × Post	-0.00638***	-0.00534***	-0.00692***	-0.00709***
	(0.000980)	(0.00108)	(0.00157)	(0.00160)
Near × Post × Z		-0.00568**	0.00107	0.00142
		(0.00242)	(0.00195)	(0.00195)
Number of mines	307	307	307	307
Mean NDVI (t-1)	.476	.476	.476	.476

Standard errors in parentheses

* $p < 0.10$, ** $p < 0.05$, *** $p < 0.01$

Table 10: Heterogeneous Treatment Effects - Mine Characteristics

	Base	Open Pit	Gold	Coal	Near Other Mine	Near Town	Old Mine
Near × Post	-0.00638***	-0.00615***	-0.00639***	-0.00675***	-0.00416***	-0.00611***	-0.00615***
	(0.000980)	(0.00174)	(0.00133)	(0.00113)	(0.00123)	(0.00150)	(0.00159)
Near × Post × Z		-0.000376	0.00000921	0.00247	-0.00449**	-0.000573	-0.000362
		(0.00210)	(0.00178)	(0.00151)	(0.00194)	(0.00193)	(0.00201)
Number of mines	307	307	307	307	307	307	307
Mean NDVI (t-1)	.476	.476	.476	.476	.476	.476	.476

Standard errors in parentheses

* $p < 0.10$, ** $p < 0.05$, *** $p < 0.01$

Table 11: Heterogeneous Treatment Effects - Environmental Conditions

	Base	Above Med. NDVI - 2000	Above Med. Precipitation - 2001	Growing Season
Near × Post	-0.00638***	-0.00526***	-0.00762***	-0.00560***
	(0.000980)	(0.00152)	(0.00163)	(0.00113)
Near × Post × Z		-0.00226	0.00247	-0.00162
		(0.00195)	(0.00194)	(0.00114)
Number of mines	307	307	307	307
Mean NDVI (t-1)	.476	.476	.476	.476

Standard errors in parentheses

* $p < 0.10$, ** $p < 0.05$, *** $p < 0.01$

12.8.3 ML heterogeneity analysis Figure 15 plots the set of the 10 least important variables used in the best performing random forest model, while Figure 16 plots the 10 most important variables from an alternative classification random forest model, trained to predict an indicator for whether the treatment effect is less than zero using the same set of predictors as in the main ML exercise.

Figure 17 plots mine-specific DID estimates from estimating the effect of mine openings on remotely sensed air pollution using Equation 4 with AOD as the outcome of interest against mine-specific DID estimamtes obtained by estimating the same specification using NDVI as the outcome of interest.

Table 12

	Base	EITI	Control of Corruption	Govt. Effectiveness	Rule of Law	Reg. Quali
Wind	-0.00123	-0.00261	-0.00190	-0.000730	-0.00280	-0.000526
	(0.00224)	(0.00412)	(0.00333)	(0.00382)	(0.00337)	(0.00375)
Wind × (Post - 3)	0.000277	0.000621	-0.00240	-0.00122	-0.000435	-0.00169
	(0.00146)	(0.00202)	(0.00189)	(0.00166)	(0.00188)	(0.00172)
Wind × (Post - 3) × Z		-0.000554	0.00402	0.00246	0.00106	0.00321
		(0.00284)	(0.00267)	(0.00271)	(0.00271)	(0.00268)
Number of mines	102	102	102	102	102	102
Mean NDVI (t-1)	.492	.492	.492	.492	.492	.492

Standard errors in parentheses
* $p < 0.10$, ** $p < 0.05$, *** $p < 0.01$

Table 13

	Base	Above Med. Mineral Rents	Above Med. GDP - 2000	Above Med. Pop - 2000
Wind	-0.00123	-0.00283	-0.00102	-0.000486
	(0.00224)	(0.00265)	(0.00282)	(0.00341)
Wind × (Post - 3)	0.000277	0.0000825	0.000147	0.00193
	(0.00146)	(0.00175)	(0.00193)	(0.00209)
Wind × (Post - 3) × Z		0.000671	0.000372	-0.00370
		(0.00274)	(0.00285)	(0.00274)
Number of mines	102	102	102	102
Mean NDVI (t-1)	.492	.492	.492	.492

Standard errors in parentheses
* $p < 0.10$, ** $p < 0.05$, *** $p < 0.01$
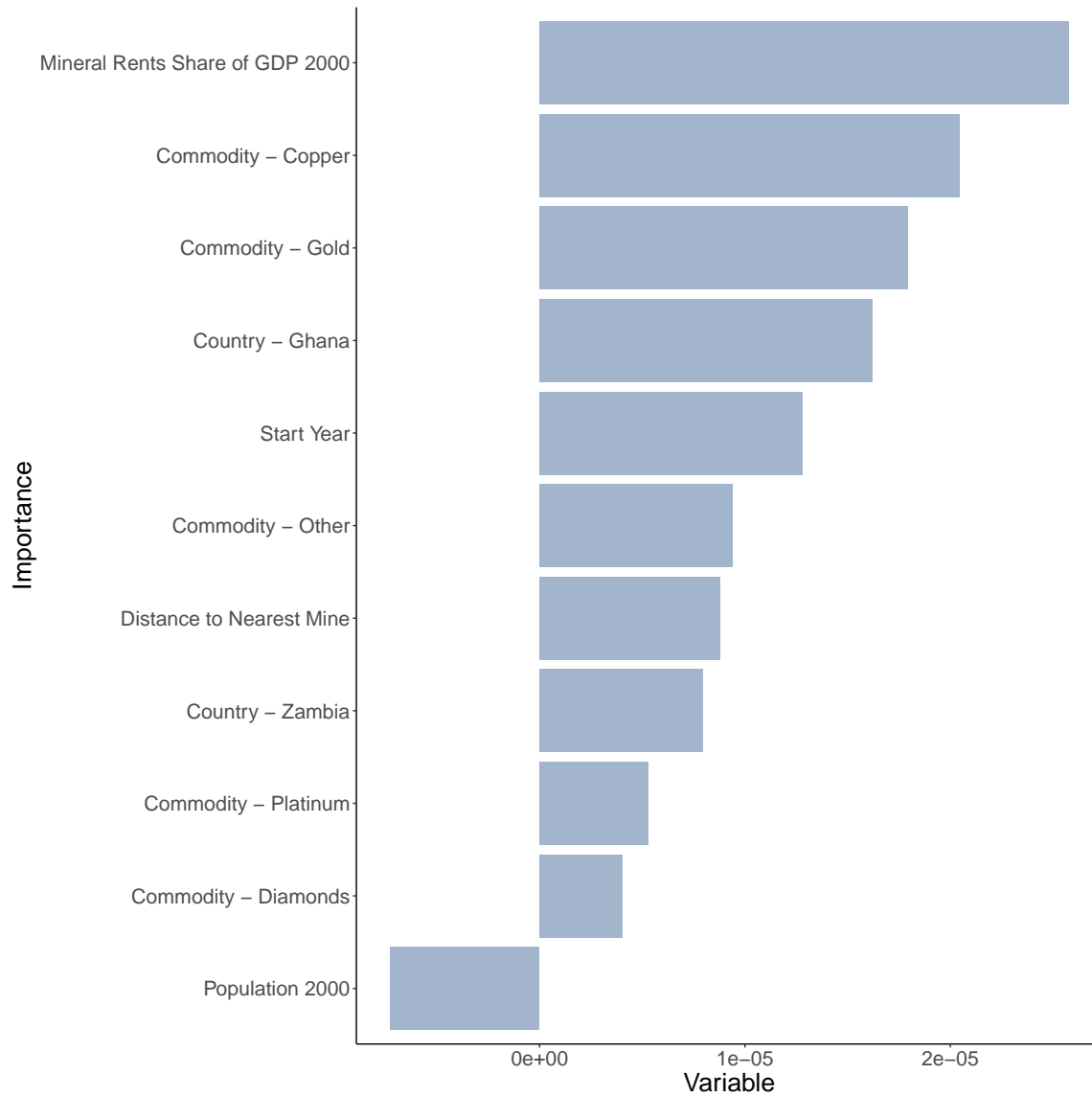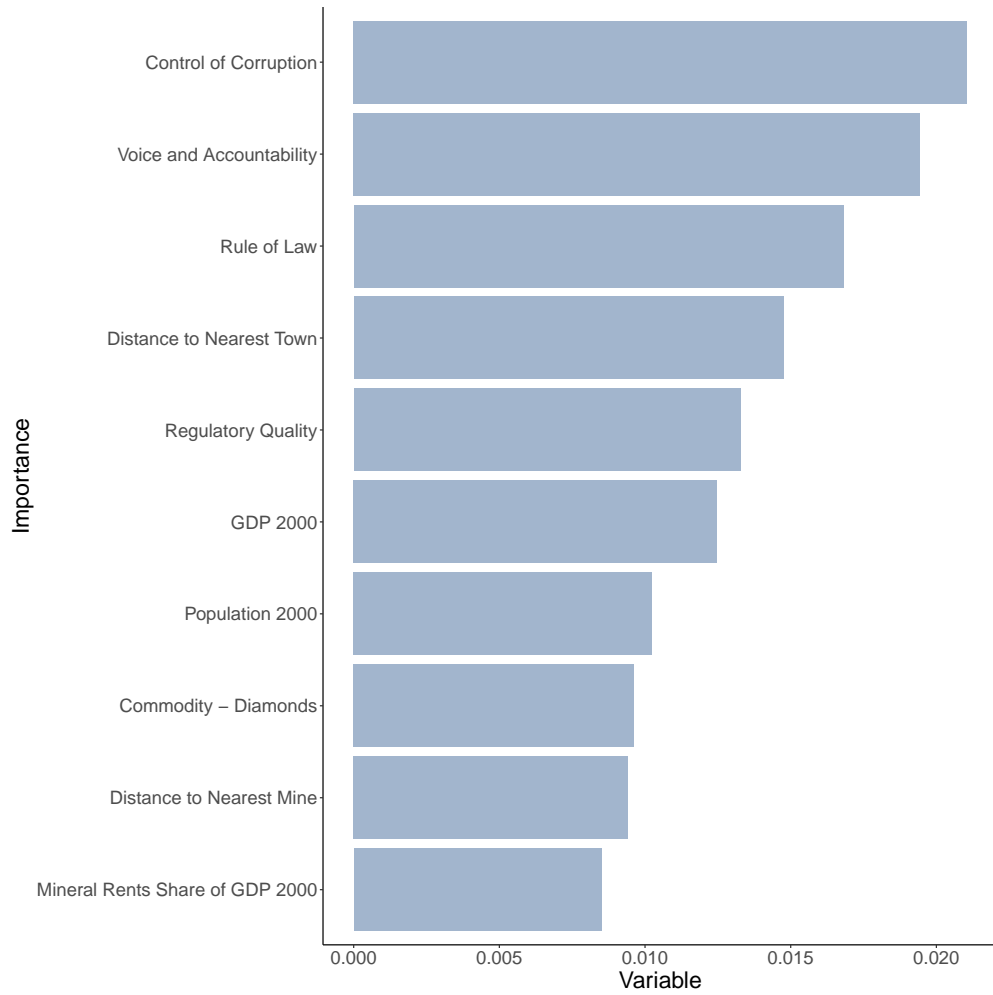
12.9 Heterogeneity - Contemporaneous Air Pollution

Figure 15: 10 Least Important Variables from ML Model

Table 14

	Base	Open Pit	Gold	Coal	Copper	Near Other Mine	Near Town	O
Wind	-0.00123	-0.00688	0.00243	-0.00407*	-0.00174	-0.00227	-0.00156	-(
	(0.00224)	(0.00555)	(0.00333)	(0.00235)	(0.00256)	(0.00328)	(0.00329)	(0
Wind × (Post - 3)	0.000277	0.00779**	0.00125	0.000267	0.00104	0.00229	-0.0000280	0.
	(0.00146)	(0.00300)	(0.00204)	(0.00164)	(0.00143)	(0.00186)	(0.00217)	(0
Wind × (Post - 3) × Z		-0.0104***	-0.00252	-0.000114	-0.00381	-0.00412	0.000698	
		(0.00338)	(0.00253)	(0.00369)	(0.00439)	(0.00281)	(0.00278)	
Number of mines	102	102	102	102	102	102	102	
Mean NDVI (t-1)	.492	.492	.492	.492	.492	.492	.492	

Standard errors in parentheses

* $p < 0.10$, ** $p < 0.05$, *** $p < 0.01$

Figure 16: Most Important Variables from Best Random Forest Model: Classification

Table 15

	Base	Above Med. AOD - 2003	Above Med. NDVI - 2003	Above Med. Precipitation -
Wind	-0.00123	0.000823	-0.00151	-0.00132
	(0.00224)	(0.00463)	(0.00338)	(0.00461)
Wind × (Post - 3)	0.000277	-0.000160	-0.00162	0.000426
	(0.00146)	(0.00151)	(0.00160)	(0.00216)
Wind × (Post - 3) × Z		0.000682	0.00298	-0.000231
		(0.00265)	(0.00258)	(0.00292)
Number of mines	102	102	102	102
Mean NDVI (t-1)	.492	.492	.492	.492

Standard errors in parentheses

* $p < 0.10$, ** $p < 0.05$, *** $p < 0.01$
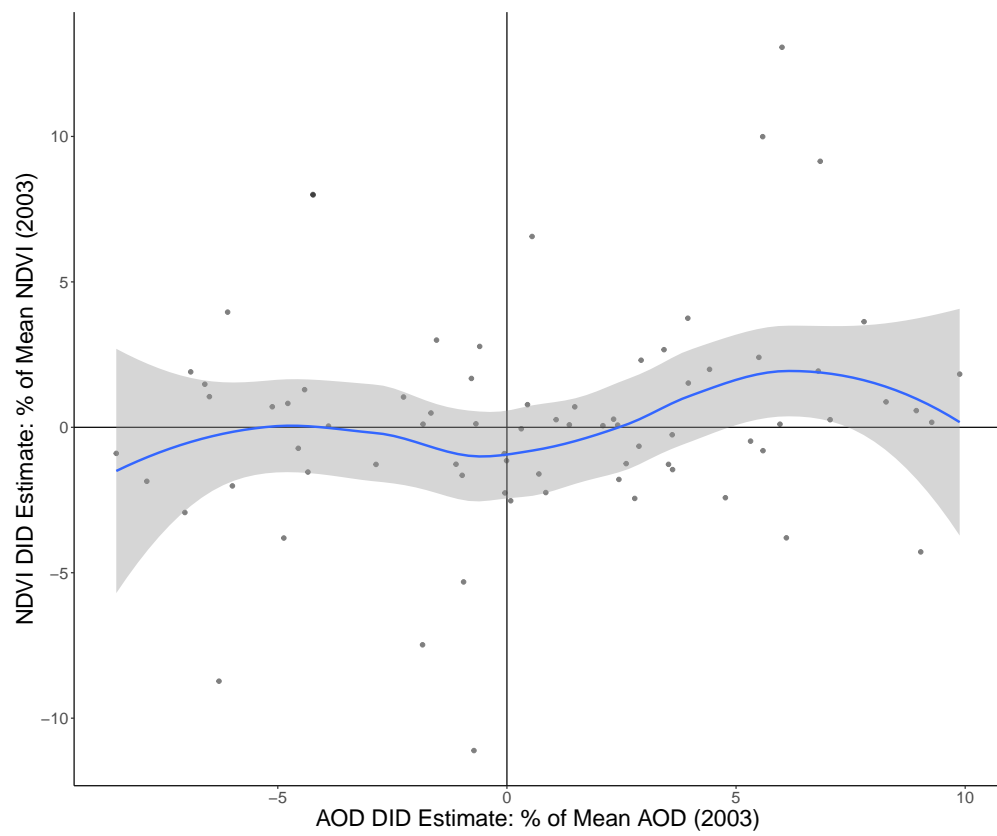
Figure 17: Mine-specific AOD DID estimates vs. NDVI DID estimates
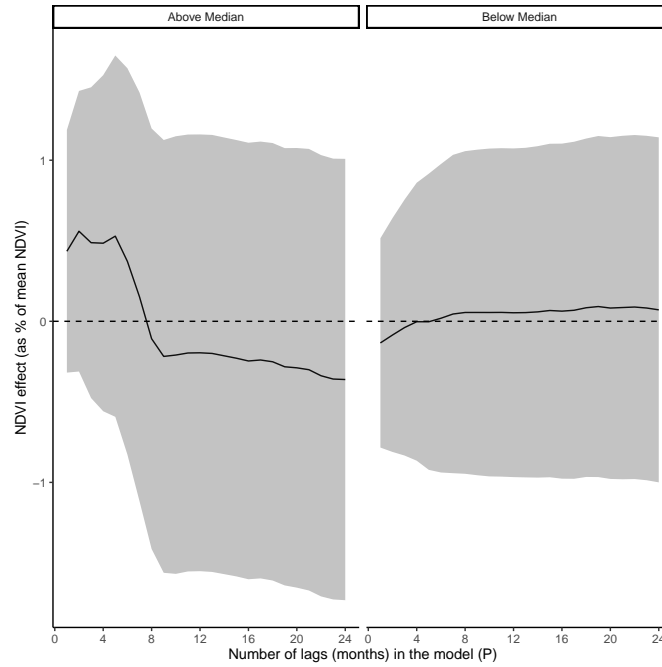
Figure 18: Heterogeneity by control of corruption
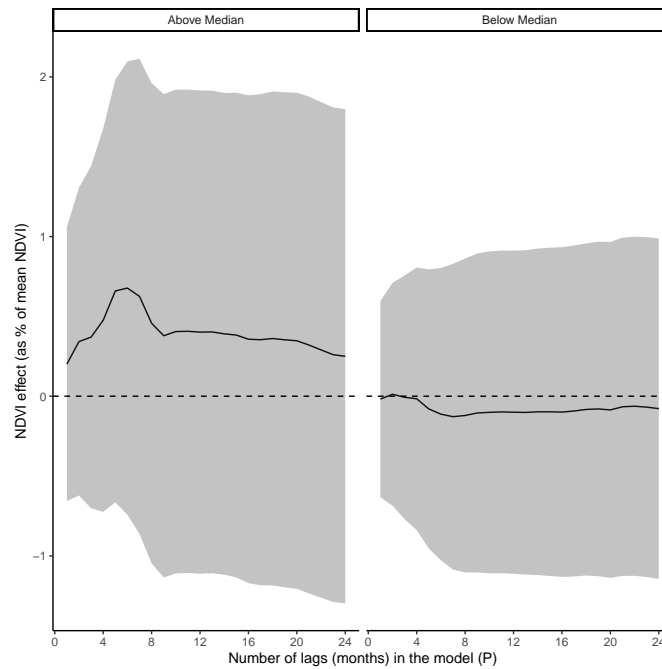
Figure 19: Heterogeneity by rule of law

12.10 Heterogeneity - Distributed Lag

Effect of Cumulative Air Pollution Exposure on NDVI

Number of Months Prior	$\sum_p^P \delta_p$	$\frac{\sum_p^P \delta_p}{\text{Mean NDVI}}$	Standard error	p
1	0.0003	0.0656	0.0011	0.7956
2	0.0006	0.1307	0.0012	0.6483
3	0.0005	0.1263	0.0014	0.6890
4	0.0007	0.1501	0.0015	0.6616
5	0.0007	0.1581	0.0016	0.6672
6	0.0005	0.1240	0.0017	0.7488
7	0.0004	0.0869	0.0018	0.8297
8	0.0002	0.0405	0.0018	0.9220
9	0.0001	0.0222	0.0018	0.9579
10	0.0001	0.0260	0.0018	0.9509
11	0.0001	0.0302	0.0018	0.9432
12	0.0001	0.0285	0.0018	0.9464
13	0.0001	0.0293	0.0018	0.9451
14	0.0001	0.0285	0.0019	0.9468
15	0.0001	0.0291	0.0019	0.9460
16	0.0001	0.0231	0.0019	0.9574
17	0.0001	0.0268	0.0019	0.9506
18	0.0002	0.0348	0.0019	0.9363
19	0.0002	0.0345	0.0019	0.9371
20	0.0001	0.0330	0.0019	0.9401
21	0.0002	0.0374	0.0019	0.9326
22	0.0001	0.0290	0.0019	0.9478
23	0.0001	0.0214	0.0019	0.9614
24	0.0001	0.0148	0.0019	0.9734

Figure 20: Heterogeneity by government effectiveness
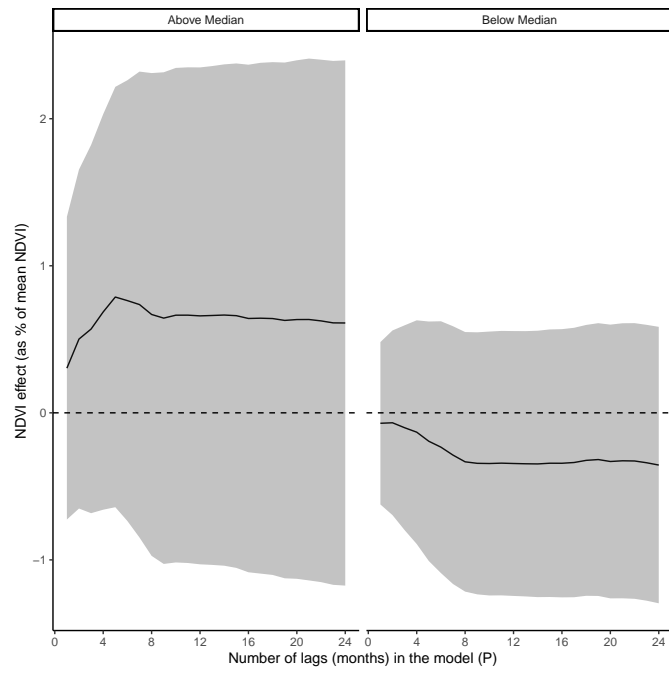
Figure 21: Heterogeneity by regulatory quality
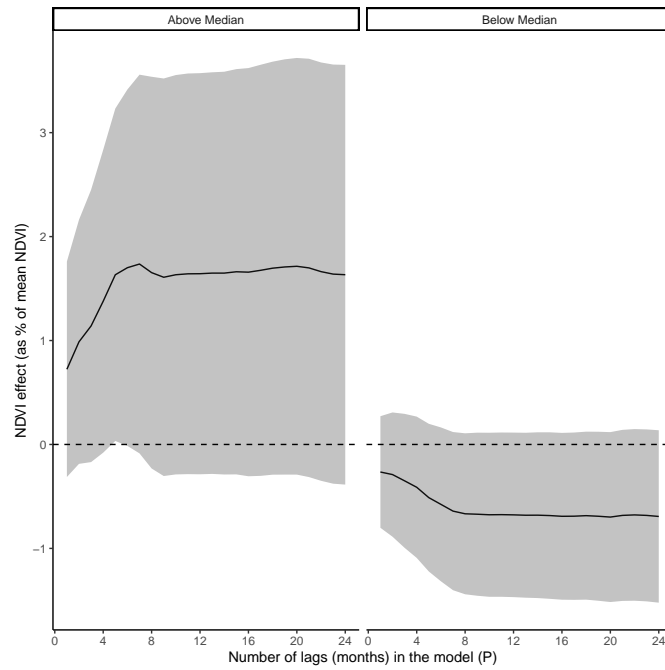
Figure 22: Heterogeneity by voice and accountability
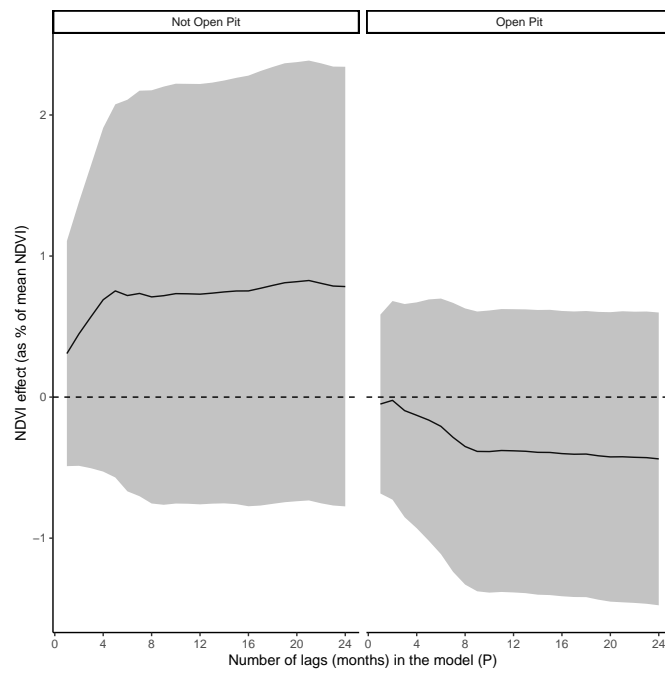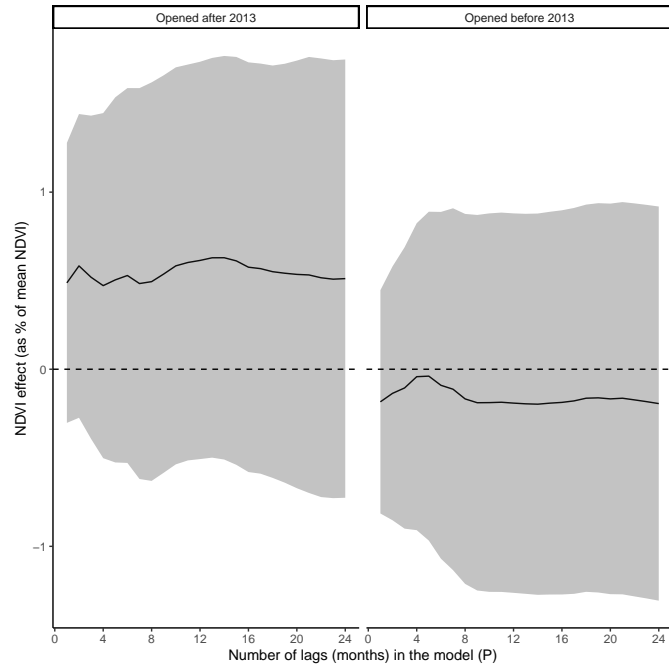

Figure 23: Heterogeneity by mine type

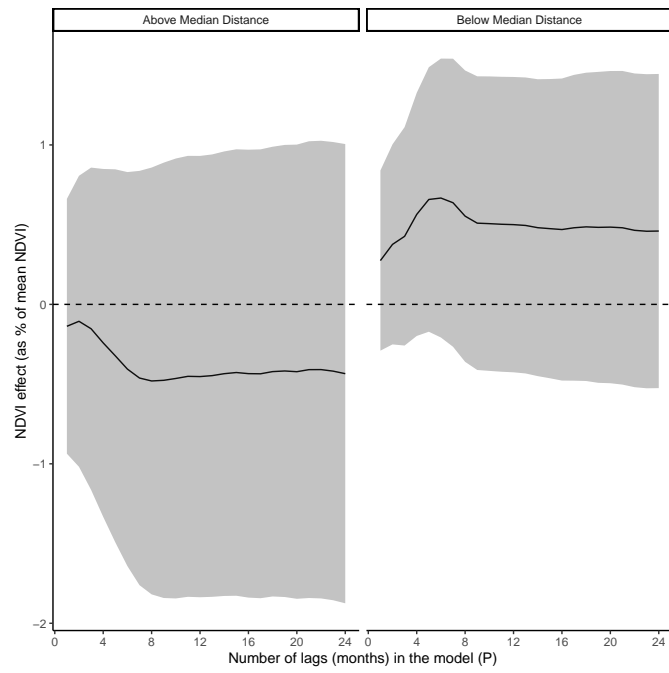Figure 24: Heterogeneity by mine age

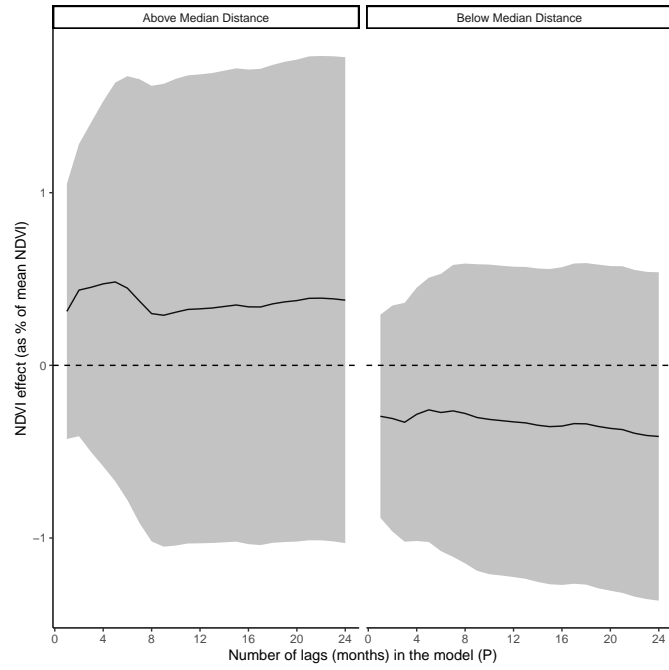
Figure 25: Heterogeneity by distance to nearest mine

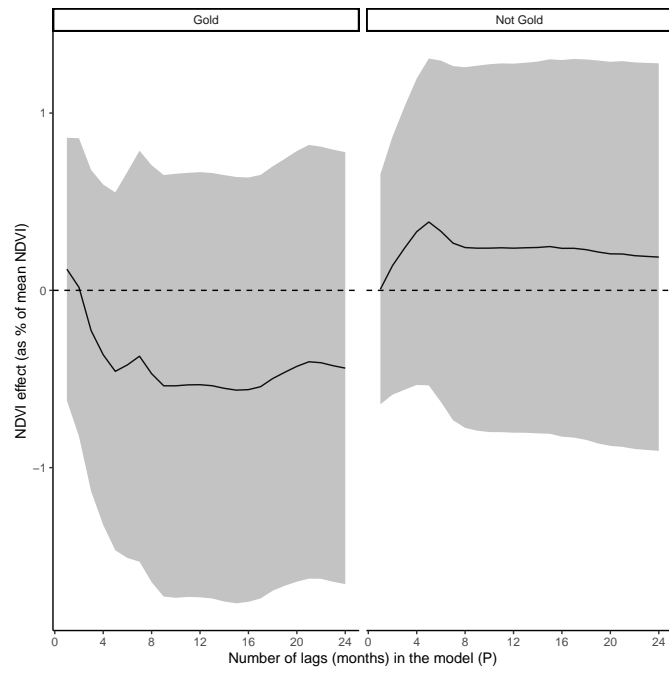Figure 26: Heterogeneity by distance to nearest town

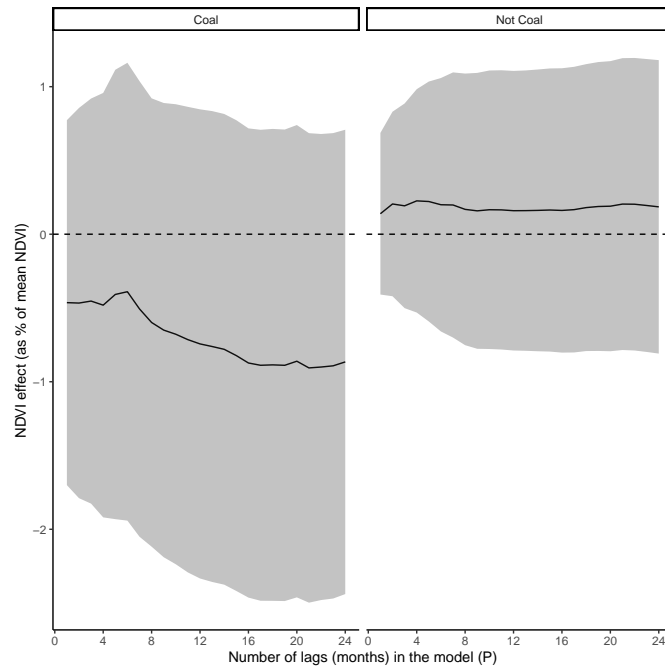Figure 27: Heterogeneity by commodity: gold
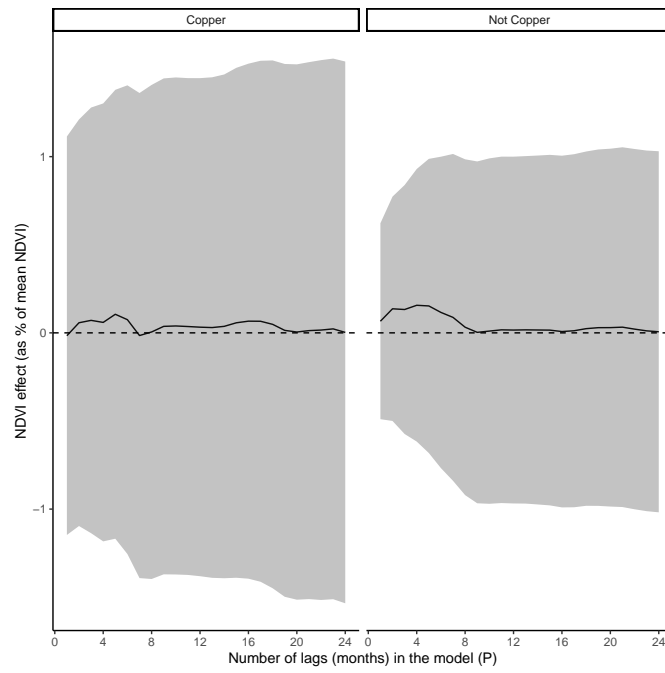
Figure 28: Heterogeneity by commodity: coal
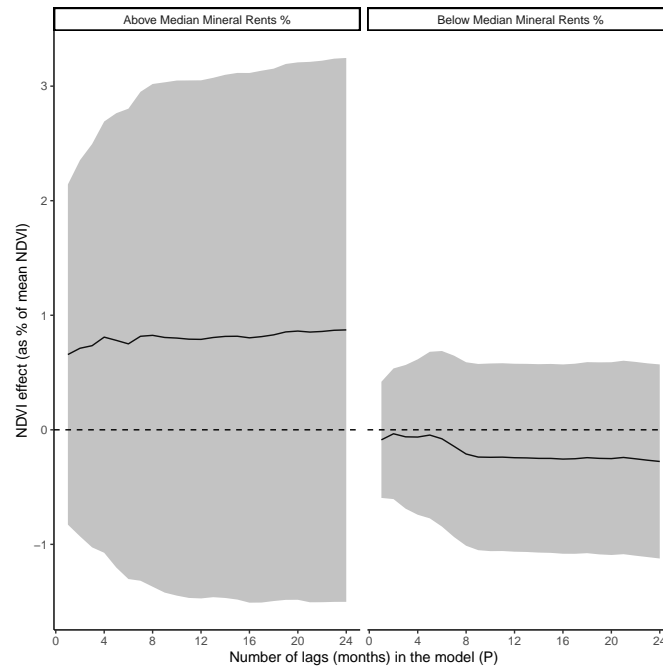

Figure 29: Heterogeneity by commodity: copper

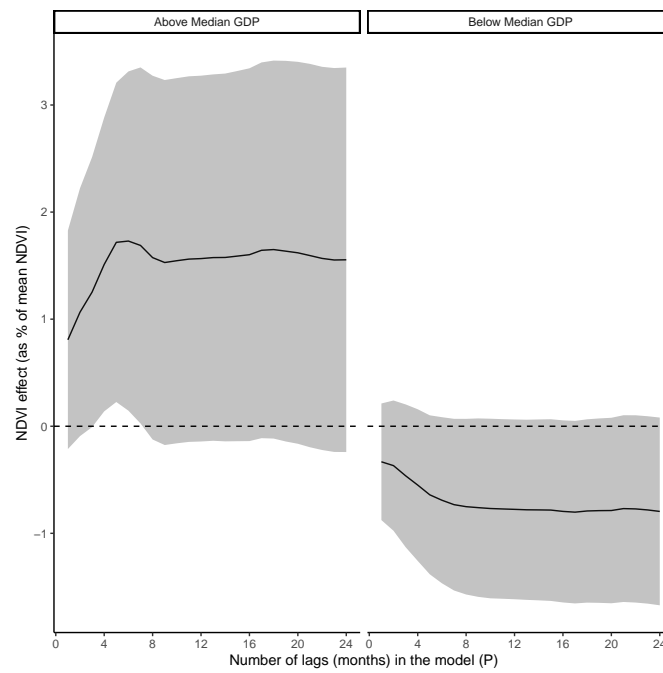Figure 30: Heterogeneity by mineral rents as share of GDP - 2000
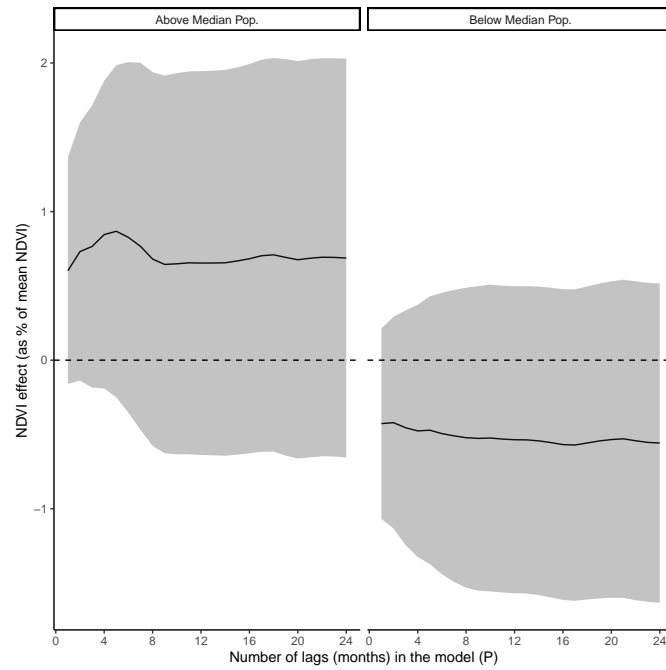

Figure 31: Heterogeneity by GDP - 2000

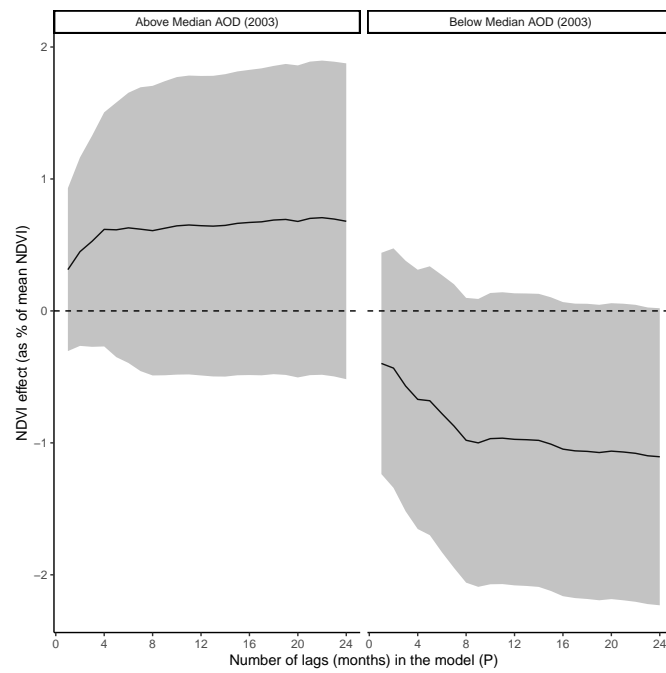Figure 32: Heterogeneity by population - 2000

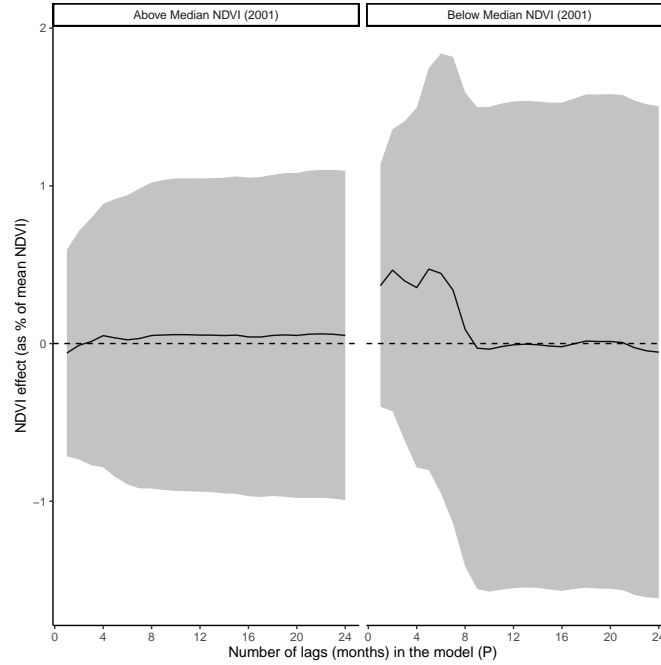Figure 33: Heterogeneity by initial pollution levels (AOD 2003)

Figure 34: Heterogeneity by initial yields (NDVI 2001)

Table 17

	Base	EITI	Control of Corruption	Govt. Effectiveness	Rule of Law	Reg. Qua
Downstream × Post	-0.0140**	-0.0129	-0.0131**	-0.0164*	-0.0126**	-0.0117
	(0.00587)	(0.00911)	(0.00600)	(0.00840)	(0.00487)	(0.0065
Downstream × Post × Z		-0.00203	-0.00185	0.00527	-0.00330	-0.0051
		(0.0119)	(0.0119)	(0.0115)	(0.0126)	(0.0121
Number of mines	38	38	38	38	38	38
Mean NDVI (t-1)	.467	.467	.467	.467	.467	.467

Standard errors in parentheses

* $p < 0.10$, ** $p < 0.05$, *** $p < 0.01$

12.11 Heterogeneity - Water

Table 18

	Base	Open Pit	Gold	Coal	Near Other Mine	Near Town	Old Mine
Downstream × Post	-0.0140**	-0.0162	-0.00849	-0.0132*	-0.000109	-0.0189***	-0.0234**
	(0.00587)	(0.0109)	(0.00511)	(0.00706)	(0.00625)	(0.00687)	(0.0100)
Downstream × Post × Z		0.00333	-0.0166	-0.00432	-0.0285**	0.00937	0.0151
		(0.0129)	(0.0147)	(0.00961)	(0.0108)	(0.0115)	(0.0122)
Number of mines	38	38	38	38	38	38	38
Mean NDVI (t-1)	.467	.467	.467	.467	.467	.467	.467

Standard errors in parentheses

* $p < 0.10$, ** $p < 0.05$, *** $p < 0.01$

Table 19

	Base	Above Med. Mineral Rents	Above Med. GDP - 2000	Above Med. Pop - 2000
Downstream × Post	-0.0140**	-0.0180***	-0.0121	-0.0193**
	(0.00587)	(0.00553)	(0.00948)	(0.00878)
Downstream × Post × Z		0.0129	-0.00406	0.0108
		(0.0151)	(0.0115)	(0.0115)
Number of mines	38	38	38	38
Mean NDVI (t-1)	.467	.467	.467	.467

Standard errors in parentheses

* $p < 0.10$, ** $p < 0.05$, *** $p < 0.01$

Table 20

	Base	Above Median Turbidity - 2000	Above Med. NDVI - 2000	Above Med. Precipi
Downstream × Post	-0.0140**	-0.0252***	-0.0107**	-0.0214*
	(0.00587)	(0.00856)	(0.00450)	(0.00975
Downstream × Post × Z		0.0199*	-0.00633	0.0146
		(0.0113)	(0.0112)	(0.0116)
Number of mines	38	38	38	38
Mean NDVI (t-1)	.467	.467	.467	.467

Standard errors in parentheses

* $p < 0.10$, ** $p < 0.05$, *** $p < 0.01$

12.12 Structural Breaks Model For each mine, I construct total luminosity for each year from 1992-2012 as the sum of nighttime light intensity across all pixels that fall within the 20-km disk around the mine centroid, in a given year. The nightlight data is provided by the DMSP OLS at a 1-km resolution. However, the DMSP-OLS data is not available to the public after 2013. From 2013 onwards, there was a switch to the Visible Infrared Imaging Radiometer Suite (VIIRS) instrument as the source of nightlights. Given that the spatial and radiometric resolution from VIIRS is higher than DMSP-OLS, Li et al. (2020) created a temporally harmonized global nighttime lights dataset from 1992-2019. Unfortunately, the temporal consistency of their harmonized data does not perform well in areas with low levels of luminosity (pixels with DN values greater than 7). Time series of nighttime light intensity for mining areas reveal a sharp jump in luminosity in 2013, when there was a switch to VIIRS. Given that the average pixel in a mining area has a DN value of 6.5, this suggests that the harmonized data is not temporally consistent for mining areas. As a result, I only estimate a structural break in nightlights for mines that opened before 2013, to avoid confounding due to the switch from DMSP to VIIRS.

I use the methods of Andrews (1993) and Andrews and Ploberger (1994) to detect a structural break in the mean of nightlights for each mine. Given a single proposed break point, the nightlights time series is split into two bins. The estimation method fits a regression of nightlights on an intercept for the data in each bin and calculates an F statistic based on the null hypothesis that the mean in nightlights is the same between the two bins. This step is repeated for all possible break points in the data to yield a time series of F-statistics. The structural break is identified as the year which yields the largest F-statistic. To test whether this structural break is statistically significant, I use the critical values for the F-statistics identified by Andrews (1993) and Andrews and Ploberger (1994), which are computed under the null hypothesis of no structural change such that the asymptotic probability that the supremum of the time series of F-statistics exceeds this critical value is $\alpha = 0.05$. In other words, if the F-statistic of the structural break is higher than the critical value, we can reject the null of no structural breaks in nightlights at the 0.05 level.

I am successfully able to estimate a structural break for 100 mines in my sample that opened prior to 2013. For the median mine, a structural break in nightlights occurs 3 years prior to the listed S&P start date, with approximately 60% of the mines having the break year between 0 and 3 years prior to the S&P defined date. This finding aligns with that of Benshaul-Tolonen [2020], who uses a local polynomial regression to show that there is a break in the trend for nightlights within 10 kilometers of a mine that occurs roughly 2 years prior to the date of a mine opening. She refers to this break as the start of the "investment" phase in a mine's life cycle. Figure 35 plots the histogram of the difference between the S&P year and the break year.
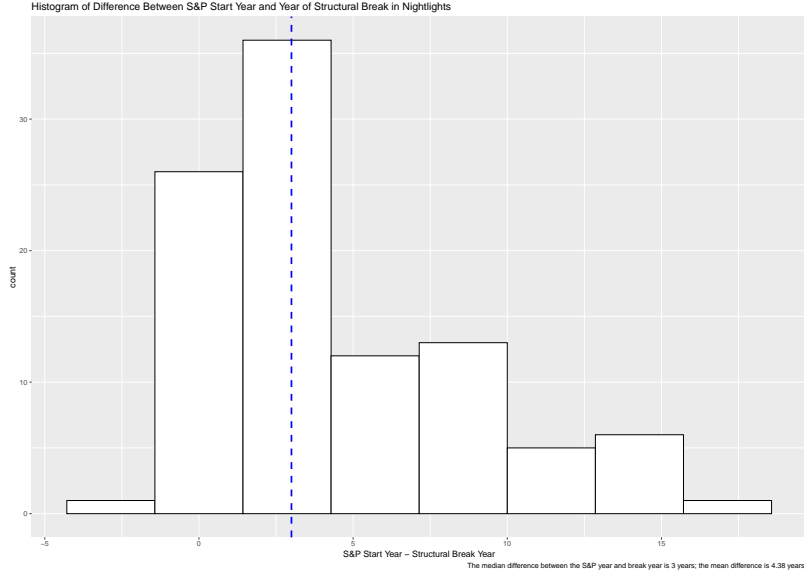
Figure 35: Difference between S&P Year and Structural Break Year

Furthermore, for most mines the year identified as the structural break visually aligns with the timing of a sharp increase in nighttime lights. Figure 36 provides an example from Goedgevonden coal mine in South Africa.
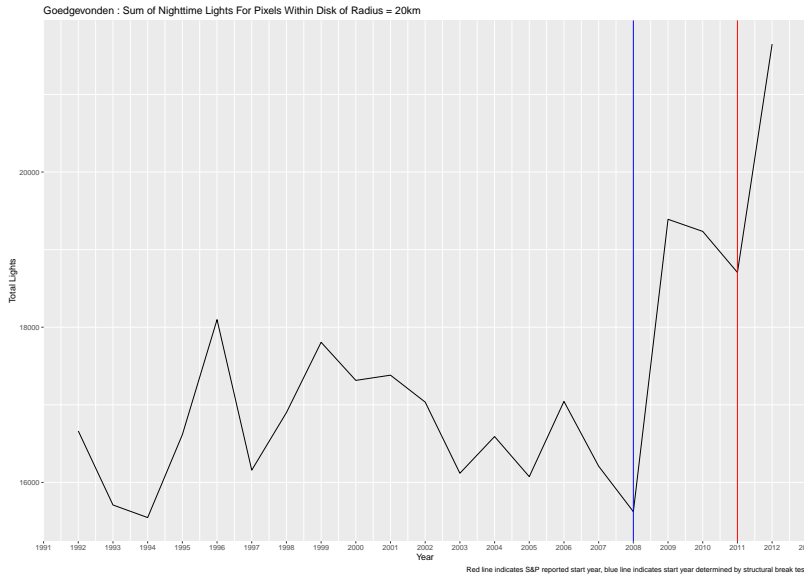

Figure 36: Time series of nightlights for Goedgevonden coal mine, South Africa

To investigate the robustness of this method for detecting structural breaks, I examine the correlation between the F-statistic from the break year and the start-date "error", defined as the difference between the S&P defined year and the break year. One might be concerned if the method is more likely to reject the null of no structural break in cases where there is a large difference between the S&P defined year and the break

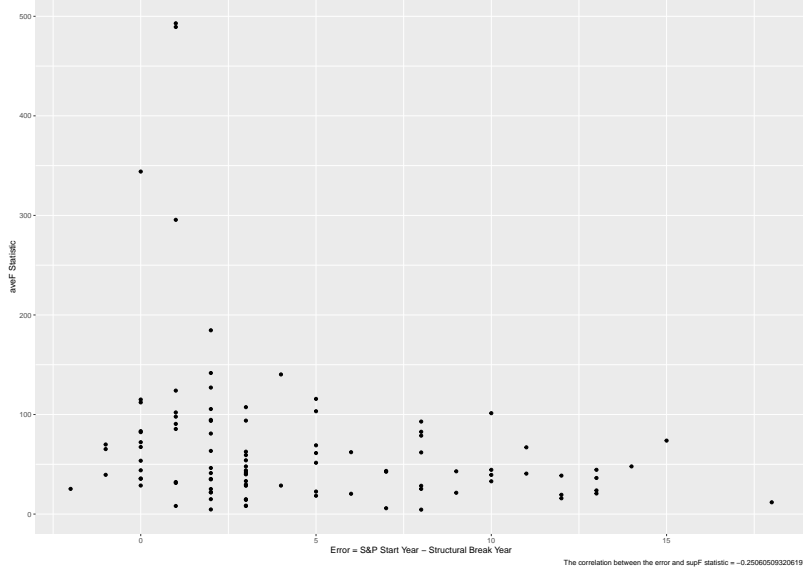year, suggesting that it would not perform well in detecting breaks that occur close to the listed date.

Figure 37: Magnitude of supF statistic vs. the difference between S&P defined start year and break year

These concerns do not seem to be borne out: in Figure 37 we see that across the domain of the "error", the sup F statistic ranges between 0-150 in most cases. In fact, the few outliers with very high supF statistics occur for cases where the S&P year and the break year are very close.

12.13 Effects of Measurement Error on DID Estimates:

Ideally, we would be able to observe farm-level yields around mining areas over time. However, this data is not available in Sub-Saharan Africa, making the use of NDVI as a proxy for yields more appealing. As NDVI is an imperfect measure of yields, I specify the following linear measurement error model from Keogh et al. (2020) to help understand how measurement error in NDVI will affect my DID estimates and the resulting share of the overall effect of mining attributed to pollution:

$$NDVI_{smt} = \theta + \mu Yield*_{smt} + v_{smt} \tag{8}$$

where NDVI on side s of mine m at time t is observed, while total yields across all farms on side s of mine m at time t is the true measure of interest and v_{smt} is noise. I assume v to be mean 0 and $cov(Yield*, v) = 0$.

I define simplified versions of the DID specifications used to estimate the overall effect of mining on NDVI and the effect of mining on NDVI through water pollution, where TO_{smt} is equal to the interaction of Near and Post in the overall specification and TW_{smt} the interaction of Downstream and Post in the water specification.

$$NDVI_{smt} = \alpha_{sm} + \lambda_{mt} + \delta Near_{sm} + \eta Post_{mt} + \beta_O TO_{smt} + \mathbf{X'_{smt}}\boldsymbol{\Gamma} + \epsilon_{smt} \tag{9}$$

$$NDVI_{smt} = \alpha_{sm} + \lambda_{mt} + \delta Downstream_{sm} + \eta Post_{mt} + \beta_W TW_{smt} + \mathbf{X'_{smt}}\boldsymbol{\Gamma} + \epsilon_{smt} \tag{10}$$

With classical measurement error, assuming v_{smt} is uncorrelated with proximity to a mine or downstream exposure and uncorrelated with the timing of a mine opening, estimates of the DID regressions using NDVI as the outcome of interest will be unbiased, though standard errors will be larger. Classical measurement error corresponds to the special case of 8 where $\theta = 0$, $\mu = 1$ and $cov(Yield, v) = cov(T, v) = 0$, where T corresponds to the main treatment and post interaction of my DID specification.

However, Proctor et al. [2023] show that assumptions of classical measurement error are unlikely to hold in regressions with remotely sensed dependent variables. First, they demonstrate that mean-reverting measurement error (negative correlation between errors in one variable and itself) is common with remotely-sensed measures, by highlighting that extreme values are systematically underestimated in remotely sensed predictions (Bound and Krueger, 1991, Ratledge et al., 2022). Mean-reverting measurement error corresponds to the case of Equation 8 where $\mu < 1$. Second, they show that differential measurement error, correlations between errors in one variable and levels of another variable, can also occur, by demonstrating non-zero covariance between errors in one variable and levels of other variables. While mean-reverting measurement error is indeed a concern in my context, differential measurement error is less so, given that it is reasonable to assume that NDVI errors should not be systematically correlated with both the timing of a mine openings and proximity or topographical placement relative to a mine.

Proctor et al. [2023] suggests that for the case with only mean-reverting error and no differential measurement error, a model using uncorrected NDVI with measurement error will tend to have attenuated coefficients. However, while mean-reverting measurement error is most common with remotely-sensed variables, differential measurement error explains most of the coefficient bias in the case of a mismeasured dependent variable. Importantly, both mean-reverting and differential measurement error can also lead to bias in standard errors of coefficients. In general, the reduced variance in the outcome variable in the presence of mean-reverting measurement error in the dependent variable could lower the sum of squared errors and underestimate standard errors on the DID coefficients of my main specification. However, when differential measurement error is also present, the direction of bias in the uncertainty parameters is theoretically ambiguous (Carroll et al., 2006).

Unfortunately, it is infeasible in my setting to implement the multiple imputation correction outlined by Proctor et al. [2023] to address issues of measurement error bias in NDVI. This is because potential data

sources for ground-based yields (One Acre Fund data, World Bank LSMS-ISA) have an insufficient number of observations that are observed for at least one year pre and post-mine openings, in both the near and far groups. Proctor et al. [2023] highlight that the calibration set should have at least 500 observations, otherwise bias can be even higher in the corrected model. Furthermore, while plot-level yields from data outside of Sub-Saharan Africa could be used for the calibration set, bias in the corrected model can be higher than in the uncorrected model if calibration locations are greater than 200km away from the locations used in the main analysis Proctor et al. [2023].

However, while the mean reverting measurement error common to remotely-sensed variables may attenuate my DID estimates, it should not affect the estimate of the share of the overall treatment effect that be explained by pollution. To understand this, I demonstrate that the attenuation bias of mean reverting measurement error should cancel out when estimating the share.

According to Proctor et al. [2023], under the most general form of the linear measurement error model, regressions of Equations 9 and 10 recover the following slope coefficients:

$$\mathbb{E}(\hat{\beta}_O) = \lambda\beta_O + \frac{\sigma_{TOv}}{\sigma_{TO}^2} \tag{11}$$

$$\mathbb{E}(\hat{\beta}_W) = \lambda\beta_W + \frac{\sigma_{TWv}}{\sigma_{TW}^2} \tag{12}$$

Given the assumption that errors in NDVI are uncorrelated with the timing of a mine opening and proximity or topographical location relative to a mine, the covariance between the main DID interaction terms and the NDVI errors should be 0. Then, once we take the ratio of $\mathbb{E}(\hat{\beta}_O)$ to $\mathbb{E}(\hat{\beta}_W)$, the mean-reverting measurement error cancels out, ensuring that we obtain an unbiased estimate for the share of the overall effect of mining on yields that can be attributed to pollution.

12.14 Effects of Measurement Error on Quantification Exercise: Given plot-level yields, the "ideal" measure of NDVI for each plot, $NDVI_p^*$, would be NDVI based on information detected by the satellite without any errors or interference and calculated over the exact boundaries of plot p. However, the NDVI measure used in Equation 7 differs from $NDVI^*$ in two ways. Dropping the t subscript for simplicity, I define the observed NDVI measure for plot p, which falls in cell c, as follows:

$$NDVI_{p(c)} = \xi NDVI_p^* + d_p + a_p$$

where d_p corresponds to deviations from "true" plot-level NDVI caused by satellite-detection errors and

a_p corresponds to deviations for plot p NDVI from the average of all plots in c. NDVI detection errors, d_p, are driven by a variety of factors, most notably cloud cover, but also surface reflectance, canopy thickness, the level of atmospheric aerosols and sensor errors (MODIS article). These detection errors make NDVI observed from satellite data an imperfect measure of NDVI in the presence of no detection errors. Indeed, low pixel quality due to detection errors can cause errors in vegetation indices to increase by 0.04-0.1. While some types of detection errors, such as satellite sensor errors, are likely uncorrelated with plot-level yields, detection errors driven by cloud cover or aerosol loading could be correlated with plot-level yields through the direct effect of atmospheric determinants on crop health. In these cases, we would have $Cov(Yield_p, d_p) \neq 0$, suggesting that d_p could introduce bias from non-classical measurement error.

Additionally, aggregation errors, a_p, are generated by the limited 500m resolution of the MODIS data, which makes it infeasible to obtain precise plot-level NDVI measures.[12] GPS-based measures of plot area from household surveys in four African countries show that over 50% of the fields in these countries are smaller than 1 acre, suggesting that the grid-cells used in my analysis likely cover multiple plots (Carletto et al., 2015). If yields are highly heterogeneous across plots within a grid-cell, averaging NDVI over the grid cells may not only weaken the correlation between grid-cell NDVI and plot-level yields, but also introduce aggregation bias into estimation of Equation 7.

I address measurement erorr in cell-level NDVI as follows. First, I limit potential bias from detection errors by calculating NDVI using only high quality pixels free of clouds and aerosols, as well as controlling for local weather variables such as cloud cover, vapor pressure and precipitation. Second, I estimate (1) a version of Equation 7 with smaller grid cells to investigate whether β_{NDVI} changes with the degree of aggregation and (2) a version of Equation 7 that aggregates plot-level yields to the grid-cell used to aggregate NDVI, so that spatial scales are consistent between the dependent and independent variables.

---

[12]While higher resolution data is available from sources like Sentinal-2 or PlanetLabs, this data does not go far enough back to cover mines that opened prior to 2014.

Table 21: Relationship between Cell-level NDVI and Cell-level Yields, cell-size = 500m

	(1) Planting	(2) Early Growing	(3) Late Growing	(4) Harvest	(5) Nonfarm
Mean NDVI	45.68	38.76	40.76	30.06	7.269
	(32.85)	(25.83)	(33.81)	(22.08)	(25.08)
Year FE	Yes	Yes	Yes	Yes	Yes
Grid cell FE	Yes	Yes	Yes	Yes	Yes
Include weather controls	Yes	Yes	Yes	Yes	Yes
Mean Yields	3005.643	3005.643	3005.643	3005.643	3005.643
Obs.	340	467	421	524	445
R-sq	0.657	0.673	0.673	0.672	0.650

Each column reports the results of an OLS regression. The unit of observation is a cell-year. The dependent variable is mean plot-level yields in kg/ha across all plots falling within a cell, in a given year. *Mean NDVI* is the average NDVI in the cell of size 500m containing the plot, across days in a particular season during the year that maize on the plot was harvested. The columns indicate the season for which NDVI is calculated during the year the plot was harvested. *Mean NDVI* is scaled so that one unit represents a 0.01 increase in NDVI. Each regression includes linear controls for cell-level averages of growing degree days, temperature and precipitation during the maize season across plots falling within the cell, as well as cell-level controls for mean temperature, precipitation, vapor pressure, cloud cover, evapotranspiration and wet days. Year and cell-level fixed effects are included in the regressions.

Table 22: Relationship between Cell-level NDVI and Cell-level Yields, cell-size = 2500m

	(1) Planting	(2) Early Growing	(3) Late Growing	(4) Harvest	(5) Nonfarm
Mean NDVI	21.96*	41.64**	0.756	29.74**	27.23**
	(12.06)	(18.23)	(16.61)	(12.99)	(10.77)
Year FE	Yes	Yes	Yes	Yes	Yes
Grid cell FE	Yes	Yes	Yes	Yes	Yes
Include weather controls	Yes	Yes	Yes	Yes	Yes
Mean Yields	3005.643	3005.643	3005.643	3005.643	3005.643
Obs.	2038	2070	2071	2057	2069
R-sq	0.588	0.585	0.583	0.585	0.586

Each column reports the results of an OLS regression. The unit of observation is a cell-year. The dependent variable is mean plot-level yields in kg/ha across all plots falling within a cell, in a given year. *Mean NDVI* is the average NDVI in the cell of size 2500m containing the plot, across days in a particular season during the year that maize on the plot was harvested. The columns indicate the season for which NDVI is calculated during the year the plot was harvested. *Mean NDVI* is scaled so that one unit represents a 0.01 increase in NDVI. Each regression includes linear controls for cell-level averages of growing degree days, temperature and precipitation during the maize season across plots falling within the cell, as well as cell-level controls for mean temperature, precipitation, vapor pressure, cloud cover, evapotranspiration and wet days. Year and cell-level fixed effects are included in the regressions.

12.15 Addressing measurement error

Table 23: Relationship between Cell-level NDVI and Cell-level Yields, cell-size = 5000m

	(1) Planting	(2) Early Growing	(3) Late Growing	(4) Harvest	(5) Nonfarm
Mean NDVI	11.93	54.57***	18.00	46.21***	34.77***
	(11.11)	(15.96)	(14.47)	(11.52)	(10.03)
Year FE	Yes	Yes	Yes	Yes	Yes
Grid cell FE	Yes	Yes	Yes	Yes	Yes
Include weather controls	Yes	Yes	Yes	Yes	Yes
Mean Yields	3005.643	3005.643	3005.643	3005.643	3005.643
Obs.	2016	2040	2038	2036	2040
R-sq	0.551	0.559	0.552	0.557	0.553

Each column reports the results of an OLS regression. The unit of observation is a cell-year. The dependent variable is mean plot-level yields in kg/ha across all plots falling within a cell, in a given year. *Mean NDVI* is the average NDVI in the cell of size 5000m containing the plot, across days in a particular season during the year that maize on the plot was harvested. The columns indicate the season for which NDVI is calculated during the year the plot was harvested. *Mean NDVI* is scaled so that one unit represents a 0.01 increase in NDVI. Each regression includes linear controls for cell-level averages of growing degree days, temperature and precipitation during the maize season across plots falling within the cell, as well as cell-level controls for mean temperature, precipitation, vapor pressure, cloud cover, evapotranspiration and wet days. Year and cell-level fixed effects are included in the regressions.